AN ABSTRACT OF THE DISSERTATION OF

Patrick T. Vallano for the degree of Doctor of Philosophy in Chemistry presented on March 6, 2001. Title: Novel Approaches to Enhancing Selectivity and Efficiency in Microscale Liquid Chromatography.

Abstract approved: Redacted for Privacy

Vincent T. Remcho

For a number of reasons, miniaturization of chromatographic columns has been a general trend over the past three decades. Methods designed to enhance selectivity and efficiency can offer improved separation power and speed, expanding on the advantages of miniaturized columns. This dissertation describes novel approaches in this direction, focusing on two areas: the development of affinity-type sorbents for capillary HPLC derived from molecular imprinted polymers (MIPs) and the study of perfusive electroosmosotic flow (EOF) and its effect on efficiency in capillary electrochromatography (CEC).

MIPs are synthetic polymers capable of selectively binding a template molecule incorporated prior to polymerization. MIPs prepared using nortripyline, a tricyclic antidepressant drug, were employed to screen a simulated chemical library, consisting of a series of structural analogs and related compounds. A parameter was introduced to quantify the selective retention of the analytes. Library compounds containing the major structural features of the template (ring structure and pendant 2° amine) exhibited the highest affinity for the MIP.

The use of macroporous packings under conditions of electroosmotic perfusion can result in improved chromatographic efficiencies. In this work, the performance of

CEC columns packed with particles having different nominal pore diameters was investigated. The results indicate that perfusive EOF can yield significant gains in efficiency and speed, especially when wide pore packings and dilute buffers are employed.

A model was developed that estimates the extent of perfusive EOF expressed as an effective particle diameter, $d_{p,eff}$. The results suggest that the observed efficiency gains are not entirely due to smaller $d_{p,eff}$ values and could perhaps be due to a decreased A term in the wide pore packings.

The electrical conductivity of CEC columns was used to assess intraparticle flow permeability under conditions of perfusion. Results for the narrow pore (100 Å) column were in agreement with theory for nonporous spheres, indicating intraparticle current was negligible, while the wide pore (1000 and 4000Å) columns exceeded theoretical values by a factor of two. These results provide evidence of the existence of "through-pores" and that intraparticle flow permeability (and potential for improved efficiency with perfusion) is greatest with wide pore packings.

Novel Approaches to Enhancing Selectivity and Efficiency in Microscale Liquid Chromatography

by Patrick T. Vallano

A DISSERTATION

submitted to

Oregon State University

in partial fulfillment
of the requirements for the
degree of

Doctor of Philosophy

Presented March 6, 2001
Commencement June 2001

Doctor of Philosophy dissertation of Patrick T. Vallano presented on March 6, 2001.

APPROVED:

Redacted for Privacy

Major Professor, representing Chemistry

Redacted for Privacy

Chair of Department of Chemistry

Redacted for Privacy

Dean of the Graduate School

I understand that my dissertation will become part of the permanent collection of Oregon State University libraries. My signature below authorizes release of my dissertation to any reader upon request.

Redacted for Privacy

Patrick T. Vallano, Author

ACKNOWLEDGEMENTS

This dissertation would not have been possible were it not for the assistance of numerous friends, colleagues, family members and faculty to whom I wish to express my heartfelt gratitude.

To begin, I want to acknowledge my advisor, Vincent T. Remcho. His guidance and support have made my tenure as a graduate student a truly memorable experience.

The support of my parents and family and their faith in my ability are greatly appreciated. My parents continue to serve as role models for me.

Individuals who have generously contributed equipment, materials, or expertise that have proved invaluable in the course of this research include Dr. Nathan Ballou, Dr. Scott Chervenick, Gabriela Chirica, Dr. Steve Petersen, Al Soeldner, and Dr. Z. Jessica Tan.

The National Science Foundation, Oregon State University Research Office and Department of Chemistry at Oregon State University have kindly provided financial support for this research.

Additionally, I have been fortunate to work alongside the following people at some time during the course of this research: Stacey Clark, Mike Cipolletti, Angela Doneanu, Mohammad Khasawneh, Daming Li, and Preston Lowe.

Lastly and most importantly I wish to thank my wife Traci. Without her encouragement, faith, love, and sacrifice, this work would surely not have been possible.

TABLE OF CONTENTS

LIST OF FIGURES

LIST OF FIGURES, CONTINUED

LIST OF TABLES

Novel Approaches to Enhancing Selectivity and Efficiency in Microscale Liquid Chromatography

1. Introduction

1.1 Introduction and Research Overview

For a number of years, high performance liquid chromatography (HPLC) has been one of the most widely used analytical techniques. Among the strengths of HPLC are a wide range of applicability and good quantitative accuracy and precision. The desire of chromatographers for increased performance, specifically with respect to efficiency and resolution, has provided a driving force for the miniaturization of HPLC columns over the past three decades. Parallel advances in microscale HPLC and capillary electrophoresis (CE) during this time have given rise to capillary electrochromatography (CEC), which can be viewed as a hybrid of these techniques. Bulk flow of mobile phase in CEC is due to electroosmosis, which exhibits a more favorable flow profile and less peak broadening as compared to laminar flow. Although electrophoretic migration is possible, CEC is a true chromatographic technique. This dissertation focuses on novel methods by which selectivity and efficiency can be enhanced in microscale HPLC and CEC, thereby increasing separation power.

This dissertation is organized as follows. At the outset, a review of relevant chromatographic theory is presented with an emphasis on the theoretical advantages of column miniaturization in HPLC and the advantages of CEC. In chapter 2, the developmental timeline of microscale HPLC is explored and major milestones

identified. To gain further perspective on the development of CEC, a short historical review of electrophoresis and the evolution of modern CE and some of its variants follow.

There are two general thrusts to research presented in this disseration: i) the development of highly selective sorbents for capillary HPLC derived from molecular imprinted polymers (MIPs) and ii) the investigation of intraparticle electoosmotic flow and its effect on efficiency in CEC. These are described briefly below.

MIPs are synthetic polymers that can be made to exhibit molecular recognition of a template molecule, which is incorporated into the solution of monomers prior to polymerization. The binding site in the polymer is complementary to the template with respect to molecular shape and orientation of functional groups and as such, binding is highly selective.

Affinity chromatography is an important analytical tool for the study of many biologically relevant molecules [1]. The technique employs biological macromolecules (e.g. receptor proteins or antibodies) as selective stationary phases. In a similar vein, the molecular recognition-based and therefore highly selective nature of template binding potentially renders MIPs useful as affinity sorbents. Chapter 3 of this dissertation explores the use of MIPs as affinity sorbents in capillary HPLC. In this research, MIPs were prepared against nortriptyline, a representative tricyclic antidepressant drug. Selective retention of the template on the MIP-based sorbent was observed in the presence of a series of structural analogs. In addition a simulated combinatorial library composed of other tricyclic antidepressants and related compounds was screened on the MIP sorbent to determine the degree to which each

test probe interacted with the nortriptyline binding sites in the polymer. A parameter was introduced, the selection index, to quantify the extent of selective retention on the MIP sorbent. Subsequently, a series of experiments was conducted to explore the mechanism of interaction between the test probes and MIP.

Intraparticle, or perfusive electroosmotic flow can occur in packed column CEC under conditions in which the electrical double layer thickness near the particle surface is small relative to the mean pore diameter of the packing particle. In general, this condition is satisfied when macroporous packings are employed with appropriate mobile phases. Advantages of operating in the perfusive regime include enhanced chromatographic efficiency, and hence, improved resolution. More importantly, separations can be conducted at higher linear velocities, resulting in shorter analysis times, without compromising efficiency. So-called perfusive packings have been employed in conventional HPLC, primarily in separations of large biomolecules (e.g. proteins) [2]. In perfusive chromatography, a decreased stagnant mobile phase mass transfer contribution to peak broadening makes possible the rapid separations without loss of resolution that are the chief benefit of the technique. Relative to HPLC, the slopes of the high velocity, mass transfer dominated region of plate height versus linear velocity curves are lower in CEC due to the "flat" profile of EOF. Therefore a reduction in stagnant mobile phase mass transfer in CEC should, in principle, allow rapid, extremely efficient separations.

Chromatographic efficiency, expressed in terms of a height equivalent to a theoretical plate, or plate height, is related to the diameter of the packing particles, with smaller particles yielding smaller plate heights (higher efficiency). Under

conditions of perfusion, with a significant fraction of the intraparticle pores in a CEC column supporting electroosmosis, the microbeads comprising the packing particles begin to dictate the true or "effective" particle diameter, and plate height is decreased. The system, in effect, acts as a bed packed with smaller particles.

Perfusive CEC systems are explored in detail in this dissertation. Commercially available reverse phase HPLC packings of various pore sizes were evaluated chromatographically under a variety of mobile phase conditions typical in CEC. Additionally, physical characterization of these packings was performed using mercury intrusion porosimetry and scanning electron microscopy.

Using the pore size distribution and chromatographic data, a model was developed that estimates the contribution of intraparticle flow in a CEC column under a given set of conditions, which is expressed in terms of an effective particle diameter. This research is presented in chapter 4. In these experiments, as the ionic strength of the mobile phase was varied, the effective particle diameter values predicted by the model were found to agree with the trends in the experimental data.

Additionally, the intraparticle flow permeability of the various packed CEC columns was evaluated using electrical conductivity measurements. In these experiments it was found that the column conductivities of the wide pore packed columns were over twofold greater than a column packed with "conventional" narrow pore particles of the same particle diameter. These observations, and the fact that the conductivity of the narrow pore column closely matched that predicted from theory for nonporous spheres, provide evidence for the existence of "through-pores" in the macroporous particles.

1.2 Theoretical Background

1.2.1 Variables Affecting Resolution in Liquid Chromatography

In liquid chromatography, separation is achieved by the differential migration of solutes based on the extent of partitioning between the stationary phase and flowing solvent (i.e. the mobile phase), upon passage through a column. The quantitative measure of the separation of any two components is resolution *(R_s)*. Resolution is an important figure of merit because describes the ability of the system to distinguish between closely spaced components in a chromatogram. The goal in chromatography is usually to obtain adequate resolution of the components of interest in a minimum amount of time.

Separations in which many components must be resolved are often the most challenging. This is typically the case when the species to be analyzed are present in a complex matrix, for example with many biological or environmental samples. Obtaining adequate separations of components within these complex matrices generally requires high resolution. In many analytical laboratories sample throughput is an important consideration. Shorter analysis times allow more samples to be analyzed per instrument per day and are therefore highly desirable in these settings. To meet these challenges, there is an ever-present need to seek ways in which chromatographic resolution can be maximized while at the same time minimizing analysis time.

At the outset, a review of the variables affecting resolution is in order. Resolution can be expressed in terms of three fundamental chromatographic parameters: retention factor, selectivity and efficiency. The dependence of resolution

on these variables is expressed in the following equation, known as the master resolution equation.

$$R_s = \frac{1}{4}\left(\frac{k}{1+k}\right)\left(\frac{\alpha-1}{\alpha}\right)\sqrt{N} \qquad (1.1)$$

The first term in equation 1.1 is retention factor *k* dependent. Retention factor for a given solute is related to its affinity for the stationary phase (it is proportional to the solute's thermodynamic partition ratio). If all other variables are held constant (e.g. mobile phase linear velocity, phase ratio, column length, etc.), a solute having a lower value of *k* will migrate through the column more rapidly (and therefore have a shorter retention time) relative to a solute with a greater *k*. Strictly defined, *k* is the equilibrium number of moles of solute in the stationary phase.

The second term in the equation contains the separation factor, or selectivity α. Selectivity, which is measured for a pair of peaks, is simply the ratio of their retention factors ($\alpha = k_2/ k_1$, where $k_2 > k_1$). Selectivity values indicate differences in the affinities of two analytes for the stationary phase. Both retention factor and selectivity are dependent upon the thermodynamics of the solute-stationary phase interaction.

The third term in the master resolution equation is efficiency *(N)* dependent. Efficiency is related to the width of the chromatographic peak and is usually expressed as the number of theoretical plates, a term carried over from distillation theory. Unlike retention factor and selectivity, efficiency is chiefly affected by physical, rather than chemical processes that occur as the solute traverses the column. These processes include molecular diffusion, slow mass transfer and other kinetic

phenomena that result in broadening of peaks as they migrate through the column. Efficiency is quantified by the following equation, which assumes Gaussian peaks:

$$N = \frac{t_r^{\,2}}{\sigma^2} \cong 16\left(\frac{t_r}{W_b}\right)^2 \qquad (1.2)$$

where t_r is the retention time of the peak , σ^2 is the peak variance in units of time and W_b is the peak width at baseline also in time units.

From equations 1.1 and 1.2 it is evident that peak broadening degrades resolution. It is desirable, then, to minimize peak broadening by understanding and minimizing (to the extent possible) its causes.

A more useful parameter with which to assess chromatographic peak dispersion is the height equivalent to a theoretical plate or plate height (H), which is given by the following expression:

$$H = \frac{\sigma^2}{L} \equiv \frac{L}{N} \qquad (1.3)$$

where L = column length. Plate height is a measure of peak broadening per unit column length. Assuming Gaussian peaks, which under most conditions is a reasonably valid assumption, plate height may be viewed as the length of column that "contains" one theoretical plate (equation 1.3)

Greater values of H correspond to broader peaks. Because plate height is a measure of peak broadening per unit length of column, it is often a more useful figure of merit than N in that it allows direct comparisons between columns of different lengths. In packed column chromatography, plate height is often expressed in its

reduced form, h, ($h = H/d_p$) in which H is normalized to the packing particle diameter d_p.

Let us now examine the phenomena that contribute to H. According to chromatographic rate theory, peak broadening arises from various kinetic factors that occur as the solute zone passes through the column. The following well-known relationship, which derives from chromatographic rate theory, expresses plate height as the sum of individual contributions:

$$H = A + \frac{B}{\mu} + C_s\mu + C_m\mu \qquad (1.4)$$

In this general form of the equation, the A term represents the plate height contribution due to eddy diffusion and the B term represents axial molecular diffusion. The contributions of slow solute mass transfer in the stationary and mobile phases are contained in the C_s and C_m terms, respectively. Mobile phase linear velocity is given by μ. It is common in chromatography to plot H versus μ graphically in so-called Van Deemter, or rate curves.

The eddy diffusion or A term in equation 1.4 arises in part from the multiple pathways in a packed bed through which solutes can flow. A molecule traveling a less torturous path will travel faster relative to the average condition. Conversely, a molecule traveling in a more difficult path will fall behind with respect to the average. The resultant chromatographic peak, a distribution of arrival times about a mean value (the peak apex), becomes broadened. It has been shown that the magnitude of the A term is proportional to the diameter of the packing particle [3].

$$A \propto d_p \qquad (1.5)$$

Axial, or longitudinal molecular diffusion, represented by the B term, is the plate height contribution due to diffusion of solute molecules along the column axis. The B coefficient is proportional to the solute's diffusion coefficient in the mobile phase. The slower the velocity of the solute zone through the column, the more time is available for diffusion to occur, thus there is an inverse relationship between mobile phase velocity and the magnitude of this contribution. In liquids, the diffusion coefficients of small molecules are low (typically on the order of 10^{-5} cm^2 s^{-1}). For this reason, the effect of axial diffusion on plate height is minimal under typical operating conditions.

A finite amount of time is required for solute molecules to enter and leave the stationary phase. The rate of this exchange has an inverse effect on plate height: a slower exchange results in broader peaks. The C_s term of the plate height equation includes this contribution to plate height. As might be expected, the value of C_s is related to the thickness of the stationary phase layer on the particle surface. For this reason, in modern liquid chromatography the stationary phase film is typically formed as a monolayer on the particle surface. Because of this, slow mass transfer in the stationary phase is usually a minor contributor to plate height.

The contribution to plate height of slow mass transfer kinetics in the mobile phase is included in the C_m term. In even the most well packed liquid chromatography column, point-to-point differences in mobile phase velocity exist. For example, velocity differences arise from the intrinsic nature of laminar, or pressure-driven flow. Consider for instance that in any microscopic flow channel within the packed bed, for example in the packing interstices, the flow velocity is at some maximum value at the

channel center and zero at the particle surface (this phenomenon is treated in greater detail in a later section). Between these extremes, flow velocity varies as a function of distance from the center. Molecules near the center of the channel will outdistance those near the particle surface, broadening the zone. Diffusion of solute molecules into and out of the various velocity regimes serves to counteract the zone broadening effect. However, as noted previously, diffusion coefficients in liquids are small and so this source of velocity inhomogeneity contributes to plate height.

Slow solute diffusion in the mobile phase results in additional zone broadening effects when porous packings are employed. Stagnant mobile phase mass transfer involves pools of non-flowing mobile phase deep inside the pores of the packing material. Solute molecules that diffuse into these pools fall behind with respect to the average, and the peak broadens. Because diffusion is the sole mechanism by which solute molecules enter and leave the pools, the slow diffusion rates of solutes in liquids exacerbate zone broadening. Stagnant mobile phase effects are amplified at high velocities.

Not surprisingly, the C_m term scales in inverse proportion to the solute's diffusion coefficient in the mobile phase D_m. The proportionality below shows the dependence of C_m on particle size and the diffusion coefficient:

$$C_m \propto \frac{d_p^{\,2}}{D_m}\mu \qquad (1.6)$$

In HPLC mobile phase mass transfer is often a major contributor to plate height at high linear velocities, due in part to the comparatively small diffusion coefficients of molecules in the liquid phase. In a C_m limited system, the ability to

achieve rapid separations is compromised by the loss of efficiency (and therefore resolution) at high mobile phase velocities.

From the viewpoint of minimizing eddy diffusion and mobile phase mass transfer contributions to plate height, small diameter particles are preferred. Although the technology exists to produce smaller particles, the typical commercially available analytical scale HPLC column is packed with 5 μm diameter particles. As discussed in the following section, the pressure drop required to drive mobile phase through a column packed with smaller particles is often prohibitive.

1.2.2 Advantages of column miniaturization

The ongoing evolution of HPLC has led to the development of ever-smaller column diameters (< 1.0 mm) over the last few decades. The impetus for this miniaturization has been the numerous advantages afforded by miniaturized columns. These advantages include:

- Improved column permeability, resulting in enhanced efficiency
- Decreased solvent consumption
- Increased mass sensitivity
- More efficient heat transfer
- Less packing material required
- More facile interfacing with mass spectrometry

Let us now examine each of these advantages in greater detail.

1.2.2.1 Enhanced Column Permeability

The permeability of a chromatographic column is a measure of its resistance to flow and can be expressed in terms of the dimensionless flow resistance parameter ϕ:

$$\phi = \frac{\Delta P d_p^{\,2}}{\mu L \eta} \tag{1.7}$$

where ΔP = pressure drop, d_p = particle diameter, L = column length, η = mobile phase viscosity and μ = mobile phase linear velocity. Evident in equation 1.7 is the direct proportionality between ΔP and ϕ. With a fixed set of operational conditions (i.e. fixed d_p, L and η), the pressure drop required to obtain a particular linear velocity is dependent upon ϕ. This is relevant in HPLC because there is an upper limit to the pressure attainable by conventional instrumentation, typically 400 bar. This in turn places constraints on L and d_p, which limit efficiency, and μ, which affects analysis time. As a result of these limits, optimizing a separation usually involves a compromise between efficiency and speed.

A useful parameter in assessing the performance characteristics of HPLC columns that incorporates pressure drop and analysis time is separation impedance E. This dimensionless parameter introduced by Knox and Bristow [4] is a measure of column efficiency per unit time and per unit pressure drop, and is defined as follows:

$$E = \left(\frac{t_o}{N}\right)\left(\frac{\Delta P}{N}\right)\left(\frac{1}{\eta}\right) = \left(\frac{H}{d_p}\right)^2 \phi \tag{1.8}$$

where t_o is the elution time of an unretained solute (i.e. a solute for which no interaction with the stationary phase occurs); and other variables as defined previously. Lower values of E correspond to better column performance. Values of E and ϕ for various column diameters are shown in Table 1.1. It is seen that E values are smaller for miniaturized columns. Thus, these columns can yield more theoretical plates in less time and with a lower pressure drop relative to conventional bores.

Table 1.1. Values of h,ϕ, and E for various column diameters (Adapted from reference 5).

Column Type	h_{min}	ϕ	E
Narrow bore and conventional packed columns ($d_c/d_p > 10$)	2	500-1000	2000-4000
Packed capillary columns ($d_c/d_p \approx 2.5$)	2	150	600
Open tubular columns	0.8	32	20

The enhanced permeability of miniaturized columns allows for further increases in efficiency by making possible the use of smaller packing particles and/or longer columns. Recall from equations 1.4 – 1.6 that plate height is related to particle size through the A and C_m terms of the plate height equation, and that efficiency is proportional to column length (equation 1.3). In spite of this, conventional columns are constrained by excessive pressure drop, which limits usable lengths and particle sizes. Most 4.6 mm I.D. columns are 150-250 mm long and employ 5 μm particles. Alternatively, the use of smaller particles can result in reduced analysis times because

when particle size is reduced, a given plate number is achievable with a shorter length of column.

1.2.2.2 Decreased Solvent Consumption

Decreasing column diameter results in a substantial reduction in the volumetric flow rate required for a given linear velocity. Volumetric flow rate (F) through a packed column is given by:

$$F = \frac{\pi d_c^{\,2} \varepsilon_{tot} \mu}{4} \qquad (3.9)$$

(d_c = column diameter, ε_{tot} = column porosity). The dependence of F on the square of column diameter translates into significant reductions in solvent consumption on miniaturization. Volumetric flow rates for various column diameters are compared in table 1.2.

Table 1.2. Comparison of flow rates for various column diameters operated at a fixed linear velocity (approximately 3 times optimum velocity).

Column Diameter (mm)	Volumetric Flow Rate (μL min^{-1})
4.60	1400
1.00	66
0.530	19
0.100	0.66
0.050	0.16

For example, downsizing to a 1.0 mm I.D. from a conventional 4.6 mm will reduce solvent consumption over 20 fold. Decreased solvent consumption is economical in terms of reduced purchase and disposal costs, as well as environmentally responsible.

1.2.2.3 Improved Mass Sensitivity

Chromatographic separations are intrinsically processes of dilution: an initial sample plug of concentration C is diluted in the mobile phase and reaches the detector as concentration C' (where C' < C). Because the majority of HPLC detectors are concentration-based, a reduction in sensitivity results from peak dilution. To understand why this process is ameliorated upon column miniaturization, it is necessary to introduce peak volume V_p. Assuming a Gaussian peak, V_p is defined as follows:

$$V_p = F W_b = \left(\frac{\mu \varepsilon_{tot} \pi d_c^{\,2}}{4} \right) W_b \qquad (1.10)$$

(W_b = peak width at baseline in units of time). V_p is simply described as the volume of mobile phase in which the peak elutes. According to equation 1.10, peak volumes are proportional to the square of column diameter; thus values of V_p for microcolumns are substantially smaller than conventional 4.6 mm I.D. columns.

The concentration of solute at the peak maximum is inversely proportional to V_p [6]. Qualitatively, this relationship can be envisioned as follows: A given mass of solute is diluted in a volume V_p yielding a concentration C. If the same mass is diluted in a smaller volume V_p', the resulting concentration C' will exceed C in proportion to

the volume difference. As indicated in table 1.3, for a fixed mass of solute injected, column miniaturization can result in substantial increases in sensitivity with concentration-based detectors (e.g. UV, fluorescence).

Table 1.3. Typical peak volumes and relative sensitivity of various column diameters. Assumed conditions: $L = 250$ mm; $k \leftrightarrows 2$; $N = 10000$; $\mu = 2.0$ mm s^{-1}; $\varepsilon_{tot} = 0.7$. (Relative sensitivity calculation assumes a fixed mass of solute injected and a concentration sensitive detector).

Column Diameter (mm)	Peak Volume V_p (μL)	Relative Sensitivity
4.60	350	1.0
1.00	17	20
0.530	4.8	75
0.100	0.17	2000
0.050	0.040	8500

1.2.2.4 Additional Advantages

The decreased cross-sectional area of miniaturized columns allows for more efficient heat transfer to and from the column interior. As a result, miniaturized columns are capable of more rapid equilibration at different temperatures relative to conventional bore columns, which makes possible the use of temperature programming as in capillary gas chromatography (GC). In addition, these columns can more effectively dissipate heat generated by the pressure drop, minimizing temperature gradients that can ultimately cause peak broadening.

Smaller volume columns require less packing material, which is beneficial if costly, "exotic" materials are used (e.g. many chiral and affinity phases). This is also the case for mobile phases and mobile phase additives.

The low volumetric flow rates of miniaturized columns also simplify interfacing to mass spectrometers. Columns may be interfaced directly using thermospray, electrospray and other means, obviating the need for flow splitting, which reduces sensitivity.

1.2.3 Extra-column Effects

Not all peak broadening occurs within the chromatographic column. In addition to the phenomena accounted for in the plate height equation (equation 1.4), which occur as the solute band passes through the column, the final peak width is affected by "extra-column effects". These include contributions from the sample injector, the injection volume, connecting tubing, detector cell volume and the detector time constant. Well-designed chromatographs are constructed such that extra-column effects comprise a small fraction (typically ≤ 10 %) of the final peak width. One disadvantage of column miniaturization is that the system becomes more susceptible to extra-column effects as column diameter decreases.

Peak volume (V_p) was defined in equation 1.10 as the peak width at baseline in units of volume. For Gaussian peaks, the final peak volume observed at the detector V_{obs} can be expressed in terms of the in-column V_p and extra-column V_{ec} contributions [7].

$$(V_{obs})^2 = (V_p)^2 + (V_{ec})^2 \qquad (1.11)$$

Dividing through by V_p^2 gives the relative increase in V_{obs} from extra-column effects:

$$\left(\frac{V_{obs}}{V_p}\right)^2 = \left[1 + \left(\frac{V_{ec}}{V_p}\right)^2\right] \qquad (1.12)$$

According to this equation, if the extra-column contribution to the final peak volume, V_{obs}, is to be limited to 10 %, then the extra-column volume must not exceed 46 % of the column peak volume. This poses less of a problem with the relatively large peak volumes encountered with conventional bore columns. However, because peak volumes are proportional to the square of column diameter, to maintain the same fraction (10%) of extra-column broadening in micro HPLC requires much more stringent control of extra-column volumes. In these cases, extra-column volumes must be significantly reduced in order to minimize the contribution to the final peak volume. As a consequence, conventional HPLC instrumentation, such as injectors, tubing and detector cells, must be modified in order to accommodate smaller diameter columns, which is one disadvantage of micro HPLC.

In addition to the dilution and mixing that occurs within extra-column volumes, a contribution to band broadening may arise from the detection electronics. The speed with which the detector responds to a change in solute concentration is affected by its time constant, τ. The time constant, which typically can be adjusted within a range of values, is useful as a filter for high frequency noise in the chromatogram. Longer time constants slow the detector response, providing enhanced signal filtering. Problems arise when the chromatographic peaks are very narrow, as is usually the case in high efficiency separations. In these instances, slow detector

response (i.e. long time constants) will result in additional peak broadening. It can be shown [8] that the maximum allowable time constant for a given fraction of peak broadening is proportional to $\frac{1}{\sqrt{N}}$. Thus, detectors employed in high efficiency separations require more rapid electronics.

1.2.4 Flow Profile and Efficiency: Advantages of Capillary Electrochromatography

As its name implies, capillary electrochromatography (CEC) can be viewed as a hybrid technique that combines features of capillary zone electrophoresis (CZE) and capillary HPLC. CEC is of interest because it combines the strengths of these techniques, namely the high efficiency of CZE and the high selectivity of HPLC, and as such can yield greater resolving power.

In CEC, two independent mechanisms are possible for the separative transport of solutes. The first is partitioning, the extent of which is governed by the thermodynamics of the solute-stationary phase interaction – the separation mechanism of HPLC. In addition, if the solutes are charged, separation by electrophoresis is possible, i.e. according to differences in their migration rates in an applied electric field. Relative migration rates, or more accurately electrophoretic mobilities, are dictated by the solute's charge and hydrodynamic radius.

CEC is performed in open tubular and packed capillary columns; the standard column material is fused silica. Open tubular CEC (OT-CEC) utilizes narrow bore capillaries, typically on the order of 10-25 μm in inner diameter. The stationary

phase, generally some type of organic polymer, is coated onto or covalently linked to the walls of the capillary. More commonly practiced is packed column CEC, which employs larger bore capillaries with typical inner diameters of 50-150 μm. Generally, these capillaries are packed with sorbents designed for and used in conventional HPLC. Typical stationary phases include reversed phase HPLC sorbents such as octadecylsilane (C18) or octyl (C8). Instrumentation in CEC is virtually identical to that in CZE. The typical set up consists of a high voltage power supply, usually capable of applying potentials up to 30 kV, and a UV absorbance detector for on-column detection. Application of an electric field along the capillary axis results in bulk flow of the mobile phase by electroosmosis. The high efficiencies observed in CEC are due to the intrinsic properties of electroosmotic flow (EOF).

Electroosmotic flow originates near the fused-silica capillary wall (or packing particle surface) due to a charge imbalance that exists at the surface-liquid interface. The surfaces of fused-silica tubing and silica-based packing materials bear a net negative charge arising from the presence of ionized silanol moieties ($Si\text{-}O^-$). When the siliceous material is placed in contact with an aqueous solution, a charge imbalance exists owing to the negatively charged surface and an excess of positively charged counterions present in the bulk solution. Electrostatic forces result in the attraction of the excess counterions to the surface. The charged surface and counterions constitute an "electrical double layer", so called because it consists of positive and negative charges. The formation of an electrical double layer at a fused silica surface is depicted schematically in figure 1.1.

The blanket of counterions near the solid surface consists of two regions. The layer nearer to the surface, the Stern layer, is comprised of a monolayer of immobile ions. Farther from the surface, a dynamic equilibrium exists between the forces of electrostatic attraction and thermal motion that results in the formation of a layer of mobile counterions able to exchange freely with ions in the bulk solution. These mobile ions constitute the diffuse or Gouy region of the double layer.

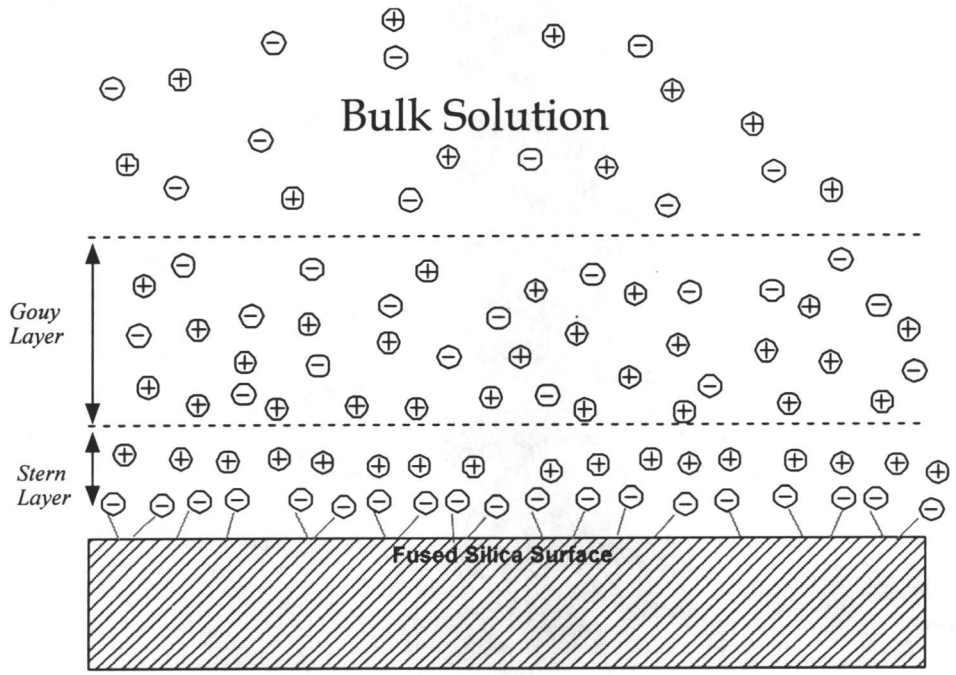

Figure 1.1. Schematic representation of the electrical double layer near the surface of fused silica capillary tubing.

The formation of the electrical double layer gives rise to a potential that varies as a function of distance from the particle surface (or capillary wall). This relationship is indicated in figure 1.2, in which potential (ψ) versus distance is plotted.

With the aid of figure 1.2, several features of the double layer can be noted. The potential at the surface (ψ_0) is dependent on the surface charge density, which in turn depends in part on the extent of silanol dissociation on a silica surface. Potential decreases with distance in a linear fashion across the Stern layer. At the interface between the Stern and Gouy layers, the potential is indicated as ψ_d. Across the diffuse region and into the bulk solution, the decay in potential is roughly exponential ($\psi \rightarrow 0$ as $x \rightarrow \infty$).

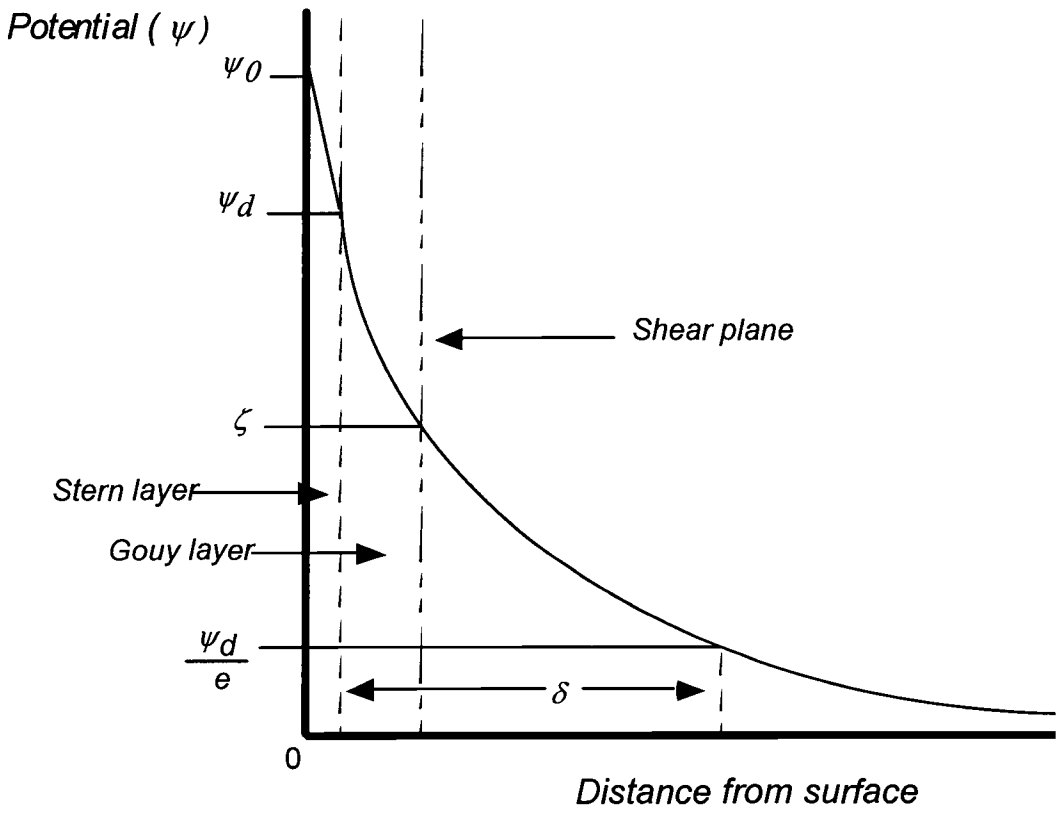

Figure 1.2. Potential as a function of distance from a charged surface. The potential at the plane of shear is the zeta potential, ζ. The distance over which the potential at the boundary of the Stern and Gouy layers, ψ_d, decays by a factor of $1/e$ is known as the double layer thickness, δ. Adapted from reference 9.

The distance over which the ψ_d decays to $1/e$ of its original value is denoted by δ, and is termed the electrical double layer "thickness" (alternatively expressed as κ^{-1}). Double layer thickness for a (1:1) electrolyte is given by the following equation, which can be derived by means of the Poisson-Boltzmann distribution and the Debye-Hückel approximation [10].

$$\delta = \kappa^{-1} = \left(\frac{\varepsilon_0 \varepsilon_r R T}{2CF^2} \right)^{1/2} \tag{1.13}$$

where ε_0 is the permittivity of vacuum, ε_r is the dielectric constant of the solution, R is the universal gas constant, T is temperature (in Kelvin), F is Faraday's constant, and C is the molar electrolyte concentration.

In the diffuse region of the double layer, a plane of shear exists that separates the counterions not free to exchange with the bulk solution from the mobile counterions. The potential at this shear plane is termed the zeta potential (ζ). Zeta potential is dependent upon double layer thickness as given by equation 1.14.

$$\zeta = \frac{\delta \sigma}{\varepsilon_0 \varepsilon_r} \tag{1.14}$$

in which σ= charge density at the shear surface (other variables as defined previously). Substitution of equation 1.13 into 1.14 yields

$$\zeta = \frac{\left[\left(\frac{\varepsilon_0 \varepsilon_r RT}{2F^2 c^2} \right)^{1/2} \right] \sigma}{\varepsilon_0 \varepsilon_r} \tag{1.15}$$

Values of δ are on the order of nm and typical values for a monovalent electrolyte are $\delta = 10$ nm for $c = 10^{-3}$ M and $\delta = 1$ nm for $c = 10^{-1}$ M. If the necessary constants and reasonable approximations of ε_r and σ are inserted into equation 1.15, it is easily determined that typical zeta potentials fall in the 25-100 mV range for silica surfaces in contact with aqueous solutions.

Upon the application of an electric field, a force is exerted on the counterions in the diffuse region and they begin to migrate toward the electrode of opposite polarity, generally the cathode. Because these migrating ions are solvated, and due to frictional forces, the bulk solution is dragged toward the respective electrode and electroosmotic flow results.

Electroosmosis is particularly advantageous as a driving force for mobile phase flow in chromatography because generates considerably less peak broadening relative to pressure-driven flow. In fact, the potential to combine the selectivity of HPLC with the favorable flow dynamics of electoosmosis has been a driving force in the development of CEC. There are three main advantages of EOF over pressure-driven flow for mobile phase propulsion in chromatography: 1) EOF flow velocity is radially uniform across a flow channel, 2) EOF flow velocity is independent of channel diameter, and 3) EOF requires no pressure drop. Each of these is explored in greater detail below.

Consider a capillary tube of radius r_c. In pressure-driven, or laminar flow, the flow velocity at any radial point in the tube $u(r)$ is a function of distance from the center as given by the Hagen-Poiseuille equation

$$u(r) = \frac{\Delta P}{4\eta L}\left(r_c{}^2 - r\right) \tag{1.16}$$

in which r is the distance from the tube center. The resultant flow velocity profile is parabolic in shape. There exists a distribution of velocities over the tube cross-section. Recall from the preceding discussion of the mobile phase mass transfer contribution to plate height that this type of velocity inhomogeneity leads to an increase band broadening. More specifically, this zone-broadening phenomenon is known as the transchannel effect [3].

Consider now electoosmotic flow through the same capillary tube. EOF velocity (υ_{eo}) at any radial point in the tube is given by the following equation:

$$\upsilon_{eo} = \frac{\varepsilon\zeta \mathrm{E}}{4\pi\eta}\left(1 - \frac{I_0(\kappa_d a)}{I_0(\kappa_d r)}\right) \tag{1.17}$$

where ε = permittivity of mobile phase, ζ = zeta potential, E = electric field strength, η = mobile phase viscosity, κ_d is the reciprocal of the thickness of the double layer, a is the distance from the center of the tube and I_0 is a zero order Bessel function of the first kind. Typically, the double layer thickness is quite small, on the order of 1 nm, and the term in parentheses reduces to 1, yielding the following expression

$$\langle v_{eo} \rangle = -\frac{\varepsilon\zeta \mathrm{E}}{4\pi\eta} \tag{1.18}$$

where $\langle \upsilon_{eo} \rangle$ indicates the average flow velocity in the tube. Equation 1.18, which is valid in the absence of double-layer overlap, shows that EOF velocity is independent of radial position in the flow channel. Thus, the flow profile is flat over most of the capillary cross section. Figure 1.3 shows an idealized view of the radial profiles of

pressure and electrically driven flow. This uniformity in flow velocity minimizes transchannel zone broadening, resulting in a lower C_m term in the plate height equation.

In packed chromatographic columns, there invariably exist local differences in packing density, which give rise to interstitial flow channels of varying diameter. With pressure driven flow, the squared dependence of velocity on channel diameter (equation 1.16) gives rise to a distribution of velocities in these channels. As in the transchannel effect, point to point differences in flow velocity contribute to zone broadening. The plate height increment due to this phenomenon is included in the eddy diffusion (A) term of the plate height equation.

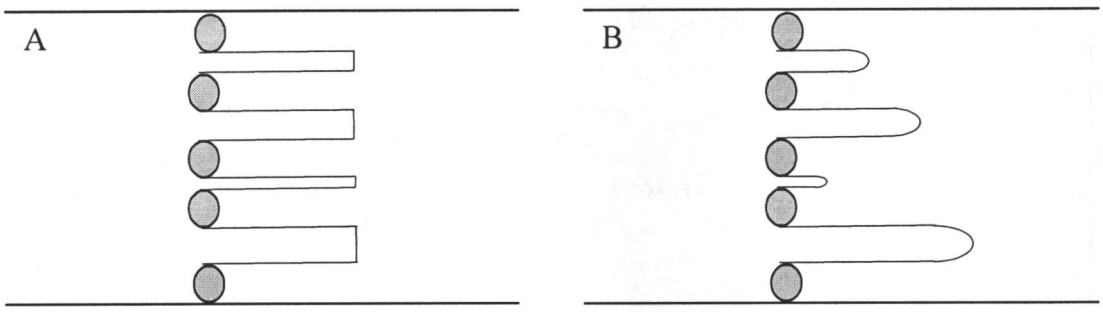

Figure 1.3. Schematic representation of electroosmotic (A) and pressure-driven (B) flow in a packed CEC column.

In contrast EOF velocity, essentially independent of channel diameter, results in a much more uniform distribution of velocities in spite of differences in local packing density, also depicted in figure 1.3. A lower A term in the plate height

equation is the expected result of the improved velocity distribution of electrically driven flow.

The third advantage of EOF is that no pressure drop is required. This is important from the standpoint of efficiency because it permits the use of smaller diameter particles. Plate height, through the A and C_m terms, is strongly dependent upon particle diameter, decreasing with a decrease in d_p. In HPLC this advantage is offset by the inverse square dependence of pressure drop on d_p (equation 1.7). The maximum pressure attainable by most commercial HPLC pumps is about 400 bar, which in most cases imposes a lower limit of 3 μm on particle diameter. With no such limit in CEC, 1.5 μm particles are regularly employed and submicron diameter particles have been used successfully by a number of research groups [11, 12].

Reduced plate height values obtained for the same columns under electrically and pressure-driven conditions have been shown to be consistently lower with the former [13, 14], a direct result of the more favorable flow dynamics of EOF. Greater efficiency, combined with the absence of pressure drop allows total column plate numbers in CEC to substantially exceed those in capillary HPLC.

An important figure of merit for a chromatographic technique is peak capacity, which is defined as the number of peaks not exceeding a specified retention factor (usually 10) and separated with unit resolution that can be contained in the column. Peak capacity, then, is a measure of a separation technique's applicability to highly complex samples (i.e. those containing many peaks). In comparison to capillary GC, peak capacity in HPLC is limited by the comparatively low efficiency of the latter. In contrast, the high separation efficiency of CEC provides increased peak capacity.

Table 1.4 compares typical column efficiency and peak capacity values achievable in CEC and capillary HPLC. It is evident that the ability to employ small particles without compromising column length is a tremendous advantage for CEC when high peak capacity is required.

To summarize, CEC has three principal advantages over microscale HPLC that arise from the improved flow dynamics of EOF: higher resolution and peak capacity and the potential for rapid separations. It is these advantages that have propelled the development of CEC in the past decade.

Table 1.4. Comparison of achievable efficiency and peak capacity in micro HPLC and CEC with various particle sizes.

	CEC		Micro HPLC	
Particle diameter (μm)	Plates per column	Peak capacity	Plates per column	Peak capacity
5	59000	147	40000	121
3	98000	189	47000 [a]	130
1.5	200000	269	24000 [b]	94

Assumed conditions: Linear velocity: 1.0 mm s^{-1}; Column length: 50 cm; High-pressure limit (micro HPLC): 400 bar; $k_{max} = 10$; Reduced plate heights: $h_{cec} = 1.7$, $h_{\mu\text{-}LC} = 2.5$.

[a] Column length limited to 35 cm due to high-pressure limit.
[b] Column length limited to 9 cm due to high-pressure limit.

2. HISTORICAL

2.1 Miniaturization in HPLC

To a large extent, the developmental timeline of microscale HPLC parallels that of conventional HPLC. Technological advances in the fields of electronics and materials science, combined with evolving theoretical descriptions of the chromatographic process, specifically the development of rate theory, have accelerated the evolution of both techniques.

The evolution and miniaturization of HPLC over the past several decades, particularly with respect to column I.D. and packing methods, have unfortunately given rise to some confusion in nomenclature. For the purpose of clarity, the system of nomenclature adopted in this dissertation is illustrated in figure 2.1. Here, columns are grouped according to I.D., packing method (if applicable), and flow resistance parameter Φ. The general terms micro HPLC and microscale HPLC are used interchangeably in this text and refer to any HPLC column having an I.D. less than 1.0 mm.

2.1.1 Semi-micro HPLC

The foundation of modern HPLC was laid in 1941, when Martin and Synge published a paper in which they described liquid-liquid partition chromatography [15]. In this seminal work, the importance of particle size and pressure drop in achieving optimum efficiency and analysis time was first identified.

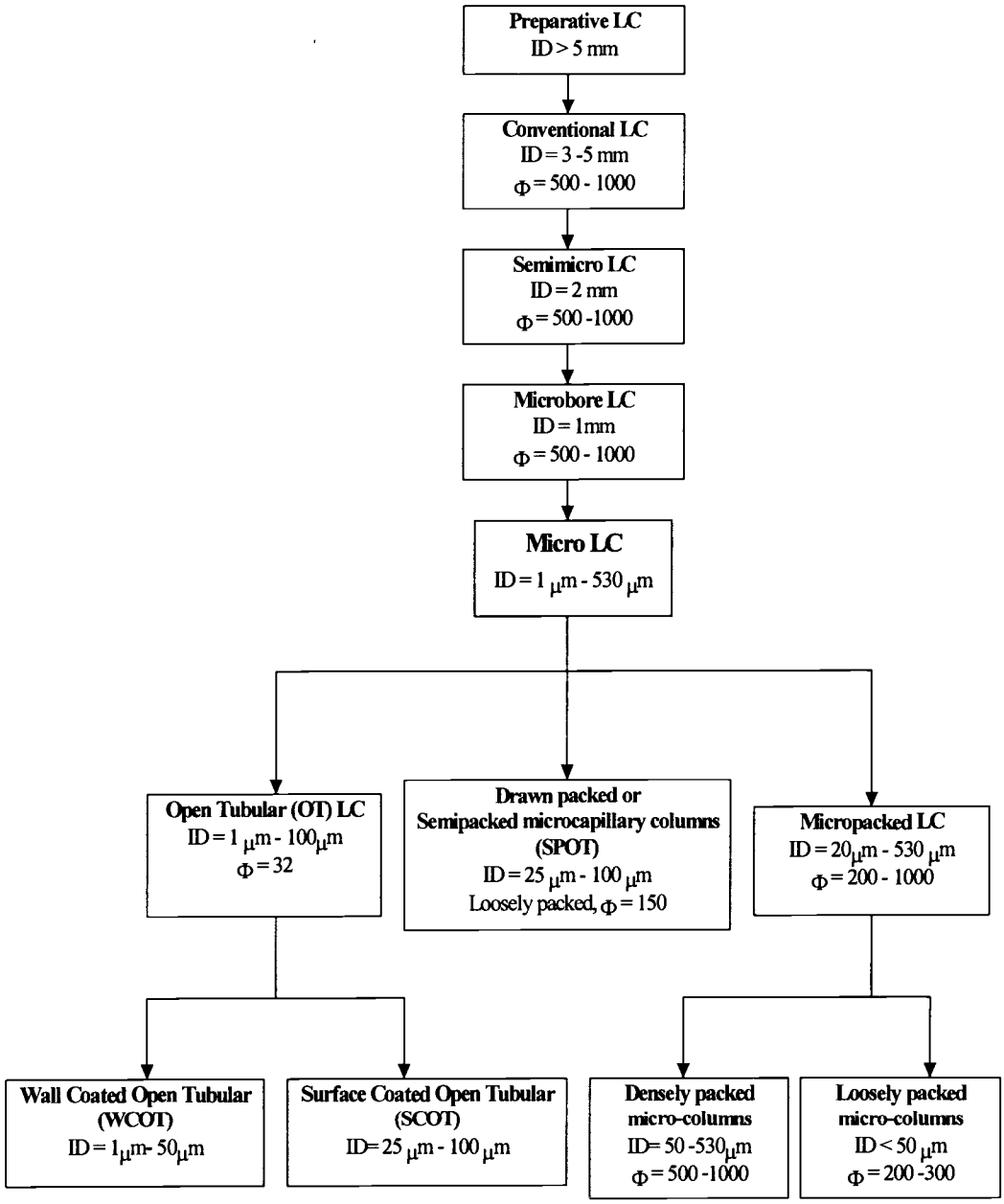

Figure 2.1. Classification and nomenclature of HPLC columns (adapted from reference 18).

By the late 1960s, after the pioneering work of Hamilton et al. [16] and Huber et al. [17] progress in optimizing HPLC separations with respect to efficiency and analysis time had been made. Tools demonstrated to enhance performance in gas

chromatography (GC), such as pellicular packings, temperature programming and capillary columns were subsequently adapted to HPLC.

Plate numbers in excess of 250000 are not unusual in GC and over the years it has been shown that comparable efficiencies could be obtained in OT-LC. Open-tubular columns have much higher permeabilities than packed columns, which allow the former to generate larger numbers of theoretical plates per unit time and unit pressure drop than the latter. The potential of OT-LC as a high efficiency separation technique was demonstrated by the achievement of 2,800,000 theoretical plates with a 27.5 m long column of 32 μm I.D [28].

To obtain open-tubular columns with a uniform stationary phase layer, however, requires skill and experience. The introduction of stationary phases covalently linked to the column wall resulted in more uniform and stable coatings, which facilitated solvent gradient elution and temperature programming. Unfortunately, covalently bonded stationary phases generally consist of a monomolecular layer and therefore have inherently low sample capacity. Exacerbating this limitation is the fact that to achieve adequate detection limits OT-LC usually requires loading capacity to be maximized.

With regard to efficiency in OT-LC, narrow I.D. columns, 10 μm and below, are required to minimize mass transfer effects, thereby achieving maximum efficiency. Peak volumes generated in columns of this size are on the order of 0.1 nL, and as such were incompatible with early HPLC detectors [29], due to excessive extra-column peak broadening. Unfortunately, this restricted the use of such columns.

Various approaches to increase the sample capacity of OT-LC columns involved the use of support materials coated on the walls of the capillaries. Supports such as silica gel, porous silica microspheres or organic polymers (e.g. polystyrene, polyacrylates) [30] have been investigated.

Fused silica capillary columns, introduced for GC in 1979 by Dandeneau and Zerenner [29], greatly accelerated the development of miniaturized separation techniques. In contrast to the fragility of glass columns and surface inhomogeneities of metal columns, the surface of fused silica is smooth and relatively inert. In addition, the polyimide cladding of fused silica tubes imparts flexibility, reducing the likelihood of breakage. In a relatively short period of time following its introduction, fused silica became the material of choice in capillary GC.

The following year, fused silica capillaries were employed in open-tubular HPLC [32]. In this application columns of various inner diameters were derivatized with octadecylsilane, the optimum results being obtained with the 30 μm I.D. capillary. In this paper *in situ* or on-column detection was introduced, which could easily be performed after removing the polyimide coating from a small section of the capillary (2 – 10 mm). The principal advantage of on-column detection is that the capillary itself serves as the detection cell, thereby minimizing the extra column volume contribution of the detection cell and increasing efficiency.

The challenge of analyzing volume-limited samples, such as single biological cells, has provided an impetus for the continued development of open-tubular HPLC. In 1989, an OT-LC system consisting of a 15 μm I.D. capillary and voltammetric detector was used to sample the contents of single neurons from the land snail *Helix*

aspersia [33]. In this application, where a low detection limit was essential, borosilicate capillary tubes, which have a more reactive surface relative to fused silica, were employed to maximize stationary phase coverage. This allowed an increased amount of sample to be loaded onto the column, lowering the detection limit. Despite the practical limitations of the technique, this type of application represents the ideal niche for open-tubular HPLC.

2.1.2 Drawn-Packed Capillaries

An alternative to the limited sample capacity of open-tubular columns and low permeability of packed columns was provided by drawn-packed microcapillary columns, or so called semi-packed microcapillary columns.

Prior to the introduction of fused silica open-tubular column, semi-packed microcapillary columns were widely used in GC. In 1978 Tsuda and Novotny achieved the first liquid phase separations in drawn-packed columns of 50 – 200 μm I.D [34].

The process of preparing these columns consists of packing the desired sorbent into 1 – 2 mm I.D. tubes and subsequently drawing the tubing to the desired diameter using a glass-drawing machine. The application of high temperatures during the drawing process results in the impression of some packing material on the walls of the tubing, conferring the characteristic "loose" packing structure of semi-packed microcapillary columns. It is this packing structure that results in the increased permeability of these columns. Unfortunately, such high temperatures preclude the

use of derivatized packing materials such as octadecylsilane. Nevertheless, it is possible to prepare a variety of chemically bonded stationary phases *in situ*, by passing the silane reagent through the capillary [35].

2.1.3 Micro packed capillaries

Several factors have driven the development of packed capillary columns for microscale HPLC. Among these have been increased sample capacity relative to open-tubular columns and increased permeability relative to conventional bore packed columns. As discussed in chapter 1, a direct result of the high permeability of micro packed capillaries is that longer columns can be used, increasing the number of theoretical plates per column relative to conventional bores.

Additionally, deleterious "wall effects" can be minimized with packed capillary columns. In a packed column, particles near the wall will, in general, be more loosely packed relative to the center of the column. The permeability of the column will therefore be nonuniform along its cross section. Ultimately this variation in packing density leads to an increase in plate height. Knox and co-workers [36, 37] have studied this phenomenon extensively. It has been shown by several workers that for a given particle diameter, radial variation in column permeability is reduced as column I.D. decreases [38, 39]. This results in a decreased range of flow velocities along the column cross-section, reduced pressure drop, and more effective dissipation of the frictional heat generated in the column.

A study conducted on packed capillaries by Wilson [40] found that higher efficiencies could be obtained for column diameter to particle diameter ratios (ρ), less than 5 due to a more ordered and uniform packing structure.

Before the benefits of micro packed capillaries could be fully exploited, however, some practical problems associated with these columns, such as increased susceptibility to extra column effects and difficulties in column packing, had to be addressed.

In 1979 Scott and Kucera introduced a low-dead-volume detection cell having a volume of 1 μL that significantly improved detection sensitivity [22]. Although this approach was successful and other configurations have since been introduced, on-column detection remains the most widely used format in spite of one limitation: detection path length. Because the capillary itself serves as the detection cell, the column I.D., which is usually quite narrow, defines path length. Due to the cylindrical geometry of the capillary tube, the effective path length is smaller than the column I.D. Therefore, sensitivity is compromised with UV absorbance detection, in which absorbance is proportional to path length.

Improvements in synthetic methodologies have resulted in particles with more uniform diameter and pore size distributions. From the small glass spheres coated with a layer of silica gel or microspheres of silica [21], to the present day commercially available material – porous, homogeneous, surface dervivatized microparticles 2 – 10 μm in diameter, the evolution of packing materials has led to increased column efficiencies. It is a well-established tenet of chromatographic theory that smaller diameter particles yield maximum efficiency. The improved uniformity

and commercial availability of particles below 5 μm in diameter over the last twenty years or so have allowed theory to be put into practice. Unfortunately, conventional analytical scale (4.6 mm I.D.) columns packed with these smaller diameter particles develop pressure drops that exceed the capability of most HPLC pumps when operated at typical linear velocities. For this reason conventional columns packed with particles less than 5 μm in diameter are seldom encountered. In contrast, the increased permeability of packed capillary columns ameliorates this problem. Efficiencies of 100,000 theoretical plates can routinely be attained when columns of 1m length containing 3 or 5 μm particles are used [41].

Advancements in column packing methodology were critical to the development of micro packed capillaries. Among these are the balanced density slurry and vacuum pulled slurry [6]. In the balanced density approach, the packing material is mixed with a solvent of similar density, usually tetrachloromethane, such that the slurry obtained is less susceptible to aggregate formation during packing. High pressures, on the order of 700 – 1000 bar, are used to force the slurry into the capillary, resulting in a homogeneous, tightly packed chromatographic bed. For glass, PTFE, and other tubing materials that are incapable of withstanding such high pressures, the packing method proposed by Ishii [6], which used a vacuum to draw the slurry into the capillary, was employed. After packing, a compression step was required to compact the bed.

The flexibility of fused silica and availability of polymeric ferrules that permit high-pressure operation greatly facilitated the development of improved packing techniques. Novotny modified the slurry packing method by using higher density

slurries, which were sonicated during packing to maintain homogeneity [41]. A solvent having the desired viscosity, acetonitrile, was used as both slurry and displacement fluid. The use of acetonitrile in this procedure also decreased the time required to pack and depressurize the column. It must be stressed that the optimum slurry and/or displacement solvent may vary with packing materials having different surface chemistries.

In view of the performance characteristics of micropacked capillaries and the versatility of the packing materials already available for conventional HPLC, it is widely considered that the micropacked capillary format of micro HPLC has the greatest potential for continued development and application.

2.2 Capillary Electroseparations Techniques and the Emergence of CEC

Over a century ago Helmholz studied the effect of the application of an electric field across a glass capillary filled with a salt solution [42] and determined that the wall of the capillary acquired a negative charge, and that upon application of the field, positively charged particles associated with the wall moved toward the cathode. This bulk transport process was subsequently termed electroosmosis.

Electrophoresis, the migration of charged particles in solution under the influence of an electric field, was a phenomenon studied extensively by electrochemists. In 1937 Tiselius exploited differences in electrophoretic mobilities of proteins to obtain separations, employing UV photography for detection [43]. In these studies, it soon became evident that resistive heating of the solution caused severe

band broadening and that none of the various attempts at cooling mechanisms could effectively eliminate the problem. In spite of this limitation, several separation techniques, including free zone electrophoresis, isotachophoresis, isoelectric focusing, all of which are based on electrophoretic transport, have become important analytical tools, particularly in the fields of biology and biochemistry.

As in HPLC, advantages of miniaturization began to be exploited in the 1960s. For example, the relatively high surface area to volume ratio of capillary tubes allows for efficient heat dissipation. In 1970 Hjerten [44] conducted electrophoretic separations in surface coated capillary tubes designed to minimize electroosmosis. In these coated columns, migration of analytes was due solely to electrophoresis. Among the advantages of conducting electrophoresis in capillary tubes were increased heat dissipation, sensitive real-time detection, applicability to volume-limited samples, and ease of automation. A paper published in 1981 by Jorgenson and Lukacs in which 75 μm I.D. glass capillaries were employed [45], was a milestone in the development of modern high performance capillary electrophoresis. By the mid to late 1980s, the material of choice for CE capillaries had become fused silica owing to its strength, flexibility, and widespread availability.

In 1984 Terabe published a paper describing a variant of capillary electrophoresis that made use of micelles in the running buffer [46]. This novel separation technique was termed micellar electrokinetic capillary chromatography or MEKC. In this technique a surfactant is dissolved in the running buffer in excess of its critical micelle concentration. Commonly, sodium dodecyl sulfate (SDS), an anionic surfactant, is used. In a typical run with cathodic EOF, SDS micelles, being

negatively charged, migrate slowly toward the cathode (the electroosmotic mobility is usually higher than the micelles' electrophoretic mobility). Because of their migration, the micelles are considered as a "pseudostationary" phase. Differential migration of solutes in MEKC can occur via two mechanisms: electrophoresis and partitioning into the micelle. Thus, MEKC can be considered a chromatographic technique. The primary advantage of MEKC over CZE is that it is possible to separate unionized solutes.

Although the introduction of this technique undoubtedly widened the applicability of capillary electrophoresis, MEKC suffers some serious limitations. Analytes having a strong affinity for the micelles are sparingly soluble in water, and only small amounts of organic modifiers can be added to enhance solubility without perturbing the micelle formation. Additionally, because the micelles migrate, there exists a finite time window in which solutes can be eluted. Peak capacity is therefore limited. A further disadvantage of MEKC is that micelles are, in general, incompatible with most ion sources for mass spectrometry.

In 1974 Pretorius, et al. published a paper in which electroosmosis was used to transport mobile phase through a packed column [47]. Although by current standards the 1.0 mm I.D. glass columns used by these researchers cannot be considered "miniaturized", this work is the predecessor of modern CEC. Pretorius and co-workers were the first to outline some of the theoretical advantages of electrically driven flow in chromatography. One of these was that an electrically driven system would less susceptible to band broadening due to irregularities (e.g. variations in packing density) in the packed bed. Rate curves generated for acetone, an unretained

solute, under pressure and electrically driven conditions predictably showed lower plate heights for the latter.

Practical problems in the implementation of electrically driven chromatography resulted in dormant research in the years following the Pretorius paper. In 1981, Jorgenson and Lukacs imposed an electric field across 170 μm I.D. glass capillaries, driving mobile phase through a bed packed with 10 μm diameter reverse phase HPLC particles [45]. A column prepared using a low-pressure packing procedure (which is not ideal for preparing efficient columns) yielded a reduced plate height of 1.9 for 9-methylanthracene, an indication of the potential of CEC to yield high efficiency. For comparison, the typical optimum reduced plate height in packed column HPLC at the time was 2.5. This application of electroosmosis for bulk transport in a micro HPLC column would subsequently be termed capillary electrokinetic chromatography, or capillary electrochromatography (CEC).

The years following the Jorgenson and Lukacs paper were again a period of relative dormancy with regard to CEC research. In 1987, Knox and Grant described the theory of CEC operation [48], but research remained sporadic until the publication of a second paper by these workers in 1991 [13]. In this second paper, the authors employed both slurry packed capillaries and drawn-packed capillaries in a comprehensive study of the effect of particle size and electrolyte concentration on electroosmotic flow velocity and plate height. Among the conclusions of this research were the following: EOF velocity was unaffected by particle size down to d_p = 1.5 μm at the electrolyte concentrations studied (indicating that double layer overlap was negligible), higher efficiencies were obtained on the same column with electrically

driven relative to pressure driven flow, and that efficiencies on the order of 500000 plates m^{-1} were possible with CEC columns packed with 1.5 μm particles.

In 1995 Yan, et al. [14] separated a mixture of 16 polycyclic aromatic hydrocarbons (PAHs), classified as "priority pollutants" by the U.S. Environmental Protection Agency, using packed column CEC with laser induced fluorescence detection (LIF). Efficiencies on the order of 150000 plates m^{-1} were obtained on columns packed with 3 μm octadecylsilane (ODS) coated particles. These researchers further demonstrated an approximately 1.5 fold increase in plate numbers for the same column operated in CEC mode versus HPLC mode.

By 1997, packed column CEC had been applied to a variety of sample types: pharmaceuticals [49], steroids in plasma and urine extracts [50], triglycerides [51], and inorganic anions [52]. As evidenced in these applications, an important advantage of CEC in the packed column format is the ability to make use of "tried and true" stationary phases originally developed for HPLC.

Though advantageous in one respect, certain limitations inherent to packed column CEC, chiefly the need for retaining frits, have driven the development of alternative column formats. In open-tubular CEC (OT-CEC) the stationary phase is usually attached to the capillary wall by covalent bonding. The initial step in the preparation of OT columns is etching of the capillary wall, which activates the silanol groups on the wall surface. The column is then treated with a reagent containing a polymerizable group (e.g. an activated double bond) that forms a covalent bond with the exposed silanols. A solution containing monomers (and cross-linker, if applicable)

is pumped through the capillary at which point polymerization occurs forming a network covalently linked to the wall of the capillary.

This approach was employed in 1997 by Tan and Remcho to produce polyacrylate stationary phases for OT-CEC [53]. In this work, in which a series of *p*-hydroxybenzoates (parabens) were separated on a 25 μm I.D. column, efficiencies as high as 200000 plates m^{-1} were obtained.

Unfortunately, as in the case of open-tubular LC, OT-CEC has some rather significant limitations that have precluded its widespread application. Relative to packed column CEC, the available surface area for solute-stationary phase interaction is significantly lower in open tubes. As a result, sample capacity is low. Additionally, to maximize efficiency requires very narrow I.D. columns (< 10 μm) be used, which further reduces surface area, and hence, sample capacity. Finally, with on-column absorbance detection, the column diameter defines detection pathlength. The requirement for such narrow tubes will necessarily result in decreased detection sensitivity.

Relatively early in the development of packed column CEC, the need for retaining frits to hold the packing in place was seen as a problem area. Frits are usually prepared by sintering (heating) silica-based packing particles *in situ* to yield a porous plug that is permeable to the mobile phase. Frit problems are usually associated with gas bubble formation during runs and peak broadening and/or tailing. A potential solution to the problems of retaining frits in packed column CEC and the low sample capacity of OT-CEC is offered by porous monoliths. In this approach, a monomer-containing mixture is polymerized inside the capillary to yield a

macroporous, monolithic medium that can support, or itself act as, the stationary phase. Bulk flow of mobile phase occurs through a network of pores, the sizes of which can be controlled by the polymerization conditions. This format has the added benefit that sections of the capillary can be removed and the column reused. For example, if the head of the capillary becomes fouled by a dirty sample, a few centimeters can simply be cut off, without ruining the entire column.

Presently in CEC, continuous polymer monoliths can be divided into three general classes: 1) organic, 2) inorganic (silica-based), and 3) hybrid organic-inorganic monoliths.

Continuous organic polymer beds for CEC have been prepared using various methods, the most common of which include acrylamide [54,55] and acrylate [56-59] based polymers. Most of these techniques require modification of the capillary surface with an anchoring reagent, to which the polymer matrix will covalently bond.

In 1997, rigid monoliths were developed for CEC that required only a single step for preparation [60-62]. These acrylate-based polymers were prepared *in situ* in untreated capillaries. To yield a rigid matrix on which solutes could be retained, a hydrophobic monomer, butyl methacrylate, was combined with a high percentage of cross-linking agent. An ionizable monomer, 2-acrylamido-2 methyl-1 propanesulfonic acid (AMPS) was incorporated into the matrix to provide sufficient surface charge density for electroosmosis. A blended porogenic solvent mixture afforded tight control over pore size and breadth of pore size distribution in the mononolith. Efficiencies of greater than 140000 plates per meter were obtained for benzene derivatives on these monoliths.

Continuous silica-based porous monoliths have been successfully employed in HPLC [63, 64]. Typically, these monoliths are prepared by a sol-gel process, which consists of polycondensation of alkoxysilanes in the presence of an organic polymer. The resultant silica skeleton contains flow-through pores having diameters on the order of a few microns. The skeleton itself is porous, with mesopores a few nanometers in diameter. The surface of the monolith is then derivatized with an organosilane reagent (e.g. octadecylsilane). The mesoporous nature of the monolith provides a high surface area for stationary phase bonding and analyte partitioning, yielding improved sample loading capacity. Varying the percentage of organic polymer in the mixture affords control over the porous properties of the monolith.

Silica based continuous beds are applicable to CEC as well. Unlike the organic monoliths, incorporation of an ionizable functionality into the polymer is unnecessary in silica beds; surface silanols can support EOF. Monoliths produced via a sol-gel method have been employed in CEC [65]. This procedure, a variation of which has been employed in capillary GC [66], was designed to yield beds that are less susceptible to shrinking and cracking, common problems with silica monoliths. Efficiencies in excess of 170000 plates m^{-1} were obtained for the various PAHs and aromatic aldehydes and ketones used as test probes.

In 1998, Chirica and Remcho reported a procedure in which a silicate polymer was employed as an entrapment medium for polyacrylate particles [67]. In this work, the particulate material was a molecular imprint polymer (MIP) prepared with dansyl-L-phenylalanine as the imprinted species. After packing MIP particles, a solution of potassium silicate was pumped hydrodynamically into the capillary, which was

subsequently heated. Polymerization of the silicate solution yielded a fine polymer network that served as a web, immobilizing the packed bed. This technique, termed silicate entrapment, has also been employed with conventional reverse phase packing media [68]. One advantage of this type of approach when used to immobilize organic polymer-based particulates is that the entrapment medium can support EOF. Thus, there is no need to incorporate an ionizable group into the polymer. This is especially important with MIPs, where the introduction of additional monomers might interfere with molecular recognition.

The past decade was a period of vigorous growth for CEC. 1997 witnessed the inception of a symposium dedicated to CEC. A recent search of the Online Computer Library Center (OCLC) First Search Database found in excess of 150 CEC papers in the first nine months of the year 2000 versus 12 for the entire year of 1995. At the time of this writing CEC remains the subject of much research interest.

3. Affinity Sorbents Derived from Molecular Imprint Polymers

Reprinted from *Journal of Chromatography A*, vol. 888, Vallano, P.T. and Remcho, V.T., "Affinity Screening by Packed Capillary High-Performance Liquid Chromatography using Molecular Imprinted Polymers", 23-34, Copyright 2000, with permission from Elsevier Science.

3.1 Introduction

Molecular imprinting is a technology in which specific recognition sites are formed in a polymer matrix by synthesis in the presence of a template molecule. The imprinted polymer is capable of selectively rebinding the template molecule through a host-guest type interaction. Although the foundations of the molecular imprinting technique were established decades ago [69, 70], the technique is enjoying a resurgence of research interest. The highly selective recognition properties of molecular imprint polymers (MIPs) rival those of natural biological media, such as receptors and antibodies. However, MIPs possess several advantages over their biological counterparts including low cost, ease of preparation, and good physical and chemical stability. In addition to their widespread use as selective stationary phases in separations, MIPs have found use as synthetic mimics of biological selectors in a number of other applications in including sensors [71], immunoassays [72] and catalysis [73]. In the interest of brevity, a short introduction to molecular imprinting will be provided in this dissertation. For a more detailed treatment, the reader is referred to a number of thorough literature reviews on the subject [74-77].

In molecular imprinting, a highly cross-linked organic polymer is synthesized in the presence of a template, or imprint, molecule. Prior to polymerization, functional groups on the template interact with those on the monomer(s). Depending on the method employed, these interactions can be reversible covalent bonds or various non-covalent intermolecular forces. Polymerization, which is begun with the activation of a free radical initiator with UV radiation or by heating, fixes the three-dimensional orientations of the functional groups associated with the template. Upon completion of polymerization, the template is removed either by hydrolysis (covalent MIPs) or by mild extraction with an appropriate solvent (non-covalent MIPs), leaving cavities, or "imprints" in the polymer that are complementary in shape and functionality to the template molecule.

MIPs are typically prepared with a molar excess of cross-linking reagent in order to impart structural rigidity, which enables the imprinted sites to retain their shapes and affords the polymer some resistance to swelling. The cavities formed through the imprinting process serve as recognition sites in which specific rebinding of the template molecule can occur. It is this recognition process that is the hallmark of MIPs.

The non-covalent approach to MIP synthesis is much more widely used for preparing MIPs as chromatographic stationary phases than is covalent imprinting. Reasons for this include the greater versatility of non-covalent imprinting with respect to the available modes of interaction and the generally more favorable kinetic properties of the recognition event.

In non-covalent molecular imprinting, methacrylic acid (MAA) is commonly used as a functional monomer. This monomer can act as a hydrogen bond donor or acceptor and has an acidic proton, enabling ionic interactions to be utilized in imprint formation. Widely used cross-linking monomers include ethylene glycol dimethacrylate (EDMA) and trimethylolpropane trimethacrylate (TRIM). In the pre-polymerization mixture, the template molecule can interact with the monomers via hydrogen bonding, ionic, π-π and hydrophobic interactions. Hydrogen bonding and ionic forces are typically dominant. The effectiveness of these interactions is highly dependent upon the polarity of the medium, thus organic solvents of low polarity are used to obtain optimal imprints. In particular, if hydrogen bonding is critical in imprinting process, aprotic solvents are preferred to minimize competition by the solvent. The non-covalent imprinting process is depicted schematically in figure 3.1.

The advantages of MIPs, in particular high selectivity and physico-chemical stability, have propelled the development of MIPs as chromatographic stationary phases, particularly in HPLC where they have been utilized mainly as chiral stationary phases (CSPs). In such applications, one enantiomer of the compound to be analyzed is employed as the template molecule. In the chromatographic separation, the template enantiomer is selectively retained on the MIP relative to its antipode.

Imprinted polymers as chiral stationary phases in HPLC generally yield higher enantioselectivites relative to conventional CSPs; values exceeding 17 have been reported [78], although in certain instances MIP columns generate less theoretical plates. Driven by high selectivity, MIP-HPLC has been employed in stereospecific separations of a variety of compounds including amino acid derivatives [79], β-

blockers [80], non-steroidal anti-inflammatory drugs (NSAIDS) [81], peptides [82], and sugars [83]. An important advantage of MIPs relative to conventional chiral stationary phases is the ability to predetermine selectivity.

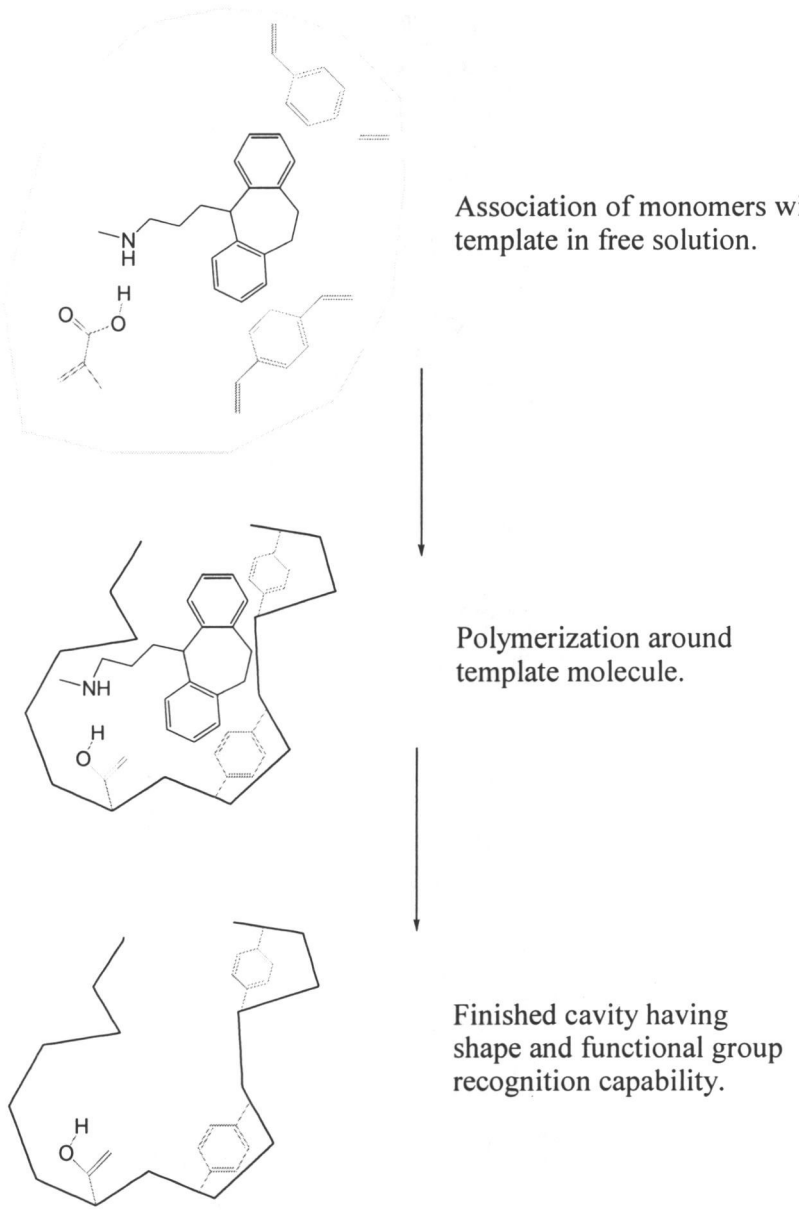

Figure 3.1. A simplified representation of the synthesis of a noncovalent molecular imprinted polymer (MIP).

Aside from chiral sorbents, one of the most promising applications of MIPs is as synthetic mimics of biological receptors and antibodies. In this approach, a template molecule is chosen that is a potent activating ligand of the receptor to be mimicked. MIP synthesis in the presence of this ligand yields a material with complementary cavities that can subsequently "recognize" the template molecule, and thereby function as a surrogate biological receptor. Immunoassays, in which synthetic antibodies have been prepared from MIPs, have shown excellent correlation with their biological counterparts [72]. In a similar vein, MIPs have been successfully utilized as mimics of biological recognition elements in biosensors [84].

The use of combinatorial chemistry techniques, from which a library of diverse compounds can be produced from an initial skeleton structure, has risen dramatically in the past ten years. Combinatorial chemistry is becoming a powerful tool in the search for novel drug compounds [85]. Techniques used to identify lead compounds from the multitude of reaction products generally involve screening for activity against some biological recognition element (e.g. enzyme, receptor, or antibody), with which the proposed new drug will interact. Included among these techniques are enzymatic and cell-based assays, enzyme linked immunosorbent assay (ELISA), radioimmunoassay, ultrafiltration, affinity chromatography and scintillation proximity assay (SPA) [86, 87].

An important subset of the receptor binding techniques is based on affinity chromatography and electrophoresis. Screening methods derived from the former, known as affinity selection chromatography [87], make use of a receptor immobilized on a solid support as the chromatographic stationary phase. In affinity selection

chromatography, elution profiles are monitored with the retention time of a given analyte correlating to its affinity for the target receptor. An advantage of this technique is that the affinity column can be coupled to a mass spectrometer, which can provide on-line structural characterization of the analytes. A second column (e.g. reversed phase) in series with the affinity column can provide multidimensional information [88] on library compounds. Additionally, receptor binding data (e.g. approximate K_d values) can be gleaned by means of affinity chromatography. The need to immobilize the receptor, however, is a limitation of traditional affinity chromatography. In addition to the often difficult chemistry required, one must ensure that the receptor is immobilized in such a way that its binding domain for the target ligand is left intact. Similarly, during chromatographic analysis, careful consideration must be given to the eluent composition to ensure that no conformational change, deleterious to molecular recognition, is induced (e.g. by pH or organic solvent composition). Ideally, the eluent should very closely approximate physiological conditions, but to fully optimize the separation often requires deviation from these "ideal" conditions.

Recently, the use of MIPs as chromatographic stationary phases for library screening has garnered attention [89, 90]. This approach is essentially affinity selection chromatography employing MIPs as receptor mimics. A ligand having a known, high binding affinity for the target receptor is chosen as the template molecule. The resultant MIP, having binding sites complementary to the high affinity ligand, then serves as a surrogate receptor against which a library of potential activators can

be screened. As in affinity selection chromatography, the elution profiles of the analytes are used as the basis to determine affinity for the MIP binding site.

This MIP-based approach to affinity chromatography, in principle, possesses several important advantages over methods that employ biological receptors. Among these are the favorable physico-chemical properties of MIPs, specifically the ability to tolerate organic solvents, pH extremes, high pressures, and elevated temperatures. The low cost and relative ease of preparation are further advantages of these polymers. In addition, the need for receptor immobilization and its associated difficulties is obviated. It is when the target biological receptor is unusually expensive, difficult or impossible to obtain that an MIP-based screening approach would be most useful. In the search for novel drug entities, the compounds generated by combinatorial synthetic techniques typically have the following features [85]: relatively low molecular weights, at least one aromatic ring, one ionizable group, and moderate polarity. These types of molecules are amenable to imprinting with existing technologies and to chromatographic analysis.

The work presented was undertaken to evaluate the use of MIPs as affinity sorbents for packed capillary HPLC. The advantages of column miniaturization in HPLC have been enumerated in this dissertation. A number of these are important from the standpoint of combinatorial library screening. The enhanced mass sensitivity achieved with miniaturized columns is of particular importance when only small quantities of analyte are available for screening. Reduced solvent consumption, a boon for economic as well as environmental reasons, is desirable when large numbers of samples are to be screened. In addition, the ease with which capillary HPLC can be

coupled to a mass spectrometer, in particular with electrospray ionization, allows valuable structural information and affinity data to be obtained simultaneously. The emergence of capillary LC-NMR as an analytical tool [91] has the potential to provide even more thorough on-line structural characterization of library compounds.

In this study, a group of structurally similar tricyclic antidepressant drugs (TCAs) and related compounds were used to simulate a combinatorial library. One of these, nortriptyline (NOR) was selected as the template molecule. The library was screened in packed capillary HPLC mode and the affinity of each library compound for the MIP, a measure of each compound's "goodness of fit" in the NOR binding site, was determined. No effort was made in this initial study to select a template molecule on the basis of its enhanced affinity for a target receptor or pharmacological activity with respect to the other test probes in the library. The specific goals of this work were: i) to quantitate the degree of selective interaction of each library compound with the MIP; and ii) based on the data generated in (i), to assess the structural features found to correlate with enhanced molecular recognition and to propose a mechanism(s) of molecular recognition on these MIPs.

3.2 Experimental

3.2.1 Materials

Functional monomers, methacrylic acid (MAA) and styrene (STYR), cross linking monomer ethylene glycol dimethacrylate (EDMA), and free radical initiator, 2,2′-azobisosobutyronitrile (AIBN) were purchased from Aldrich Chemical Co. (Milwaukee, WI, USA) and used as received. HPLC grade toluene, purchased from

Fisher Scientific (Pittsburgh, PA, USA), was dried over 4 Å molecular sieves prior to use. The antidepressant drugs and other compounds employed in the study were purchased from Sigma Chemical Co. (St. Louis, MO, USA).

3.2.2 Preparation of Molecular Imprint Polymers

Nortriptyline (NOR), obtained in its hydrochloride salt form, was converted to the free base by extraction into toluene using 1 M NaOH. An appropriate amount of free base NOR (approximately 0.35 mmol) was added to a solution of EDMA (6.25 mmol), MAA (1.25 mmol) and STYR (1.25 mmol) in toluene. The volume ratio of toluene to total monomers was maintained at 2:1. The solution was prepared in a 20 ml glass scintillation vial, which was immersed in an ice bath during the addition of the reagents, and stirred constantly using a magnetic stirrer to ensure homogeneity. The total volume of the mixture of monomers and toluene was approximately 5 mL. Following the dissolution of 0.015 g AIBN, the mixture was purged with a stream of N_2 for 5 min, after which the vial was capped and transferred to a freezer (˜10 °C) where it was illuminated with a UV lamp and allowed to polymerize for 24 h. Following polymerization, the resultant solid block of polymer was recovered by breaking the scintillation vial. The block of material was ground into fine particles using a mortar and pestle. It should be noted that the entire block of bulk polymer appeared to be uniform in its physical characteristics, e.g. optical properties (white, opaque), texture, and hardness. The particles were then wet-sieved with methanol through a nylon mesh filter having a nominal mesh opening of 30 μm (Spectrum Inc., Laguna Hills, CA, USA). Fines were removed by multiple sedimentation steps in

acetone. The particles were then dried at 50 °C for 12 h prior to use. "Blank" polymer was prepared for use as a control by the same procedure in the absence of template. Although the bulk polymerization methodology employed here yields rather large and irregularly shaped particles, which are undesirable from the viewpoint of chromatographic efficiency, the synthesis is less complex and easier to optimize relative to other strategies designed to provide smaller and more uniform particles.

3.2.3 Preparation of Packed Capillary Columns

Fused silica capillary tubing (I.D. 250 μm, O.D. 360 μm) was purchased from Polymicro Technologies (Phoenix, AZ, USA) and cut to lengths of approximately 40 cm prior to packing. A retaining frit was prepared at the column outlet by tapping the capillary tip into a paste consisting of 7 μm Nucleosil Si Particles (Meta Chem Technologies, Torrance, CA, USA) and potassium silicate (Kasil #1, PQ Corp., Valley Forge, PA, USA) followed by curing at 80 °C for approximately 24 h. A slurry was prepared by adding 10 mg finished MIP particles to 1 mL acetonitrile. The slurry was pumped into a fritted capillary using an Isco 100 DX syringe pump (Isco Inc, Lincoln, NE, USA) in constant pressure mode with which a pressure of 1500-2000 psi was maintained during packing. After the desired length of capillary was packed, the pump was stopped and the pressure allowed to slowly bleed to zero. The packed capillary was subsequently coupled to a section of bare fused silica tubing of the same inner diameter via a Teflon sleeve. In order to minimize dead volume at the coupling, the following measures were taken. First, the ends of the capillaries were cut squarely using a specially designed cutter with a rotating diamond blade (Hewlett-Packard,

Waldbronn, Germany). While viewed under a microscope, the capillaries were carefully butted together inside a section Teflon tubing approximately 5 mm in length. This provided a liquid tight joint while introducing a minimum of dead volume. For subsequent on-column detection, a detection window was made in this open section of capillary by removing a small (1 mm) section of the polyimide coating. Prior to chromatographic evaluation, the packed capillary was flushed with a solution of acetic acid in methanol (10:90 v/v) to extract any residual template from the polymer. No effort was made to ascertain the recovery of template molecule from the polymer. To serve as a control, an additional capillary column was packed with "blank" polymer and conditioned using an identical procedure.

3.2.4 Instrumentation

All reagents employed in the capillary HPLC experiments were HPLC grade and were used as received from Fisher Scientific (Pittsburgh, PA, USA) or Mallinkcrodt (St. Louis, MO, USA). The HPLC system consisted of an Hitachi L-6000 HPLC pump (Hitachi Ltd., Tokyo, Japan) or an Isco 100 DX syringe pump (Isco Inc., Lincoln, NE, USA), a Unicam 4225 UV detector (Thermo Separation Products, San Jose, CA, USA), and a Valco microinjection valve (Valco Instrument Co., Houston, TX, USA) with a 60 nL (fixed) loop volume. Data were collected using an Apple Power Macintosh 6100/66 (Apple Computer, Cupertino, CA, USA) equipped with a PowerChrom System 2.0 (ADInstruments, Milford, MA, USA) chromatography data system. Unless otherwise specified, in all HPLC experiments

mobile phase was delivered in constant pressure mode with a detection wavelength of 220 nm. The void time (t_o) was determined by the elution time of a small negative peak observed upon injection of the sample solvent (acetonitrile).

3.3 Results/Discussion

3.3.1 Library Screening

A simulated combinatorial library was assembled from a group of structurally similar tricyclic antidepressant drugs and related compounds shown in figure 3.2.

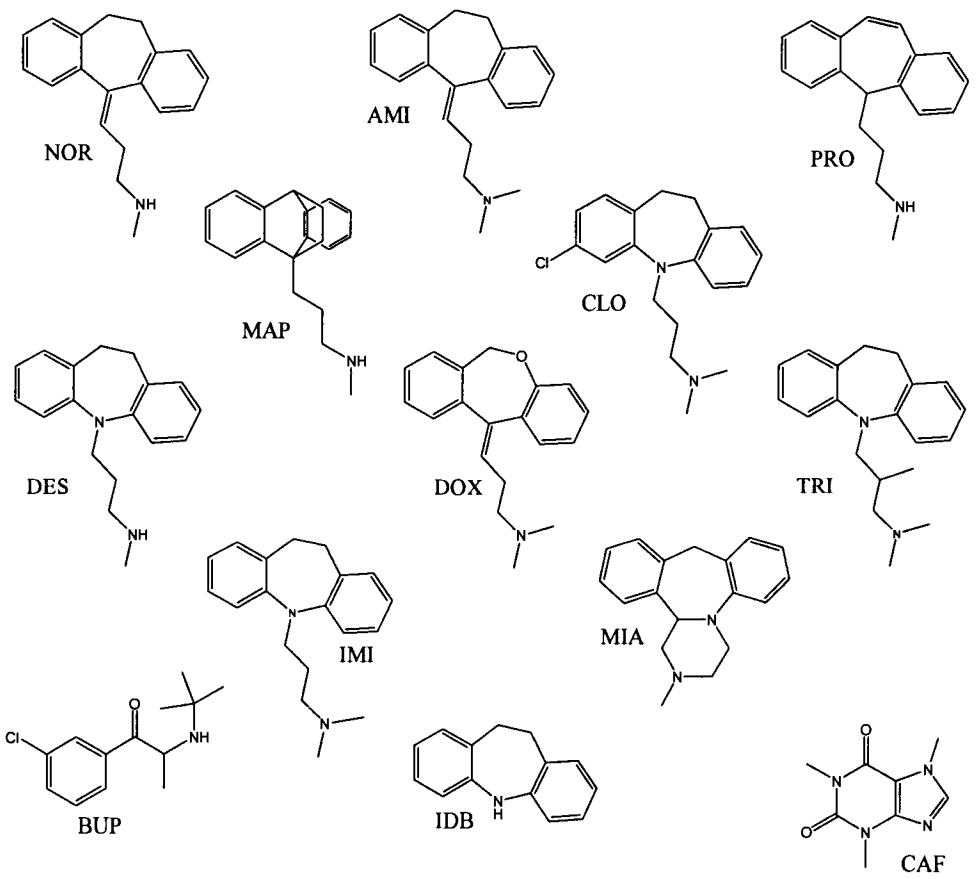

Figure 3.2 Structures of compounds in the simulated combinatorial library.

Caffeine was included in the library as a structurally dissimilar and unrelated test probe. MIPs were prepared as described previously using NOR as the imprint molecule.

Following careful optimization of the chromatographic conditions, the library was screened by capillary HPLC using packed MIP capillary columns prepared as described previously. Retention factors (k) were calculated for each library compound on the MIP and blank columns and are shown in figure 3.3. As expected, the template species, NOR, was the most strongly retained of the library compounds. To determine the extent of non-specific retention on the MIP, the library was run under identical chromatographic conditions on a capillary packed with blank polymer (herein referred to as "blank" capillary).

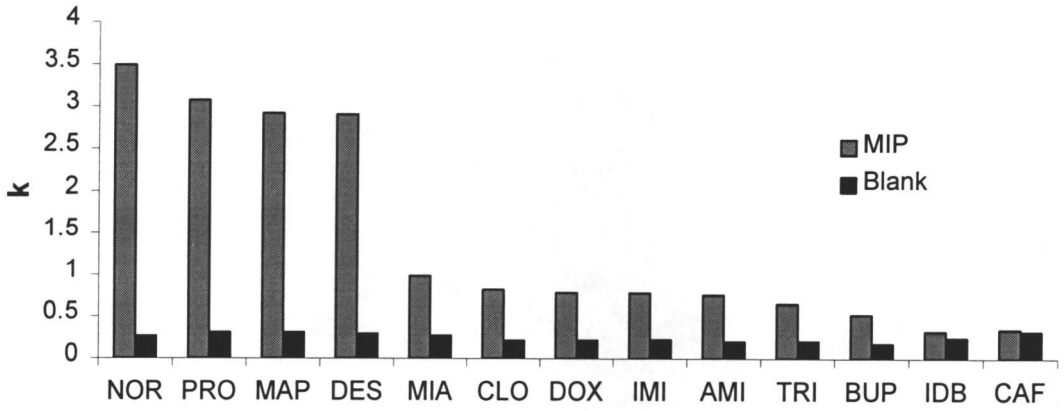

Figure 3.3 Comparison of k values for library compounds on NOR-imprinted MIP and blank polymer capillaries. Data points represent the mean of three runs. Eluent: 0.02% v/v trifluoroacetic acid (TFA), 0.015% v/v triethylamine (TEA) in CH_3CN.

For a given compound, the ratio of its retention factors on the MIP and "blank" columns (k^{MIP}/k^{blank}) is of interest as it provides a quantitative measure of the compound's selective affinity for the MIP. This ratio, for which the term selection factor will be introduced, would be expected to be highest for the template molecule, in this case NOR. The selection factors for the other compounds in the library are useful in comparing their relative affinities for the MIP. A more useful parameter with which to obtain a relative measure of affinity of a compound for the MIP recognition cavity is the selection index, which is introduced as follows:

$$selection\ index\ (compound\ n) = \frac{\left(k_n^{(MIP)} / k_n^{(Blank)}\right) - 1}{\left(k_{template}^{(MIP)} / k_{template}^{(Blank)}\right) - 1} \qquad (3.1)$$

The selection index is obtained by normalizing the selection factor for compound n to the selection factor calculated for the template molecule. It is useful to note several salient features of this equation. By definition, the selection index for the template is 1, thus as the ratio $k^{(MIP)}/k^{(Blank)}$ (the selection factor) for library compound n approaches the template selection factor ($k_{template}^{(MIP)}/k_{template}^{(Blank)}$), the selection index for compound n approaches 1. If library compound n exhibits very little selective retention on the MIP (i.e. when the selection factor$\rightarrow$ 1), the selection index approaches zero. This equation is similar in form to the retention index used by Ramström, et al. [90], differing in the limit $k_n^{(MIP)}/k_n^{(Blank)} \rightarrow 1$. The selection index, then, provides a measure of the relative "goodness of fit" of the various library compounds into the NOR binding pocket in the MIP.

Using equation 1, selection indices for the library were calculated and are shown in figure 3.4. Upon inspection of these data, some trends are observed. The secondary amine antidepressants, PRO, DES and MAP exhibit greater affinity for the MIP than do the tertiary amines; selection indices for the former are approximately a factor of three greater than the latter. This behavior is not surprising in view of the fact that NOR (the template) is a secondary amine. AMI, the tertiary amine analog of NOR, exhibits relatively weak affinity for the MIP (selection index = 0.2).

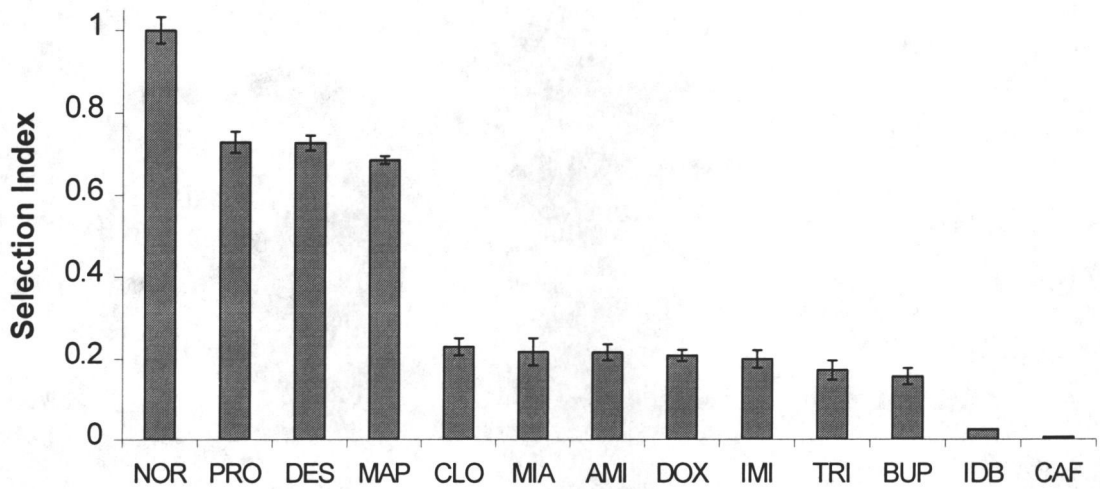

Figure 3.4 Selection indices for simulated combinatorial library. Error bars indicate ± 1 standard deviation (s.d.) determined from three injections. s.d. for IDB and CAF < 0.001.

One possible explanation of the more favorable interaction of the secondary amine TCAs with the MIP is steric hindrance at the pendant amine. It is plausible that the additional methyl group on the tertiary amine TCAs impedes hydrogen bond formation with a methacrylic acid moiety on the MIP. The involvement of hydrogen

bonding in molecular recognition is supported by the results of studies of the effect of eluent composition on retention.

The compounds with the least affinity for the MIP are BUP, IDB, and CAF. BUP is an antidepressant that is pharmacologically similar to the TCAs [92], but lacks the tricyclic structure. Interestingly, although BUP contains a secondary amine (figure 3.2), it exhibits rather weak affinity for the NOR binding pocket, having the lowest selection index of the antidepressants tested. This behavior implies that the secondary amine functionality and tricyclic structure are necessary to maximize interaction ("fit") with the binding cavities in the MIP. IDB is a structural precursor to the dibenzazepine TCAs (IMI, DES, CLO, and TRI) that lacks the pendant group. IDB exhibited minimal recognition, having a selection index of only 0.02. Thus, the ring structure alone is insufficient for a favorable interaction with the binding cavity. As expected CAF, a test probe included in the library to evaluate the MIP's ability to discriminate against a structurally dissimilar (and pharmacologically unrelated) compound, showed virtually no selective interaction (selection index < 0.01). These observations are generally in agreement with the anticipated result: the most structurally dissimilar compounds in the library with respect to the template were the least "recognized" by the MIP. Clearly, the tricylic ring structure and pendant amine together are important structural elements in the recognition process.

3.3.2 Chromatography

The MIP sorbent was employed to separate NOR from a series of tertiary amine structural analogs. As illustrated in figure 3.5a, resolution of NOR from the structural analogs is achieved in about 5 minutes. Although a measure of selectivity was obtained between NOR and the various secondary amine antidepressants on this sorbent (refer to the *k* values in figure 3.3), no separations could be obtained due to low efficiencies and poor peak shapes. Similarly, in chromatogram shown in figure 3.5a, the tertiary amine TCAs (AMI, IMI, CLO, DOX, and TRI) coelute despite slight differences in their *k* values. Also apparent in this chromatogram is the severe tailing of the template molecule. Such behavior is well documented with MIP sorbents and has been attributed to slow adsorption/desorption kinetics and nonlinear binding isotherms [93, 94]. It should be noted that the MIP particles employed here were obtained by grinding and sieving bulk polymer, which yielded irregular particles on the order of 15-25 μm in diameter. Chromatographic theory predicts low efficiencies for such particles, undoubtedly this is a factor in observed peak shapes. Efforts have been made to synthesize more chromatographically desirable MIP particles (i.e. uniformly sized, small, and spherical), most notably by means of dispersion [95] and two step swelling or "seed" polymerization [96]. Although successful in the end goal, there is unfortunately a precipitous increase in complexity with these approaches relative to bulk polymerization. Because optimization of selectivity was the primary focus in this work, bulk polymerization was employed. However, research is currently underway in our laboratory to develop MIPs with more favorable chromatographic properties.

Figure 3.5b shows the same test mixture run on the blank column. In addition to the absence of molecular recognition, it is interesting to note the overall improvement in the shape of the coeluted peak in this blank run, which suggests very little interaction between the analytes and sorbent. The selection index values shown in figure 3.4 for the tertiary amine test probes range from about 0.18 to 0.25 (i.e. there is some "recognition" on the MIP). It can be seen from a comparison of figures 3.5a and b that AMI, IMI, CLO, DOX, and TRI are preferentially retained on the MIP sorbent, although to a much lesser extent than the template molecule.

Shorter columns and slightly faster linear velocities were employed to effect faster separations of NOR from the five tertiary amine TCAs, shown in figure 3.6. As seen, separations were achieved on this MIP sorbent in less than 60 s. It must be emphasized that all of the separations presented here were performed isocratically and at ambient temperature (approximately 25 °C). Gradient elution and elevated temperature are often necessary in MIP chromatography to improve peak shape [97], thereby enhancing resolution and reducing analysis time. Under the conditions employed here, however, rapid separations were achieved without the need for these modifications, thus simplifying the analysis.

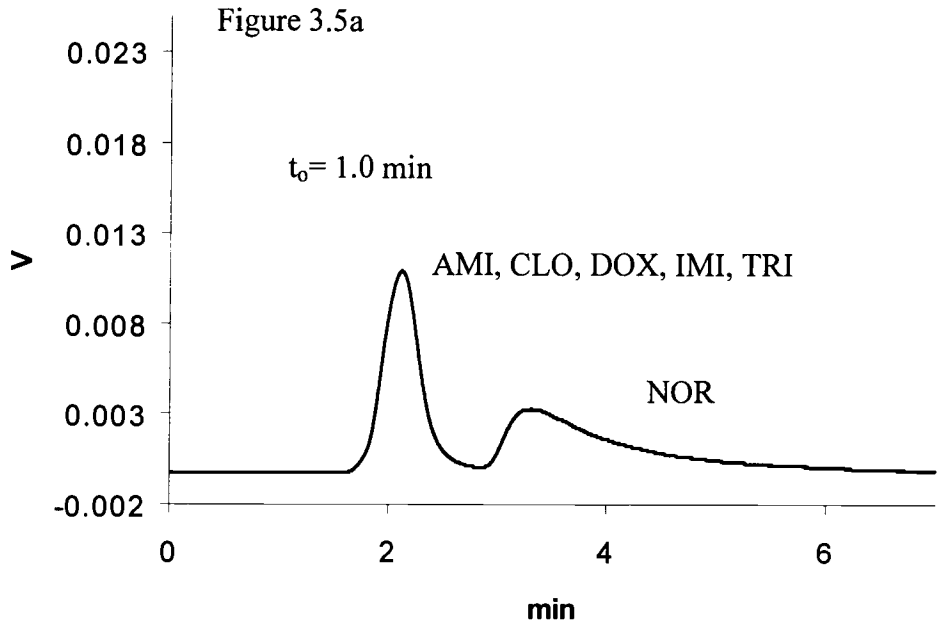

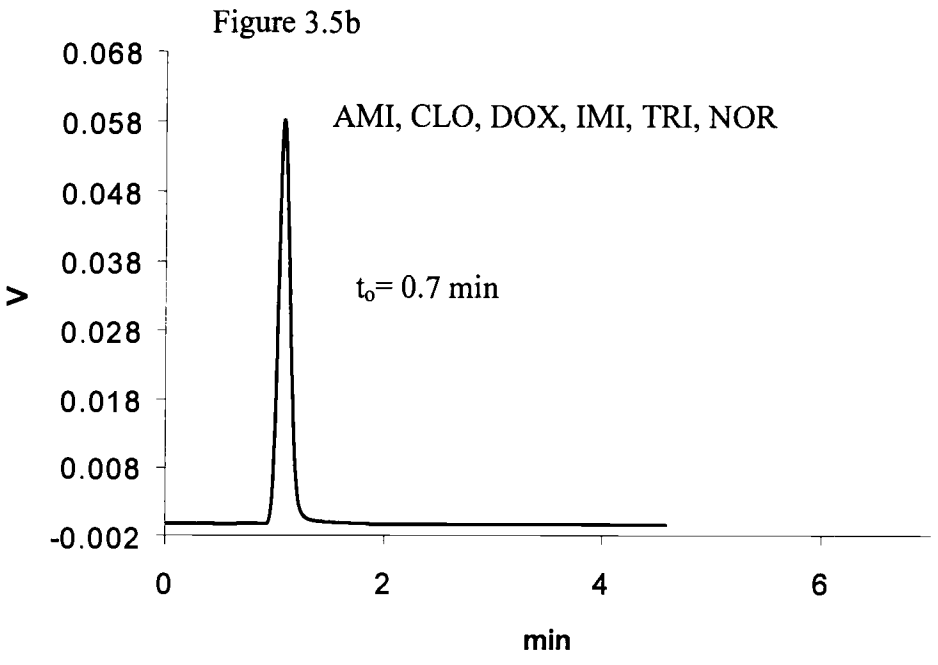

Figure 3.5 Analysis of TCA test mixture. Run conditions: Pressure: 50 bar; Eluent: 0.02% TFA v/v, 0.0075% TEA v/v in CH_3CN. Sample: 0.5 mg/mL (each) AMI, IMI, DOX, TRI, CLO, 1.5 mg/mL NOR in CH_3CN. (A) MIP Capillary: I.D. 250 μm, L_{bed}: 28 cm. (B) Blank Capillary: I.D. 250 μm, L_{bed}: 29 cm.

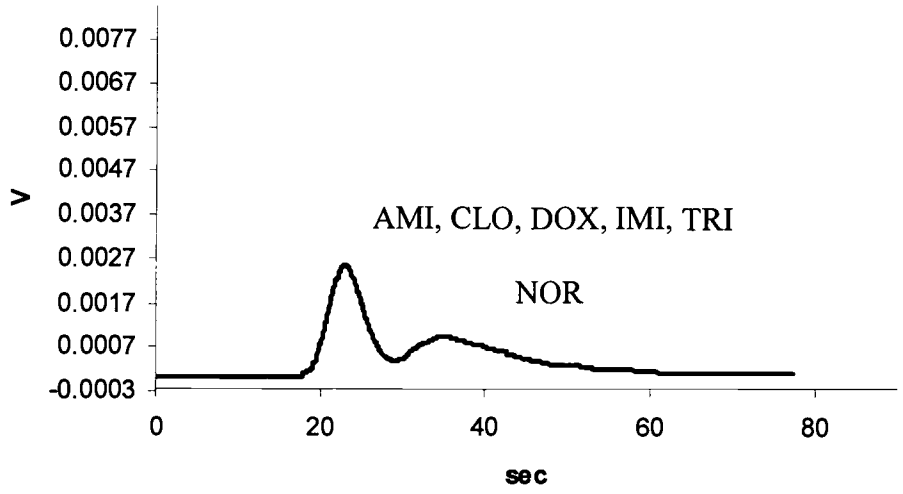

Figure 3.6. Rapid separation of NOR from a series of structural analogs on an MIP sorbent. Capillary I.D.: 250 μm; Eluent: 0.02% TFA v/v, 0.0075% v/v TEA in CH_3CN; L_{bed}: 11.5 cm; Linear Velocity: 13 mm/s; Pressure: 50 bar.

3.3.3 Investigation of separation mechanism

In an effort to elucidate the mechanism of molecular recognition on the MIP, a series of experiments was conducted in which the eluent composition was varied. The mixture of NOR and the five tertiary amine TCAs was used as a test sample and the effect on the retention behavior of the TCAs (i.e. retention factors) was observed. The optimum eluent for the separation consisted of 0.02% trifluoroacetic acid (TFA) v/v, 0.0075% triethylamine (TEA) v/v in CH_3CN, and a representative chromatogram is shown in figure 3.5 A. This eluent was used as a reference point from which to begin the eluent composition study. The test mixture was run on the MIP and blank columns under the following conditions: 1) optimized eluent (control), 2) vary TFA concentration, holding TEA constant, 3) vary TEA concentration, holding TFA

constant, 3) omit TFA and TEA, and 4) incorporate an aqueous component. Finally, the test mixture was analyzed on an MIP prepared without methacrylic acid.

The TFA concentration in the eluent was varied over the range of 0 to 0.1% v/v. The results for the MIP and blank columns are shown in figure 3.7a. Surprisingly, it was found that when the TFA was omitted, all six TCAs were strongly retained on the MIP and blank columns. So strong was the retention in the absence of TFA that no peak elution was observed and hence k values could only be estimated[1]. As such, the extent of selective retention on the MIP could not be determined. As the TFA concentration is increased there is an overall decrease in k on both columns. On the MIP, selective retention of NOR is readily apparent and decreases with increasing TFA content. At 0.1% TFA, selectivity is decreased to the point where NOR retention on the MIP and blank are comparable. Extrapolation of the MIP data to 0% TFA would predict a relatively large measure of molecular recognition superimposed on a strong nonspecific component of retention. TFA evidently plays a role not only in disrupting molecular recognition, but in attenuating nonspecific sorption on these polymers.

Next, the percentage of TEA was varied from 0 to 0.075% v/v while the TFA concentration was fixed at 0.02%. As shown in figure 3.7b, in the absence of TEA, the tricyclic antidepressants were minimally retained (k <1) on both columns. Increasing the concentration up to 0.015 % results in a moderate increase for each compound on the blank polymer. Although the same general trend of increased k with

---

[1] Due to low plate numbers and the sensitivity of the available detector, k values greater than approximately 15 could not accurately be determined on these columns.

% TEA is observed on both columns, selective retention of NOR on the MIP sorbent becomes apparent upon addition of TEA, and increases with the amount added. In contrast, no noticeable difference in retention exists between the template and the other TCAs on the blank polymer. At 0.075% TEA, extremely strong retention (not measurable) is once again observed on both columns.

These data indicate the presence of specific and nonspecific components of retention acting in concert on this MIP. Upon inspection of figure 3.7, it is seen that near the optimum TFA and TEA concentrations, the nonspecific component is effectively disrupted while the specific component is sufficiently maintained such that resolution of NOR from the tertiary amine analogs is possible.

When the acid and base modifiers were omitted from the eluent (neat CH_3CN), runs of the test mixture were characterized by strong retention of the TCAs on both the MIP and blank columns. In addition, the peaks were unusually broad and poorly shaped. For this reason molecular recognition of NOR on the MIP, though observed, was not quantitated.

Incorporation of an aqueous component was next studied. The optimized "control" eluent was modified by the addition of a 10 mM sodium acetate buffer to yield the following: (95:5) v/v CH_3CN: 10 mM sodium acetate pH=3.0 containing 0.02% TFA, 0.0075% TEA v/v (final volume). From the resultant run of the test mixture, shown in figure 3.8, it is evident that the aqueous component disrupts molecular recognition. Retention of the TCAs on the blank column was essentially unchanged relative to the control eluent, where only weak retention was observed.

Figure 3.7a

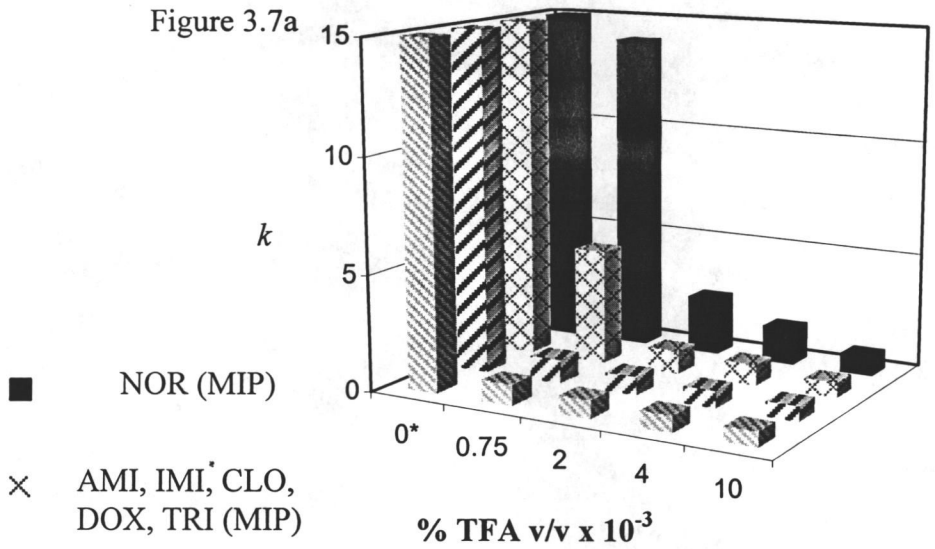

Figure 3.7b

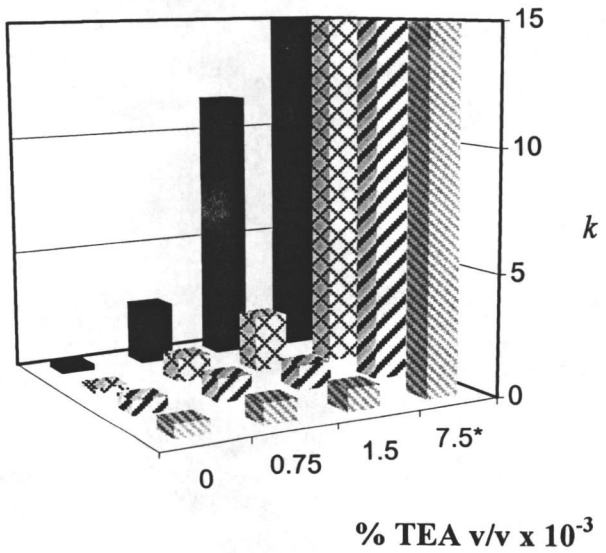

Figure 3.7. Effect of acid and base modifier concentration on retention. (A) TEA held concentration held constant at 0.0075% v/v, (B) TFA concentration held constant at 0.02% v/v, * $k > 15$; exact value not determined.

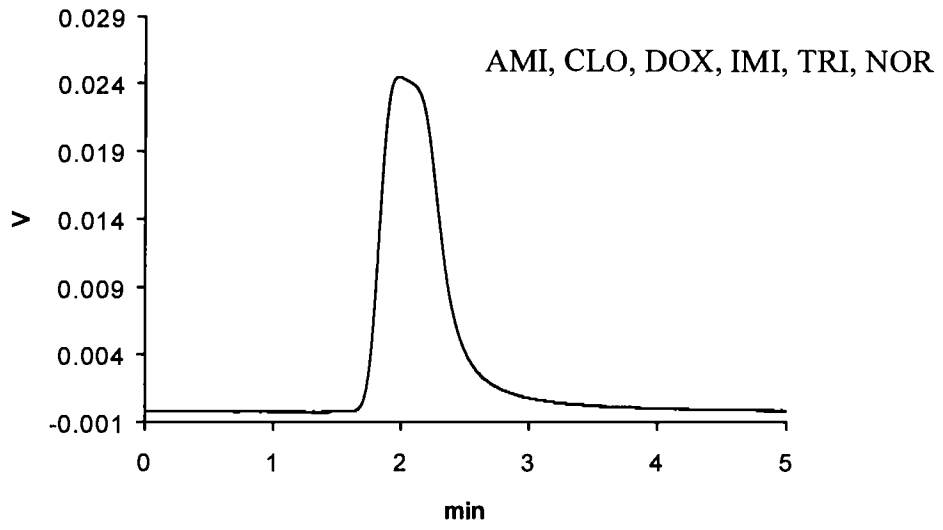

Figure 3.8. Effect of an aqueous modifier on molecular recognition (MIP capillary). Eluent: CH_3CN: 10 mM sodium acetate pH 3.0 (95:5) containing 0.02% TFA, 0.0075% TEA v/v (final volume). Sample: 0.5 mg/mL (each) AMI, IMI, DOX, TRI, CLO; 1.5 mg/mL NOR in CH_3CN; Pressure: 50 bar.

Results obtained for the test mixture on an MIP prepared without methacrylic acid are presented in table 3.1. These data show that very little retention and no molecular recognition were obtained with the control eluent. From these data it could be argued that an ionic interaction between a protonated amine on an analyte and dissociated methacrylic acid moiety on the MIP is important in the recognition process. This is unlikely, however, in view of the fact that selective retention of NOR increases upon addition of TEA to the eluent. If ionic interactions were dominant, one would expect that TEA would compete for the ionized sites on the polymer, resulting in an overall decrease in selectivity. Indeed, the addition of TEA to a (nonaqueous) CH_3CN eluent has been shown to decrease retention and selectivity in separations of diaminonapthalene isomers on methacrylic acid-based MIPs [96]. Such behavior is

consistent with an ion exchange model [79] developed to describe retention on MIPs in the presence of aqueous/organic eluents. This behavior was not observed in the present study. Instead, the addition of TEA through the range studied resulted in an increase in selective retention (figure 3.7).

TCA	*k*
NOR	0.19
AMI	0.18
CLO	0.19
DOX	0.18
IMI	0.18
TRI	0.18

Table 3.1. Retention data for NOR and selected TCAs on an MIP sorbent prepared without methacrylic acid. Eluent: 0.02% TFA v/v, 0.0075% TEA v/v in CH_3CN.

Furthermore, in the presence of ionic interactions between the pendant amine and the polymer, a correlation might be expected between selection index values and analyte basicities. Such a correlation, however, was not observed. Consider the following six TCA test probes ranked in order of decreasing pKa [98]: PRO > MAP > DES > NOR > IMI > CLO > DOX. Selection index values, however, rank as follows: NOR > PRO > DES > MAP> CLO > DOX > IMI. No apparent correlation is found. It must be noted, however, that these pKa values were determined in aqueous solution and the actual values might be expected to vary considerably in the nonaqueous conditions employed here. Nevertheless, these data are useful in providing a measure of *relative* base strengths.

These results suggest that a critical element of molecular recognition on this MIP is hydrogen bonding between the pendant amine of the TCAs and a methacrylic acid moiety on the polymer. The interaction is apparently more favorable at the less sterically hindered secondary amine group. This hypothesis is supported by the disruption of molecular recognition observed upon addition of a potent hydrogen bonding agent (e.g. water, TFA) to the eluent. The nonspecific component of retention on these polymers was disrupted by the addition of TFA. It is likely, then, that hydrogen bonding also plays a role in this nonspecific sorption. With MIP sorbents, it is generally desirable to eliminate or at least minimize any nonspecific retention. In this work, attenuation of nonspecific retention was accomplished by judicious use of TFA and TEA as mobile phase modifiers. The precise role of these modifiers is complex and probably involves multiple effects that include influence on the charge states of the polymer acid groups and analytes as well as providing hydrogen bonding competition. In this study, the net effect of the modifiers is to disrupt of nonspecific sorption while maintaining to an acceptable degree the interaction(s) responsible for molecular recognition. Eluents of similar composition (i.e. acid and base modifiers in an anhydrous polar organic solvent such as CH_3CN) have been employed in chiral HPLC with cyclodextrin stationary phases [99] where they are thought to affect the interaction of polar functional groups such as amines with the hydroxyl groups on the cyclodextrin. Additional mechanistic studies on MIPs are needed to more fully explore the role of these modifiers under these conditions.

3.4 Conclusion

The goal of this study was to prepare an MIP using one of a group of structural analogs as a template and subsequently to screen this group of analogs against the MIP. The primary purpose of the screening analysis was to determine if certain compounds in the "library" would interact more favorably with the MIP relative to others and if so, to evaluate any observed differences in terms of the structures of the test probes. The selection index data provided a quantitative measure of the "goodness of fit" of each library compound into the NOR binding pocket and revealed that some of the test probes did in fact exhibit better "fit" than others. The results of the screening analysis also demonstrated the ability of the MIP to discriminate against structurally dissimilar compounds.

The "best fit" compounds in the library were those that possessed both the tricyclic structure and a pendant secondary amine group – structural features shared by the template molecule. Tricyclic compounds with a tertiary amine exhibited an intermediate degree of interaction with the MIP while the most structurally dissimilar species exhibited the least. The experimental data suggest that hydrogen bond formation between the test compounds and the polymer is important in molecular recognition. In general, multiple types of intermolecular forces (e.g. hydrogen bonding, π-π interactions, etc.) acting in concert can serve to maximize molecular recognition in noncovalent MIPs.

This work demonstrates that high selectivity, affinity-type separations can be achieved using MIP sorbents. In principle, an MIP-based technique could be useful as

a preliminary step in screening libraries generated by combinatorial techniques. This approach has the advantages that MIPs are inexpensive and relatively simple to produce, especially important when the target receptor(s) are difficult or impossible to obtain, and are stable in a broad range of chemical environments. Utilizing MIPs in an initial screening step could serve to identify those compounds in the library worthy of immediate study by bioassay techniques, thereby enabling a limited supply of biological material to be conserved and used to screen a more highly focused group of compounds.

4. Modeling Interparticle and Intraparticle (Perfusive) Electroosmotic Flow in Capillary Electrochromatography

4.1 Introduction

The primary reason capillary electrochromatography (CEC) has garnered the attention of many separation scientists over the past decade or so [100-103] is the technique's efficiency advantage relative to HPLC. Specifically, sources of peak dispersion arising from nonuniformity in flow velocity, namely eddy diffusion and mobile phase mass transfer effects, are generally smaller in CEC than HPLC, as is overall plate height.

Chromatographic rate theory predicts lower plate heights when smaller diameter packing particles are employed [3, 7]. For this reason, practitioners of HPLC generally employ the smallest particles practically possible (usually 3 – 5 μm in diameter). This maxim holds for CEC as well. In contrast to HPLC, the absence of pressure drop facilitates the use of submicron particles in CEC, which in principle should provide maximum efficiency. This approach has yielded promising results [11, 12], though it presents a number of practical limitations. Chief among these are difficulties in column preparation due to the small particle size and a lack of commercial availability of the particles.

Macroporous packings present an alternative pathway to improving efficiency in CEC because, under the proper conditions, the macropores in such particles can

support EOF [104]. Widely available from a number of manufacturers, macroporous particles are typically larger in diameter (e.g. 5 –10 μm) and have mean pore diameters above 500 Å. As are most typical silica based HPLC packings, macroporous particles are corpuscular in nature, produced by sol-gel methods in which colloidal silica particles ("microbeads") coalesce under controlled conditions to form porous spheres composed of agglomerates of microbeads [105]. Pore size can be adjusted by altering the size of the silica sol particles and their packing density. One advantage that immediately accrues to the use of these media is the relative ease of capillary packing. The practical complications associated with packing submicron particles, clogging for example, are avoided. Additionally, larger diameter particles can be well packed using conventional slurry packing methods.

In the "through-pore", or perfusive EOF regime, analyte molecules in the mobile phase sample two distinct regions of space, that between packing particles (the interstitial space) and the spaces in the pores of the particles (the intraparticle region). This is depicted schematically in figure 1. In the interstitial space, flow channel diameter is proportional to the diameter of the packing particle (d_p). For this reason, individual sources of flow velocity inhomogeneity (with the associated diffusion distances, persistence of velocity spans, etc.) are scaled to particle diameter [3]. The flow channel diameter in the intraparticle region is independent of d_p and instead is a function of the diameter of microbeads constituting the particle. Under conditions such that a considerable fraction of the total column flow occurs through the particles, the *effective* particle diameter $d_{p,eff}$, which is dictated to a large extent by the microbead diameter, will therefore be lower than d_p.

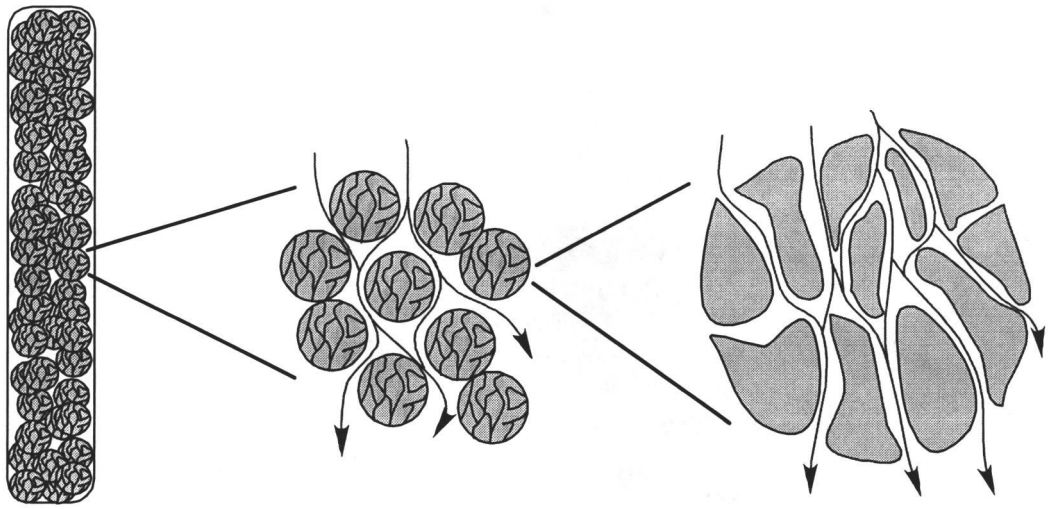

Figure 4.1. Schematic representation of interparticle and intraparticle flow in a packed CEC column. Arrows indicate mobile phase streampaths.

In addition to a smaller effective particle diameter, operating in a perfusive EOF mode provides a further advantage in that a substantially lower contribution of stagnant mobile phase mass transfer to plate height is expected. With conventional small pore media, fluid occupying the pores is generally stagnant. Broadening of the analyte zone occurs due to slow diffusion between the stagnant and mobile fluids, and is greater in magnitude at higher flow velocities. This phenomenon manifests itself as an increasingly positive slope on the high velocity side of plate height versus linear velocity curves, also known as rate curves. In contrast, the fluid in much of the pore space in a perfusive system is no longer stagnant and as a consequence the system takes on the characteristics of a bed composed of small diameter, essentially nonporous particles, which are ideal from the standpoint of efficiency.

Recent studies on the use of macroporous packings in CEC have demonstrated the predicted improvements in efficiency brought about by intraparticle EOF [104,

106]. Using 7 μm d_p, 4000 Å pore Nucleosil C18 particles, Stol, et al. [106] observed plate heights only slightly greater than those generated with 1.5 μm nonporous particles. Reduced plate heights as low as 0.34 were obtained for fluorene.

When assessing column performance, reduced parameters are recommended [3, 107] in which plate height is scaled to d_p. In the perfusive EOF regime, however, reduced parameters calculated by scaling to d_p are not representative because the "effective" particle diameter is less than d_p. On this basis, it would be useful to devise a method by which the effective particle diameter for a given set of conditions could be estimated. Although the effective particle diameter has no physical meaning, such a parameter would allow for: i) more accurate scaling of plate height and velocity, thus facilitating comparisons of different conditions and determinations of plate height coefficients; and ii) estimation of the gain in efficiency as the perfusive character of the packings is increased. In this paper, a model has been developed by which the extent of intraparticle flow in CEC columns packed with different pore sizes of macroporous particles was estimated for a range of eluent ionic strengths. By means of the model, an effective particle diameter was obtained for each test condition. The values generated predict the trends observed in the experimental data.

4.2 Theory

As discussed in chapter 1, the electrical double layer, which forms near charged surfaces, gives rise to electroosmotic flow. In CEC with conventional sorbents, electrical double layer formation is the result of a net negative charge present

at the surface of the silica packing particles and the capillary wall. Application of an electric potential gradient along the capillary axis causes mobile ions in the double layer to migrate resulting in EOF. Rice and Whitehead [108] published a thorough treatment of EOF in cylindrical capillary tubes in which EOF velocity V was shown to be a function of radial position in the tube r described as follows:

$$V(r) = \frac{\varepsilon_0 \varepsilon_r \zeta E}{\eta}\left[1 - \frac{I_0(\kappa r)}{I_0(\kappa a)}\right] \qquad (4.1)$$

where ε_0 is the permittivity of vacuum, ε_r is the dielectric constant of the solution, ζ is the zeta potential (the potential at the shear plane), E is the applied electric field strength, η is the solution viscosity, I_0 is a zero order modified Bessel function of the first kind, κ is the reciprocal of the electrical double layer thickness, r is the distance from the tube center, and a is the tube diameter. The double layer "thickness" δ is the distance (from the wall) at which the potential decays to $1/e$, or 0.37 of its value at the wall and for a (1:1) univalent electrolyte is given by

$$\delta = \kappa^{-1} = \left(\frac{\varepsilon_0 \varepsilon_r R T}{2CF^2}\right)^{1/2} \qquad (4.2)$$

in which R is the universal gas constant, T is absolute temperature, C is the molar concentration of electrolyte, and F is Faraday's constant. Apparent in equation 2 is the inverse square root relationship between double layer thickness and electrolyte concentration. The electrokinetic radius, κa, is the ratio of channel radius to double layer thickness.

Under conditions in which the flow channel diameter is large relative to the double layer thickness, typical in CEC with interstitial flow, the term in brackets in

equation 4.1 approaches zero and the expression reduces to the familiar Smoluchowski equation [109] in which V is essentially independent of radial position in the channel.

$$V = \frac{\varepsilon_0 \varepsilon_r \zeta E}{\eta} \tag{4.3}$$

However, in narrow flow channels such as those in the pores of the packing material, values of κa will be much smaller than in the interstitial channels and the term in brackets in equation 1 must be considered. A useful parameter with which to evaluate V in such conditions is the relative EOF velocity V_{rel} [110], which is derived as follows. From equation 4.1, the cross sectional average velocity can be obtained:

$$\overline{V} = \frac{\varepsilon_0 \varepsilon_r \zeta E}{\eta}\left[1 - \frac{2I_1(\kappa a)}{\kappa a I_0(\kappa a)}\right] \tag{4.4}$$

where I_1 is a first order modified Bessel function of the first kind. For $\kappa a >> 1$, the term in brackets in equation 4 approaches unity, and expressions 4.3 and 4.4 become equivalent. If, for clarity, the average velocity at large κa is expressed as $\overline{V}_\infty$, then the relative EOF velocity, V_{rel} is given by:

$$V_{rel} = \frac{\overline{V}}{\overline{V}_\infty} = \left[1 - \frac{2I_1(\kappa a)}{\kappa a I_0(\kappa a)}\right] \tag{4.5}$$

Figure 4.2 is a plot of V_{rel} versus κa, which helps to illustrate the salient features of equation 5. Although for finite values of κa, $V_{rel} < 1$, there is an asymptotic approach toward unity such that at large κa (>50), V_{rel} is essentially equal to $\overline{V}_\infty$, hence the validity of the Smoluchowski equation. In contrast, for $\kappa a < 10$, a sharp dependence of V_{rel} on κa is observed.

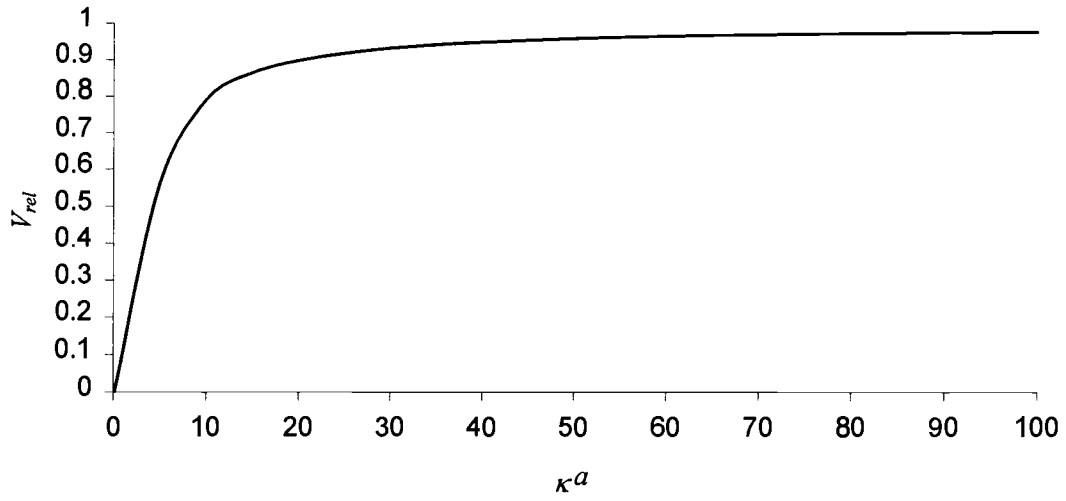

Figure 4.2. Relative EOF velocity as a function of electrokinetic radius κa.

4.2.1 Model Design

The goal of this study was to develop a model that could be used to estimate the contribution of intraparticle EOF to the total flow in the packed column for a given nominal pore size of packing and eluent ionic strength. To that end, a model was designed in which a weighted average channel diameter was determined for a column under a given set of operating conditions. In addition to the interstitial space, intraparticle pores with diameters in the range 50 – 10000 Å, readily determinable by mercury intrusion porosimetry, were considered. An overview of the model is as follows. Initially, the fraction of total void space in the column accessible by the mobile phase, the total column porosity, was estimated. The intraparticle pores under consideration were then partitioned into intervals of 10 Å. Using pore size distribution data for the packings obtained by mercury intrusion porosimetry, the volume fraction

for each interval (i.e. its fraction of the total column void space) was determined. In a similar manner, the volume fraction of the interstitial space was estimated. Next, the relative magnitude of EOF velocity in each channel diameter interval was estimated by treating the channels as parallel cylindrical capillary tubes of equal length. With this assumption, relative EOF velocity was determined using the well known Rice and Whitehead relationships, in which EOF velocity is a function of κa in the channel. The volume fractions and estimations of relative EOF velocity, calculated for each of the 10 Å intervals representing the intraparticle region and for the interstitial region, were used as weighting factors in calculating an average flow channel diameter for a given set of conditions. The average *channel* diameter obtained from the model was subsequently converted to an average effective *particle* diameter to enable a more facile interpretation of the results.

4.2.2 Calculation of Weighting Factors

Pore size distributions for the different nominal pore diameter Nucleosil packings were determined by mercury intrusion porosimetry. Pore diameters from 50-10000 Å were partitioned into 995 intervals, each spanning 10 Å. Using the porosimetry data, a given interval's fraction of the total pore volume f_i was calculated by determining the fraction of the total area under the pore size distribution curve contributed by the interval.

$$f_i = \left(\frac{Interval\ Volume}{Cumulative\ Pore\ Volume} \right) \tag{4.6}$$

The 10 Å interval i was then assigned a nominal pore (channel) diameter d_{ch} equal to the midpoint of the interval. For example, if pores between 250 and 260 Å in diameter constituted 1% of the total pore volume, then the volume contribution was considered to arise from 255 Å pores (i.e. d_{ch} = 255 Å). In this way, the pore size distribution data were discretized with the large number of intervals ensuring minimal loss of coherence.

The fraction of void space in the column occupied by the mobile phase, ε_{tot} is given by

$$\varepsilon_{tot} = \varepsilon_i + \varepsilon_p(1 - \varepsilon_i) \tag{4.7}$$

where ε_i is the fraction of interstitial free space in the column (the interstitial porosity) and ε_p is the particle porosity. The fraction of total column void space contributed by the pores of the packing particles is then

$$\varepsilon_{pore} = \frac{\varepsilon_p(1-\varepsilon_i)}{\varepsilon_{tot}} \tag{4.8}$$

For well packed chromatographic columns, ε_i is typically on the order of 0.4 [3] and equation 4.8 reduces to $\varepsilon_{pore} = 0.6\left(\frac{\varepsilon_p}{\varepsilon_{tot}}\right)$. Values of ε_p for the Nucleosil materials were obtained from the porosimetry data. The fraction of total column void space contributed by the packing interstices is $1 - \varepsilon_{pore}$.

For the intraparticle pores, the volume fraction weighting factor χ_v for a given 10 Å pore diameter interval i is defined as the fraction of total column volume contributed by interval i. The sum of χ_v over all intervals is therefore equal to ε_{pore}.

$$\chi_v \text{ (interval } i) = (f_i)(\varepsilon_{pore}) \tag{4.9}$$

$$\sum_{i=1}^{i=995} \chi_v i = \varepsilon_{pore} \tag{4.10}$$

The volume fraction weighting factor for the interstitial channels is $1 - \varepsilon_{pore}$.

The relative EOF velocity weighting factor, χ_e for pore interval i is equal to the relative EOF velocity for a cylinder of the appropriate diameter, given by equation 4.5. Thus:

$$\chi_{e(i)} = \left[1 - \frac{2I_1(\kappa a_i)}{\kappa a_i I_0(\kappa a_i)}\right] \tag{4.11}$$

in which a_i is the nominal pore radius (0.5 d_{ch}) of the interval. The value of κ is dependent upon the ionic strength of the eluent. For the interstitial space, the channel radius a was estimated from the particle diameter d_p and the interstitial porosity using the following relationship [111].

$$a = 0.21 d_p \left(\frac{\varepsilon_i}{1 - \varepsilon_i}\right) \tag{4.12}$$

4.2.3 Weighted Average Particle Diameter

To calculate a weighted average particle diameter, χ_v and χ_e were combined into a single lumped weighting factor χ_l for each channel under consideration.

$$\chi_l(i) = [\chi_v(i)][\chi_e(i)] \tag{4.13}$$

An average channel diameter $\overline{d_{ch}}$ was subsequently obtained by calculating the weighted average of the individual flow channels

$$\overline{d_{ch}} = \frac{\overbrace{(\chi_1 1)(d_{ch}1) + \ldots + (\chi_1 995)(d_{ch}995)}^{\textit{Intraparticle Contribution}} + \overbrace{(\chi_1\, int)(d_{ch}\, int)}^{\textit{Interstitial (int) Contribution}}}{\chi_1 1 + \ldots + \chi_1 995 + \chi_1\, int} \qquad (4.14)$$

Rearranging equation 4.12 and once again setting $\varepsilon_i = 0.4$, $\overline{d_{ch}}$ was converted to an effective particle diameter $d_{p,eff}$

$$d_{p,eff} = 3.57\,\overline{d_{ch}} \qquad (4.15)$$

The effective particle diameter for a given type of packing is dependent upon the pore size distribution of the material, its porosity and the ionic strength of the eluent. At lower ionic strengths, where the double layer thickness δ is large relative to the mean pore diameter of the packing (i.e. small κa), a larger $d_{p,eff}$ is predicted. As ionic strength is increased, a greater fraction of the pores can support EOF, resulting in a lower $d_{p,eff}$. In contrast to the macroporous particles employed in this study, conventional (e.g. 60-80 Å pore diameter) HPLC packings in general possess an insufficient fraction of pores large enough to support EOF. With such particles the interstitial contribution dominates equation 4.14 and $d_{p,eff} \approx d_p$. Alternatively, if a packing were employed having a uniform distribution of macropores in which vigorous electroosmosis could occur, a limiting value of $d_{p,eff}$ would be reached because the intraparticle pore space in a typical column constitutes only 40-50% of the total volume accessible to the mobile phase. The remaining fraction arises from the interstitial space. In practice, the relatively broad pore size distributions of many macroporous packings, which often include a fraction of mesopores (< 500Å), impose more stringent limits on the minimum achievable value of $d_{p,eff}$.

In the work presented here, commercially available macroporous silica HPLC packings (Nucleosil, Macherey-Nagel, Duren, Germany) of three different nominal pore diameters were examined using typical CEC eluents with a range of ionic strengths. An unretained test probe, acetone, was employed to monitor plate height as a function of eluent ionic strength. The model described above was used to estimate $d_{p,eff}$ for each combination of packing and eluent ionic strength. Values of $d_{p,eff}$ obtained from the model were then used to reconstruct experimental reduced plate height versus reduced velocity plots.

4.3 Experimental

4.3.1 Materials and Reagents

Concentrated hydrochloric acid (37%) and HPLC grade acetone were purchased from Mallinckrodt, St. Louis, MO USA. Ultrapure grade (99.9+%) tris (hydroxymethyl) aminomethane (Tris) was obtained from Aldrich Chemical, Milwaukee, WI USA. HPLC grade acetonitrile was purchased from Fisher Scientific, Pittsburgh, PA USA. All water used in this study was filtered and deionized using a Barnstead Series 582 water purification system (Barnstead/Thermolyne Corporation, Dubuque, IA USA). Fused silica capillary tubing of 75 μm I.D., 360 μm O.D., was purchased from Polymicro Technologies, Inc., Phoenix, AZ USA. Nucleosil C18 silica particles (d_p = 7 μm) with nominal pore diameters of 500, 1000, and 4000 Å were obtained from Meta Chem Technologies, Torrance, CA USA.

The desired concentrations of Tris buffer were obtained by first preparing a 500 mM stock solution of Tris (base form), and subsequently diluting in deionized

H_2O to 100 mM. The pH of this 100 mM solution was adjusted to 8.0 by titration with concentrated HCl, after which dilutions were performed to yield 75, 50, 25, 10, and 1.0 mM buffer solutions. The concentration of protonated Tris (acid form), necessary for double layer thickness calculations, was estimated using the Henderson-Hasselbach equation. Appropriate volumes of each buffer were mixed with acetonitrile to yield (20:80) (v/v) buffer: acetonitrile solutions, which were then employed as eluents in the capillary electrochromatography experiments. In this system, ionic strength I is essentially equal to the concentration of Tris in the acid form. It should be noted that the various Tris concentrations employed in this study are identified herein according to their nominal values, i.e. the total concentration of Tris in the aqueous component of the mobile phase (1, 10, 25, 50, 75, and 100 mM). In calculating values of δ, however, the final concentration of ionized Tris (determined as described above and accounting for the 1:5 v/v dilution in acetonitrile) was used.

4.3.2 Preparation of Capillary Columns

The initial step in capillary preparation was the formation of a frit to retain the particles during packing. After cutting to the desired length, one end of the capillary tube was tapped into dry packing material until the material protruded a short distance into the tube. The packing material was sintered by heating with an electric arc fusion splicer (Alcoa Fujikura, Tokyo, Japan). A slurry was made by suspending 10 mg of particles in 1.0 mL acetonitrile. Using an Isco 100 DX syringe pump (Isco, Inc., Lincoln, NE USA) with 50% (v/v) acetonitrile: water as the packing solvent, the

particles were forced into the capillary tube by applying an initial pressure of 1000 psi after which the pressure was increased gradually to 3500 psi. When the packed bed reached at least 25 cm, a second frit was made approximately 24 cm from the first frit, again by sintering with the fusion splicer. After sintering, the pump was stopped and the pressure slowly allowed to decay to zero. Finally the capillary was reverse flushed (i.e. with the original frit at the inlet) in order to expel the loose packing downstream from the outlet frit. The section of capillary immediately downstream from the outlet frit served as the detection window. It was necessary to use a sharp knife to scrape away some of the polyimide cladding a short distance downstream from the frit in order to provide a fully unobstructed window for detection. The distance from the outlet frit to the point of detection was 1 mm or less for each column. The dimensions of the columns employed in this study are summarized in Table 4.1.

Table 4.1. Physical dimensions of capillary columns used in this study.

Packing Type (Nucleosil C18)		I.D. (μm)	L_{bed} (cm)	L_{tot} (cm)
d_p (μm)	Pore Diameter (Å)			
7	500	75	24.0	32.5
7	1000	75	24.0	32.6
7	4000	75	24.1	32.6

4.3.3 Capillary Electrochromatography

All CEC runs were conducted on a Hewlett-Packard ^{3D}CE instrument (Hewlett-Packard Co., Waldbronn, Germany) equipped for external pressurization. The instrument's standard photodiode array detector was used to monitor the UV absorbance of acetone at 280 nm. External pressure, typically 5 bar, was applied to the inlet and outlet mobile phase vials in all CEC experiments to minimize bubble formation. The capillary temperature was held at 25 °C. Acetone samples were prepared for each experiment by diluting HPLC grade acetone (1:10) v/v in the appropriate mobile phase and injected electrokinetically ($^{+}$5 kV, 3 s) onto the column. To minimize the possibility of sample focusing, the mobile phase used to prepare the acetone sample was identical to that used for the analysis. The retention time of acetone, an essentially unretained compound with no net electrophoretic mobility, was used to estimate the mobile phase linear velocity, μ. An approximate value for the diffusion coefficient for acetone in the mobile phase D_m was obtained using the Wilke-Chang equation [112] ($D_m = 3.1 \times 10^{-5}$ cm^{2}s^{-1}). Data points presented in the text represent the mean values from three replicate injections.

4.3.4 Physical Characterization of Nucleosil Packing Materials

Pore size distributions of the Nucleosil packing materials were investigated by mercury intrusion porosimetry. These analyses were performed by Micromeritics (Norcross, GA USA) using a Micromeritics AutoPore mercury porosimeter. Scanning

electron microscopy (SEM) images of the packings were obtained using an AmRay 3300 FE scanning electron microscope (AmRay, Bedford, MA USA).

4.3.5 Data Analysis

Chromatographic data were collected and processed using the Hewlett-Packard ChemStation software (Hewlett-Packard Co., Waldbronn, Germany), standard equipment on the instrument. Rate curves and others graphs were prepared with Microsoft Excel (Microsoft Corporation, Renton, WA USA). Analysis of the porosimetry data was performed using GraphPad Prism (GraphPad Software, Inc., San Diego, CA USA).

4.4 Results/Discussion

4.4.1 Physical Characterization of the Nucleosil Particles

The pore size distributions of the Nucleosil particles obtained by mercury porosimetry are shown in figure 4.3. Each material exhibited a broad, bimodal distribution, with a maximum at approximately 120 Å (mesopores) and another at some larger diameter (macropores), the exact value of which depended on the material. The second maxima in the distributions occur at approximately 600 Å, 800 Å, and 1600 Å, respectively for the 500 Å, 1000 Å, and 4000 Å (quoted) nominal pore sizes. These distributions show that although all the packings possess some amount of macropores (greater than 500 Å in diameter), expectedly the 1000 and 4000 Å media contain greater fractions of the largest pores (above 1500 Å). The characteristics of

these pore size distributions are important in accounting for the observed chromatographic behavior of these packing materials. The physical parameters gleaned from the porosimetry analyses of these materials are summarized in table 4.2.

Table 4.2. Physical characteristics of Nucleosil packings determined by mercury intrusion porosimetry

Nominal Pore Diameter (Å)	Cumulative Pore Volume (mLg^{-1})	ε_p	Median Pore Diameter (Å)
500	0.8820	0.69	620
1000	1.049	0.80	980
4000	0.7971	0.69	1580

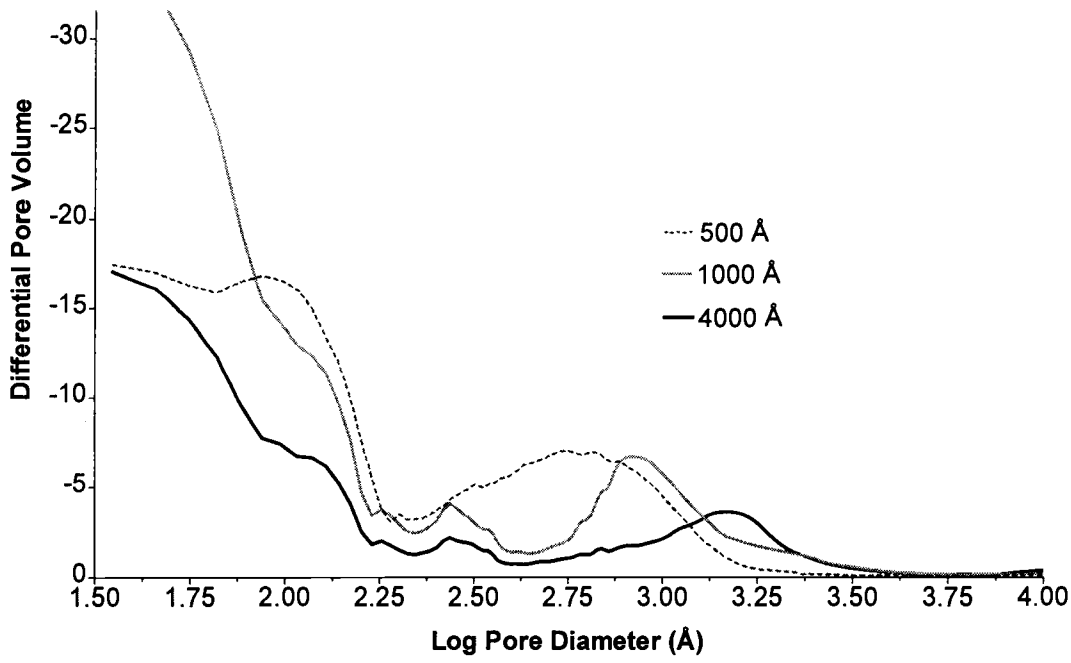

Figure 4.3. Pore size distributions of Nucleosil packings determined by mercury intrusion porosimetry.

These results are in agreement with those previously reported for 5 μm d_p macroporous Nucleosil particles performed by Tanaka, et al. [113]. Through mercury intrusion porosimetry and electron microscopy analyses, these workers showed that each nominal pore size of packing tested consisted of a mixture of different particles, each having distinct pore sizes and structures.

Scanning electron micrographs of the particles provided some useful insight into the pore structures of the packings used in this study. Images obtained for the 500, 1000, and 4000 Å nominal pore sizes are presented in figure 4.4 a-c. The corpuscular structure of these media, as well as the different types of particles present, is evident in these images. The preponderance of macroporous particles in the 1000 and 4000 Å packings, relative to the 500 Å, is clearly visible. In agreement with the porosimetry data, the 4000 Å packing (figure 3.4 c) appears to possess the greatest fraction of the largest pore size particles.

Transmission electron micrographs of 5 μm d_p Nucleosil particles [113] better illustrate the characteristic pore structures of these macroporous packings. The TEM images presented in figures 4.5 a and b of the 1000 and 4000 Å materials show that a large fraction of the pores are through-pores (500 Å were not analyzed by these workers).

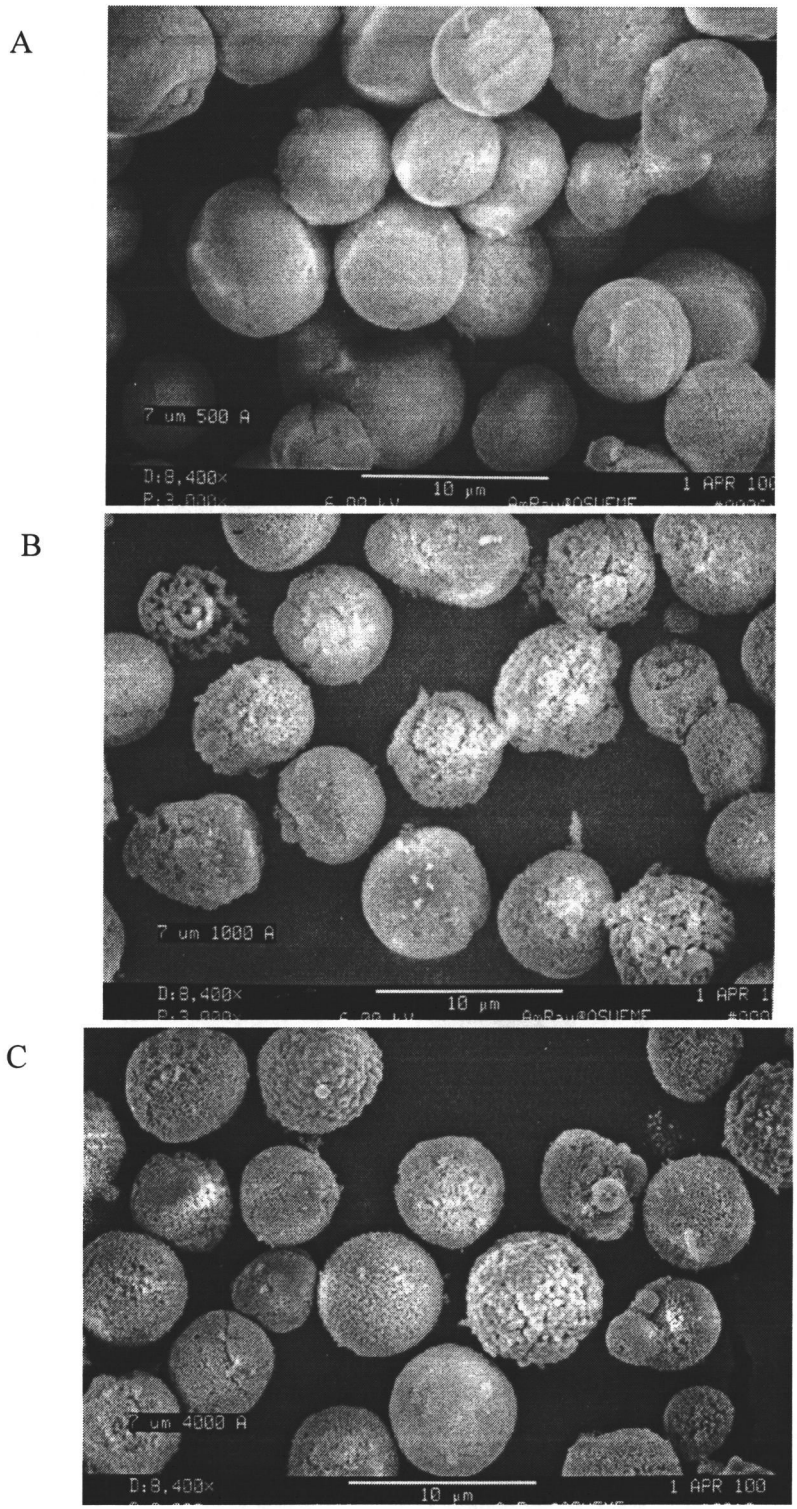

Figure 4.4. Scanning electron micrographs of the Nucleosil packings employed in this study. (A) 500 Å, (B) 1000 Å, (C) 4000 Å.

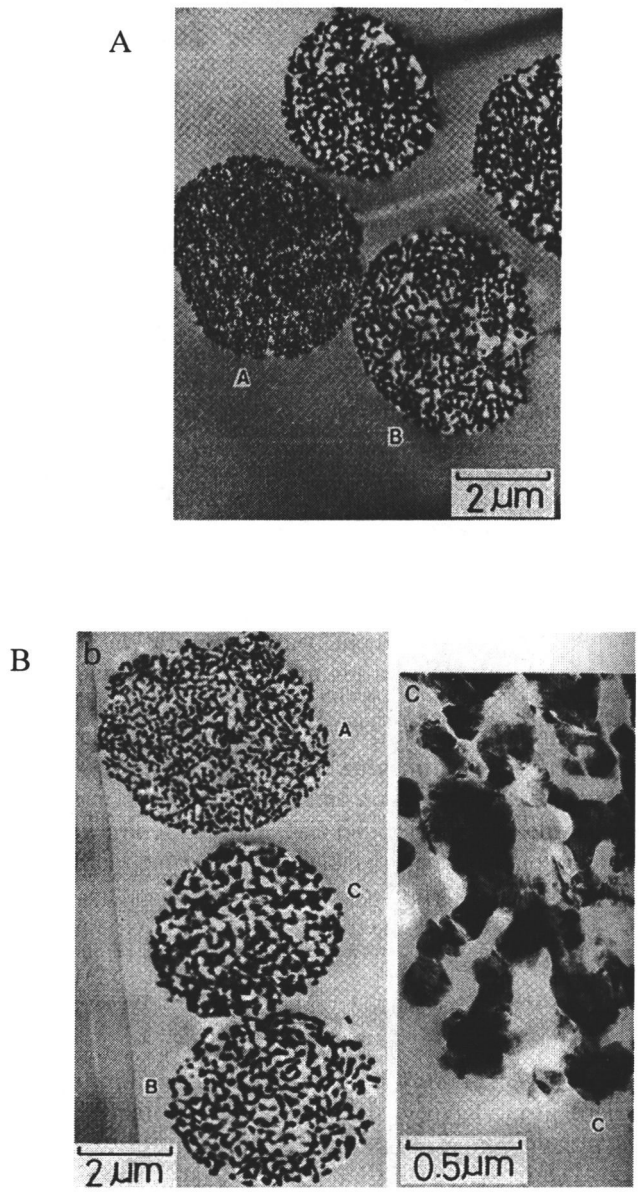

Figure 4.5. Transmission electron micrographs of 5 µm d_p Nucleosil particles. (A) 1000 Å, (B) 4000 Å. The letter notation (a-c) in the insets indicates the subtypes of particles that constitute each packing material. From [113] with permission from Elsevier Science.

4.4.2 Electrochromatography

Chromatographic results for the 500, 1000, and 4000 Å nominal pore diameter packings at various buffer concentrations are summarized in figures 4.6 a-c and 4.7 a-c in which reduced plate height h ($h = H/d_p$) is plotted against reduced velocity v ($v = \mu d_p/D_m$). In order to best illustrate the trends present in these data sets, the results are presented in two ways. In figure 4.6, findings for the three types of packings at 1, 50 and 100 mM Tris are plotted as series and grouped according to Tris concentration, while figure 4.7 shows the full data set with buffer concentrations plotted as series and grouped according to nominal pore size.

Several interesting features of these curves warrant an in-depth examination of these data. At the lowest Tris concentration, 1.0 mM, the curves differ in their shapes as well as relative positions on the y-axis. For the 500 and 1000 Å columns, a minimum in the curves is observed at $h \approx 1.2$ and 0.9 and $v \approx 3.6$ and 5.0 respectively. The 4000 Å capillary exhibited not only lower plate heights over the entire velocity range, but a flatter curve at high v with a barely discernable minimum at $h \approx 0.6$, $v \approx 6.8$. In view of the fact that the Nucleosil materials are of the same 7 μm nominal d_p (verified by SEM), these results suggest that there was some extent of intraparticle flow occurring at buffer concentrations as low as 1.0 mM. It should be noted that the maximum velocity in each of these data sets was obtained at the highest obtainable electric field strength (i.e. a potential of $^{+}30$ kV applied to the shortest length of column possible with the instrument used).

As the buffer concentration was increased to 10 mM, no improvement in plate height was seen for the 500 Å column (there was actually a modest increase in h_{min}).

In addition, the shape of the curve is roughly the same as that for the 500 Å – 1.0 mM Tris data set. For the 1000 Å column, h_{min} decreased slightly to around 0.8. The 4000 Å column, however, showed no plate height minimum up to $v \approx 7.0$, at which $h \approx 0.4$. The shape of this curve differs slightly from the 4000 Å-1.0 mM data set, with a lower h at a given v, especially at $v > 3.0$. Importantly, no minimum was observed in this curve. It can be inferred from the shape of this curve that a minimum, if it exists, will lie somewhat to the right of (i.e. at a higher velocity than) that observed for the 1.0 mM Tris buffer. Again, the limit of 30 kV, imposed by the instrument, precluded the investigation of higher velocities.

At 25 mM Tris, the curve generated by the 500 Å data set is scarcely different from the 500 Å – 1.0 mM curve. Although the lowest observed h for the 4000 Å – 25 mM curve was approximately equal to that of the 4000 Å 10 mM curve ($h \approx 0.4$), it was achieved at a lower v ($v \approx 5.6$ vs. 7.0). Thus, the shape of the curve again changed as Tris concentration was increased. A similar change in curve shape was observed for the 1000 Å – 25 mM data set where, relative to the 1000 Å – 10 mM and 1000 Å –1.0 mM data, the curve is shifted to lower h values with the divergence increasing with v. Additionally, the 1000 Å and 4000 Å curves begin to overlap, in particular at lower values of v, which suggests that on going from 10 to 25 mM Tris, the extent of change in the curve shape was greater for the 1000 Å column.

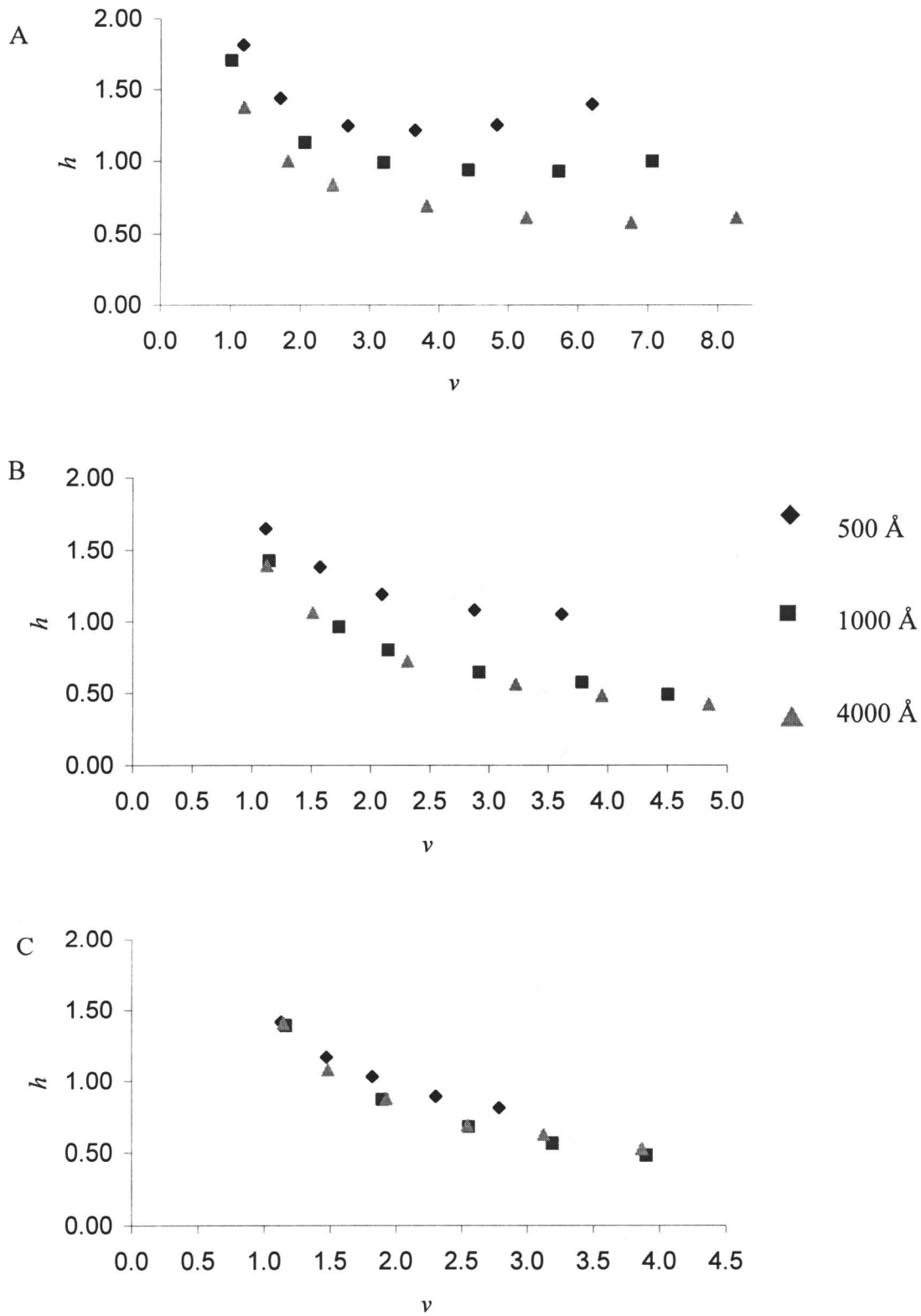

Figure 4.6. Rate curves: (A) 1.0, (B) 50, and (C) 100 mM Tris.

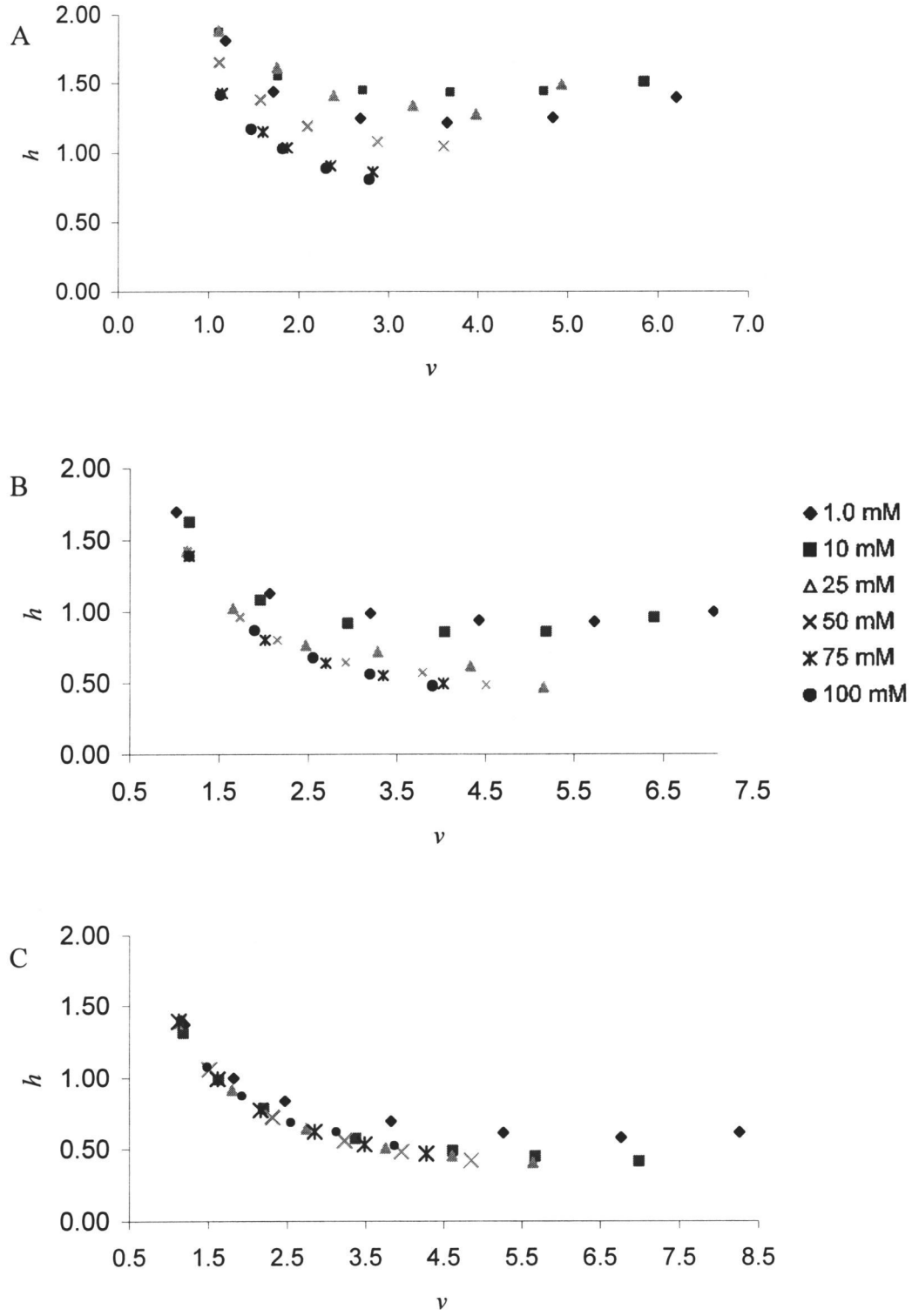

Figure 4.7. Rate curves: (A) capillary 1-500 Å pores, (B) capillary 2-1000 Å pores, and (C) capillary 3-4000 Å pores.

Increasing the Tris concentration to 50 mM resulted in a similar change in the shape of the 500 Å curve. The lowest observed reduced plate height of 1.0 was obtained at the maximum achievable reduced velocity, $\nu \approx 3.6$ with the curve bearing no observable h_{min}. With respect to the 1000 Å – 50 mM and 4000 Å – 50 mM data sets, further small changes in the curves, continuations of the same trend, were observed. Interestingly, the 1000 Å – 50 mM and 4000 Å – 50 mM curves are virtually superimposable, the latter with $h \approx 0.4$ at a relatively low $\nu \approx 4.8$.

At the highest Tris concentrations (75 and 100 mM), no noticeable changes in the 1000 Å and 4000 Å curves were observed. The 500 Å – 75 mM curve, however, showed a marked shift to lower h values, toward the 1000 Å – 75 mM and 4000 Å – 75 mM curves. This again appears to be an extension of the previous trends. At the maximum velocity $\nu = 2.8$, the reduced plate height was approximately 0.85, a significant decrease relative to results for the same column with 1.0 mM Tris. A further shift toward lower h and convergence with the larger pore sizes is seen for the 500 Å – 100 mM curve, where $h \approx 0.80$ was obtained at a maximum velocity of 2.8.

To summarize, at the most dilute buffer concentrations (i.e. 1.0 and 10 mM), the ability of the columns to generate a low plate height ranked according to the nominal pore size of the packing ($h_{500\,\text{Å}} > h_{1000\,\text{Å}} > h_{4000\,\text{Å}}$). The curves also exhibited different shapes, particularly in the high velocity regions, with the larger nominal pore sizes having the more shallow slopes. Increasing the Tris concentration resulted in changes in the shapes of the curves generated for each packing material, with the 1000 Å and 4000 Å curves starting to converge at a Tris concentration of 50 mM. Here a limiting point was reached for these larger pore packings, as no changes were apparent

as Tris was increased to 75 and 100 mM. Further changes, however, were observed for the 500 Å curves, which at 100 mM Tris had closely approached the curves for the larger pore sizes. It should be noted also that linear velocity versus field strength plots were obtained for each condition in the study. Thus Joule heating effects, even at 100 mM Tris, were determined to be negligible.

These data and the observed trends provide evidence of electroomosis in the pores of these particles. Moreover these results suggest that 1) a fraction of macropores exists in the 1000 Å and 4000 Å packings capable of supporting electroosmosis with Tris concentrations as low as 1.0 mM, and 2) the fraction supporting EOF can be increased, up to a point, by increasing the buffer concentration, thereby compressing the double layer.

The limiting behavior of the *h* vs. *v* curves can be rationalized as follows. Each type of packing possesses a certain fraction of macropores that can support EOF under the conditions of the experiment. At the most dilute buffer concentration, the benefit of lower *h* due to intraparticle flow, if any, will be most pronounced for the packing having the greatest fraction of the largest pores, in this case the 4000 Å packing. When the buffer is made more concentrated, compressing the double layer, improvements in *h* will be made as a greater number of smaller diameter pores can now support EOF. However a point is reached at which no further reduction in *h* is possible: flow exists in a large fraction of the available macropores. The buffer concentration at which this limiting point is reached is necessarily dependent upon the pore size distribution and average pore size of the packing; the larger pore media reach a limit at a lower buffer concentration relative to smaller pore sizes.

4.4.3 Application of Model

For illustrative purposes, values of the weighting factors χ_v and χ_e obtained for three representative pore size intervals, 100, 1000, and 4000 Å at different eluent buffer concentrations are provided in table 4.3. Values of δ derived using equation 2 for the range of Tris concentrations used are shown in table 4.4. In these calculations, a dielectric constant (ε_r) of 45, determined previously for (80:20) mixtures of acetonitrile and water [114], was assumed for each eluent.

Table 4.3. Weighting factors χ_v, χ_e, and χ_l for three of the 995 intraparticle pore size intervals used in the estimation of $d_{p,eff}$.

Nom. Pore Diam. (Å)	Pore Interval (d_{ch}) (Å)	χ_v (x 10^{-3})	χ_e			χ_l (x 10^{-4})			ε_{pore}
			1.0 mM	50 mM	100 mM	1.0 mM	50 mM	100 mM	
500	100	9.8	0.006	0.229	0.353	0.59	22	35	0.51
	1000	2.7	0.345	0.878	0.913	9.3	24	25	
	4000	0.06	0.789	0.969	0.978	0.31	0.38	0.38	
1000	100	5.9	0.006	0.229	0.353	0.35	14	21	0.54
	1000	3.1	0.345	0.878	0.913	11	27	0.28	
	4000	1.5	0.789	0.969	0.978	12	15	15	
4000	100	3.9	0.006	0.229	0.353	0.23	8.9	14	0.52
	1000	1.4	0.345	0.878	0.913	4.8	12	13	
	4000	1.9	0.789	0.969	0.978	15	18	19	

The pore diameter intervals and associated weighting factors shown in table 4.3 are three out of the 995 total intervals that represent the intraparticle pore space

considered in the model. It is at the lowest buffer concentration where the differences in the packings are most pronounced.

Table 4.4. Double layer thickness (δ) values at the Tris concentrations employed in the study calculated as described in the text. (Note: δ values reflect 1:5 dilution of Tris in acetonitrile.)

Nominal Tris Concentration (mM)	δ(Å)
1.0	224
10	70.7
25	44.7
50	31.6
75	25.8
100	22.4

Table 4.5. Values of $d_{p,eff}$ generated by the model.

Nominal Pore Diameter (Å)	$d_{p,eff}$ (μm)					
	1.0 mM	10 mM	25 mM	50 mM	75 mM	100 mM
500	5.81	4.84	4.57	4.40	4.32	4.26
1000	5.16	4.39	4.21	4.09	4.02	3.98
4000	4.96	4.37	4.24	4.15	4.11	4.08

The $d_{p,eff}$ values generated by the model are presented in table 4.5. It can be seen that the general trends observed in the experimental data are reflected also in the $d_{p,eff}$ values. For example, at the lowest Tris concentration, 1.0 mM, the model predicts a considerably higher contribution of intraparticle EOF for the 4000 Å

packing relative to the 500 Å, manifest in a smaller $d_{p,eff}$ value. In addition, $d_{p,eff}$ for the 1000 Å media lies between the 500 and 4000 Å. Examining once again the experimental data in figures 4.6 and 4.7, it is found that the model correctly predicts the trend $h_{500\text{ Å}} > h_{1000\text{ Å}} > h_{4000\text{ Å}}$ observed for 1.0 mM Tris. As Tris concentration is increased to 100 mM, the model further predicts the observed convergence of the rate curves for the three packing types. That the 1000 Å packing possesses a slightly smaller $d_{p,eff}$ than the 4000 Å material at this Tris concentration is a consequence of the preponderance of 800-1200 Å pores in the former, which at higher Tris concentrations can support EOF thereby weighting the average toward a smaller $d_{p,eff}$.

The $d_{p,eff}$ values generated by the model help to illustrate some practical implications of perfusive electroosmosis not obvious from the experimental data alone. In CEC, as in most chromatographic techniques, it is desirable not only to achieve high efficiencies, but to do so in a minimal amount of time. With the larger pore packings (1000 Å and 4000 Å) there is only a marginal decrease in $d_{p,eff}$ as Tris concentration is increased above 50 mM. However, EOF velocity decreases as the square root of buffer concentration, thus limiting the achievable linear velocity. There exists, then, a set of conditions that yields the optimum combination of speed and efficiency. Recall from the rate curves in figure 4.7 that no minimum was observed for 4000 Å packing for Tris concentrations as low as 10 mM. At 10 mM Tris, a very low h of 0.42 was obtained at a relatively high v of 7.0, at which the maximum potential of 30 kV of the instrument was applied. Clearly, this set of conditions offers the best combination of speed and efficiency, as evidenced by the separation of polyaromatic hydrocarbons (PAHs) in figure 4.8.

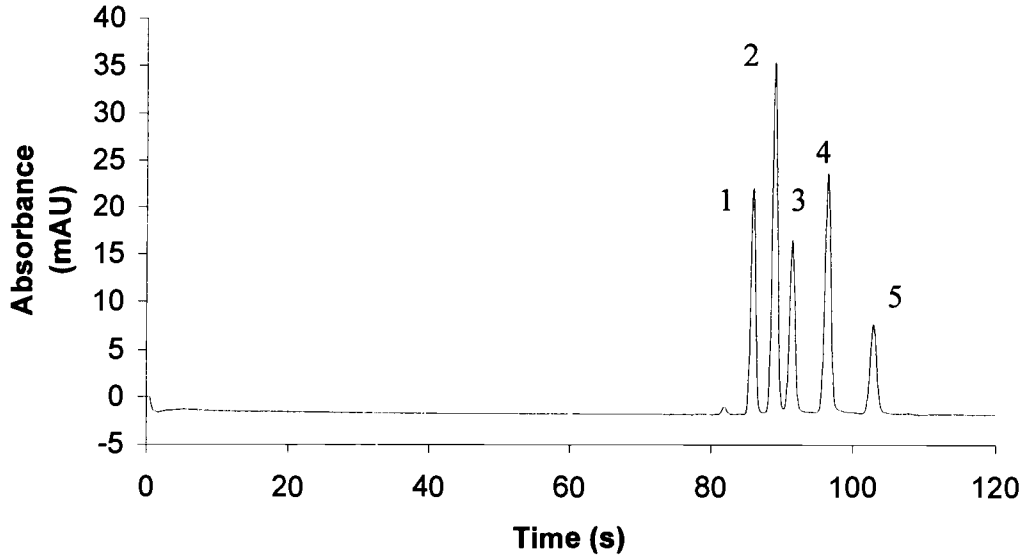

Figure 4.8. Separation of polyaromatic hydrocarbons on capillary 3 (4000 Å pores). Peaks: (1) naphthalene (308000 plates m^{-1}), (2) acenaphthene (289000 plates m^{-1}), (3) anthracene (272000 plates m^{-1}), (4) pyrene (264000 plates m^{-1}), (5) chrysene (237000 plates m^{-1}). Conditions: Mobile Phase: (20:80) 10 mM Tris pH 8.0: acetonitrile; Separation Voltage: +30 kV; $\mu = 3.1$ mm s^{-1}. Injection: +3 kV, 3 s; Detection: UV 230 nm; Capillary Dimensions: as indicated in table 4.1; Sample: 75 µg/mL each compound in mobile phase.

One advantage to expressing the contribution of intraparticle flow in these macroporous packings in terms of an effective particle diameter, rather than effective channel diameter, is the ability to generate rate curves in more familiar terms. In addition, reduced parameters based on $d_{p,eff}$ should allow for a more accurate assessment of the relationship between h and v, than do parameters based on nominal d_p.

To that end, the experimental rate curves obtained for the three columns were replotted with h and v values determined by scaling to the appropriate $d_{p,eff}$ values. These are shown in figure 4.9.

If the improvements in plate height with increasing perfusive character of the packings were attributable solely to a decrease in effective particle diameter, the rate curves of the "effective" reduced parameters for a given column should be quite similar regardless of Tris concentration. That is, normalization of plate height and linear velocity to $d_{p,eff}$ should account for the observed differences in efficiency. This, however, is not observed. Inspection of the curves in figure 4.9 reveals that the curves exhibit a trend similar to the "uncorrected" data shown in figure 4.7. With the exception of one anomalous data set, the 500 Å – 1.0 mM Tris, the curves tend toward lower h values as Tris concentration increases.

It is interesting to note that the degree of difference in the "effective" rate curves in figure 4.9 appears to correlate inversely with the pore size of the packing. That is, the differences are most pronounced for the 500 Å material and least so for the 4000 Å. As shown previously, the 4000 Å packing exhibited the highest perfusive character at the lowest Tris concentration of 1.0 mM; it is possible that larger differences exist at lower buffer concentrations.

It can be concluded from this data that reductions in $d_{p,eff}$ with increased perfusion alone do not explain the observed plate height improvements. The differences in the rate curves in figure 4.9 imply that increasing the perfusive character of the packing causes the column not only to take on the characteristics of a bed of smaller particles, but a bed of more tightly packed particles.

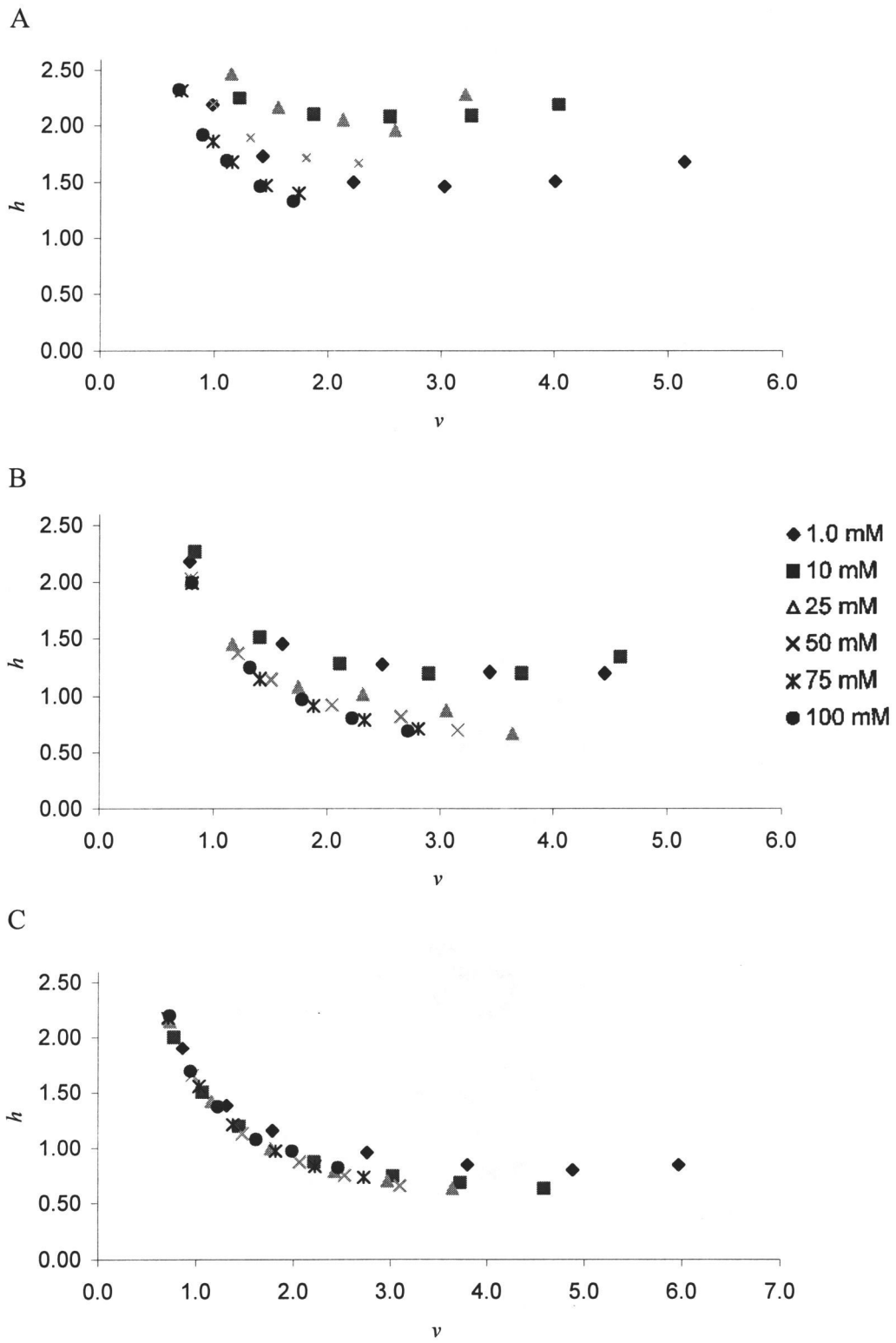

Figure 4.9 Rate curves with reduced parameters calculated based on $d_{p,eff}$. (A) Capillary 1, 500 Å pores; (B) capillary 2, 1000 Å pores; capillary 3, 4000 Å pores.

The Knox equation, $h = Av^{1/3} + B/v + Cv$, is a semi-empirical equation used to describe the behavior of rate curves in packed column liquid chromatography [107]. The A term in this expression includes the coupled effects of eddy diffusion and mobile phase mass transfer, the B term longitudinal molecular diffusion, and the C term stationary phase and stagnant mobile phase mass transfer effects. It is evident from the curves in figure 4.9 that differences in the magnitude of plate height coefficients A and C exist (the curves converge in the low velocity B term dominated region). Although a lower C term with increased perfusion is not surprising owing to stagnant mobile phase effects, the shapes of the curves and range of velocities tested suggest that the disparity in the curves is due primarily to differences in the A term of the plate height equation. Differences in the A term may arise from geometric effects in the intraparticle flow channels, perhaps the result of lower tortuosity factors for the wider pore media. In such cases, a decreased multipath (eddy diffusion) contribution to h may result. Values of the plate height coefficients can be obtained by curve fitting, usually with the Knox equation. However, to yield meaningful values requires a wider range of velocities (i.e. the inclusion of higher velocities) than was possible in this study. In principle, if $d_{p,eff}$ is precisely known, improvements in the plate height coefficients, if any, can be discerned.

4.5 Conclusion

Improved chromatographic efficiency with increasing perfusive character of the packing medium was observed with commercially available reversed phase

packings and typical CEC eluents. Experimental rate curves obtained for the larger pore packings, 4000 and 1000 Å Nucleosil, suggest the presence of intraparticle EOF at buffer concentrations as low as 1.0 mM. From a practical point of view, the experimental data indicate that optimum chromatographic performance (i.e. speed and efficiency) can be achieved with macroporous packings and relatively low buffer concentrations.

The extent of intraparticle EOF under a range of eluent conditions was estimated and expressed in terms of an effective particle diameter. Although this model predicts the trends in the data, it is difficult to assess the accuracy of the $d_{p,eff}$ values it yields. Rate curves of reduced parameters calculated with $d_{p,eff}$ values indicate that in addition to a smaller effective particle diameter, wide pore media operated under perfusive conditions may yield lower A term (possibly tortuosity dependent) contributions to plate height.

5. Assessment of Intraparticle Flow Permeability of Capillary Chromatographic Columns using Electrical Conductivity

Vallano, P.T.; Remcho, V.T., Submitted to *Journal of Physical Chemistry B*, September 2000, in press.

5.1 Introduction

Intraparticle, or perfusive electroosmosis is known to improve column performance in CEC. Specifically perfusive EOF leads to substantially increased efficiencies and shorter analysis times due to a decrease in the effective particle diameter and a smaller stagnant mobile phase contribution to plate height [115].

The structure and uniformity of the packed bed are of critical importance to the performance of a chromatographic column, particularly with respect to band broadening. Variations in packing density between regions of the packed bed give rise to flow velocity induced broadening of peaks, one of the phenomena associated with eddy diffusion [3]. A highly variable packing structure amplifies this effect and can severely limit column performance. As noted in chapter 1, one of the advantages of packed column CEC over capillary HPLC is that the former is much less susceptible to this type of velocity inhomogeneity. Under typical CEC operating conditions, EOF velocity is essentially independent of flow channel diameter, and thus will vary only slightly between more or less densely packed regions of the column. Nevertheless, packing uniformity remains vitally important in CEC if efficiency and peak capacity are to be maximized.

[113] and confirmed in our laboratory for macroporous Nucleosil particles produced by Macherey-Nagel (Duren, Germany) reveal that a given packing consists of multiple subtypes of particles that vary in morphology. Information gleaned from the physical characterization of these packings as well as from packed column conductivity data could provide insight into the following: 1) the approximate pore diameter below which ion transport is minimal, and, potentially, above which pores act as "through-pores"; and 2) differences in the packings with respect to geometric impediments to ion transport, perhaps arising from tortuosity, that affect intraparticle current flow. The assumed operating principle is that the extent of intraparticle current transport in columns packed with macroporous particles could be useful in providing a measure of flow permeability *through* such particles under conditions where the double layer thickness is small relative to the mean pore diameter.

Using the conductivity of a CEC column as a means to evaluate intraparticle permeability requires that the electroosmotic contribution to current flow, which results from ion transport within the electrical double layer, be small relative to the current flow in the bulk solution. To obtain a precise value of the electroosmotic current contribution in a packed column would be an exceedingly complex endeavor, thereofore in this work we make use of a capillaric model in which the column is treated as a bundle of parallel cylindrical capillary tubes of varying diameter, for which a series of equations describing current flow has been well established [108]. As will be seen, the values predicted by the model in combination with the experimental data indicate that electroosmotic current can indeed be neglected in this study.

5.2 Theory

The magnitude of electrical current I_p transported through a tube packed with chromatographic particles is lower than that in an open tube I_o of the same diameter due to two factors. First, a decrease in conductance results from a reduction in the free cross sectional area of the packed tube by a factor ε (the porosity) relative to an open tube. The conductance of the packed tube is further reduced by a decrease in effective ion mobilities arising from geometrical constraints. As described by Boyack and Giddings [117], this latter effect can be expressed in terms of a ratio of effective and free solution ion mobilities, termed the obstruction factor ξ, which includes a tortuosity term T and a constrictive factor C.

$$\xi = C T^{-2} \qquad (5.1)$$

The tortuosity term T^{-2} accounts for the reduction in effective migration rate due to nonalignment of flow channels with the field axis. This nonalignment acts to decrease the effective electric field strength and increase migration distance per unit displacement along the tube axis, hence the squared dependence on T. The constrictive factor C represents the reducing effect of channels of differing cross sectional area on electric field strength.

Accounting for these effects, the conductance of a packed tube G_p is decreased a factor $\varepsilon\xi$ relative to an open tube of identical diameter G_o. In a chromatography column packed with nonporous particles, the total porosity ε_{tot} is equal to the interstitial porosity ε_i, thus

$$G_p = G_o \varepsilon_i \xi \qquad (5.2)$$

Equation 5.2 can be written in terms of conductivity and rearranged as follows

$$\frac{\kappa_p}{\kappa_o} = \varepsilon_i \xi \qquad (5.3)$$

where κ_p and κ_o are conductivities of the packed and open tubes, respectively.

In practice, it is difficult to obtain precise values of C and T, thereby limiting the utility of equation 5.3. As a result, semi empirical relationships have often been used to describe the conductivity of porous media, in which the ratio κ_p/κ_o is usually expressed as a function of porosity [118-121].

As in HPLC, most packing materials used in CEC are porous and as such transport of ions through as well as around the particles is possible. If macroporous packings are employed that possess a large fraction of through-pores compared to conventional porous particles, significant current flow through the particles might be expected. In such cases, where intraparticle as well as interparticle current transport is important, increased κ_p/κ_o values would be expected.

In the presence of electroosmotic flow (EOF), charge transport within the electrochemical double layer contributes to the total current in the CEC column. In their thorough treatment of electroosmosis in cylindrical capillary tubes, Rice and Whitehead derived the following expression for the magnitude of electoosmotic current [108].

$$I_e = I_b \frac{(\varepsilon_0 \varepsilon_r \zeta \kappa)^2}{\eta C \Lambda_b} \left[-1 + \frac{2 I_1(\kappa a)}{\kappa a I_0(\kappa a)} + \frac{I_1^2(\kappa a)}{I_0^2(\kappa a)} \right] \qquad (5.4)$$

in which I_e is the electroosmotic current, I_b is the current in the bulk solution, ε_0 is the permittivity of vacuum, ε_r is the dielectric constant of the bulk solution, ζ is the zeta

potential, κ is the reciprocal of the double layer thickness, η is the solution viscosity, C is the molar concentration of electrolyte, Λ_b is the molar conductivity of the bulk solution, and a is the radius of the capillary tube. I_0 and I_1 are zero and first order, respectively, modified Bessel functions of the first kind. Equation 5.4 is limited by the use of the Debye-Hückel approximation for a (1:1) electrolyte and as such is valid only for low values (<100 mV) of ζ.

The ratio I_e/I_b, termed the relative conductivity λ, can be expressed in terms of the following equation, which was derived from the Rice and Whitehead equations by Wan [111].

$$\lambda = \frac{2\varepsilon_0\varepsilon_r F^2}{\Lambda_b RT}\zeta^2\left[-1+\frac{2I_1(\kappa a)}{\kappa a I_0(\kappa a)}+\frac{I_1^{\,2}(\kappa a)}{I_0^{\,2}(\kappa a)}\right] \qquad (5.5)$$

Estimations of λ for the different columns and eluent conditions employed in this study were obtained as follows. The general structure of a model previously published [115] and described in detail in chapter 4 was employed to calculate a volume averaged packed bed conductivity $\bar{\lambda}$. Briefly, pores with diameters ranging from 50- 10000 Å were partitioned into 995 intervals of width 10 Å. From pore size distributions for the packings obtained by mercury intrusion porosimetry, the fraction of total column void volume contributed by each pore interval was determined. In these calculations, an interstitial porosity of 0.4 was assumed [3]. The volume fractions determined for the intraparticle pore intervals and the interstitial region were subsequently used as weighting factors to obtain volume averaged relative conductivity values for each column at each of the three buffer concentrations used. Treating each of the columns as comprising a bundle of capillary tubes of varying

diameter, equation 4 was used to calculate the relative conductivity for each pore interval and for the interstitial space. The zeta potential was estimated for each column and buffer concentration from electroosmotic mobility measurements [114] and assumed to be equal on the outer particle surface and on surfaces within the pores. For the intraparticle pores, channel radius a was set equal to the midpoint of the pore radius interval, e.g. pores in the diameter range 290-300 Å were assigned a = 147.5 Å. For the interstitial space, the relation $d_{ch} = 0.28\ d_p$ [111] was used to estimate channel diameter from particle diameter (d_p) assuming a uniform, well packed bed. Volume fraction weighting factors χ_v, calculated for each pore interval and the interstitial space, were subsequently used in the determination of a volume averaged relative conductivity as indicated below.

Intraparticle Contribution *Interstitial Contribution*

$$\bar{\lambda} = \frac{\chi_{v1}\lambda_1 + \ldots + \chi_{v995}\lambda_{995} + \chi_{v\,\mathrm{int}}\lambda_{\mathrm{int}}}{\chi_{v1} + \ldots + \chi_{v995} + \chi_{v\,\mathrm{int}}} \qquad (5.6)$$

5.3 Experimental

Concentrated hydrochloric acid (37%) was purchased from Mallinckrodt, St. Louis, MO USA. Ultrapure grade (99.9+%) tris (hydroxymethyl) aminomethane (Tris) was obtained from Aldrich Chemical, Milwaukee, WI USA. HPLC grade acetonitrile was purchased from Fisher Scientific, Pittsburgh, PA USA. Water was thoroughly filtered and deionized using a Barnstead Series 582 water purification system (Barnstead/Thermolyne Corporation, Dubuque, IA USA). Fused silica

capillary tubing of 75 μm I.D., 360 μm O.D., was purchased from Polymicro Technologies, Inc., Phoenix, AZ USA. Nucleosil C18 silica particles (d_p = 7 μm) with nominal pore diameters of 100, 300, 500, 1000, and 4000 Å were obtained from Meta Chem Technologies, Torrance, CA USA.

The desired concentrations of Tris buffer were obtained by preparing a 100 mM solution of Tris (base form) adjusted to pH 8.0 by titration with concentrated HCl. This buffer solution was subsequently diluted in deionized H_2O to yield 50 and 25 mM solutions. The concentration of protonated Tris (acid form), necessary for double layer thickness calculations, was estimated using the Henderson-Hasselbach equation (in this system, ionic strength I is essentially equal to the concentration of Tris in the acid form). Appropriate volumes of each buffer were mixed with acetonitrile to yield (20:80) (v/v) Tris: acetonitrile solutions, the final buffer concentrations of which were 20, 10 and 5 mM. These solutions were employed as eluents in the capillary electrochromatography experiments.

Packed capillary columns were prepared using the slurry packing procedure described in chapter 4. The physical dimensions of the columns used in this study are illustrated in Table 5.1.

Current measurements were conducted using a Hewlett-Packard ^{3D}CE instrument (Hewlett-Packard Co., Waldbronn, Germany) equipped for external pressurization. During the runs, an external pressure of 5 bar was applied to the inlet and outlet mobile phase vials to minimize bubble formation within the capillary. A capillary temperature of 25 °C was maintained during the experiments. Current data was collected with the Hewlett-Packard Chemstation software package at a sampling

rate of 100 points min^{-1}. The data presented in the text represent the mean value of a minimum of 150 data points.

Table 5.1. Physical dimensions of the capillary columns used in this study. All packings were Nucleosil ODS 7 μm particle diameter. For each column: ID: 75 μm OD: 360 μm.

Nominal Pore Diameter of Packing (Å)	L_{bed} (cm)	L_{tot} (cm)
100	24.5	33.0
300	24.0	32.5
500	24.0	32.5
1000	24.0	32.6
4000	24.1	32.6

Pore size distributions of the Nucleosil packing materials were investigated by mercury intrusion porosimetry. These analyses were performed by Micromeritics Instrument Corporation (Norcross, GA USA) using a Micromeritics AutoPore mercury porosimeter. Analysis of the porosimetry data was performed using GraphPad Prism (GraphPad Software, Inc., San Diego, CA USA) and Microsoft Excel (Renton, WA USA) software. Scanning electron micrographs were obtained using an AmRay 3300 FE scanning electron microscope (AmRay, Bedford, MA USA).

5.4 Results and Discussion

As is the case with most CEC columns, the capillaries in this study consisted of a packed bed and an open section on which detection is performed. Because the total column conductivity κ_t is the directly measurable quantity in these experiments, it was necessary to determine κ_p, the conductivity of the packed bed, by indirect means. With the assumption that the current is uniform over the length of the capillary and that the system obeys Ohm's law, κ_p can be expressed in terms of measurable quantities as follows

$$\kappa_p = \left[\frac{L_t}{L_p \kappa_t} - \frac{L_o}{L_p \kappa_o} \right]^{-1} \tag{5.7}$$

in which L_t is the total column length, L_p is the packed bed length, L_o is the open section length, and κ_o is the conductivity of the open section. κ_o was determined through a separate set of experiments using an open fused silica capillary tube of the same internal diameter and same lot of tubing as the packed columns.

At the outset, a review of the estimated contributions of electroosmotic conductivity is in order. In table 5.2, volume averaged relative conductivity values are presented. Most of the values are below 0.02 and in all cases are less than 0.04. At the highest Tris concentration of 20 mM, the relative conductivity values are 0.0013 or less for each of the columns. On this basis, it can be concluded that differences in κ_p/κ_o values are attributable primarily to ion transport in the bulk solution.

Table 5.2. Volume averaged relative conductivity values for the packed columns calculated as described in the text.

Column	Volume Averaged Relative Conductivity		
	5 mM Tris	10 mM Tris	20 mM Tris
100 Å	0.018	0.013	7.2×10^{-5}
300 Å	0.029	0.020	0.0013
500 Å	0.038	0.012	7.2×10^{-5}
1000 Å	0.025	0.017	1.2×10^{-4}
4000 Å	0.024	0.015	9.2×10^{-5}

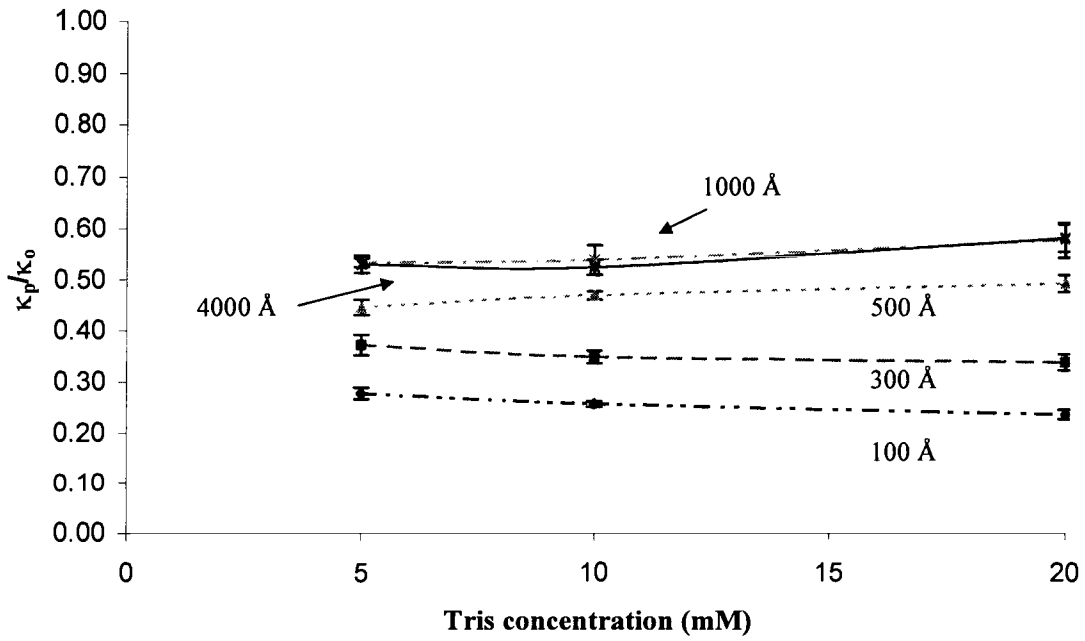

Figure 5.1. κ_p/κ_o values as a function of Tris concentration for the five packed capillary columns. Error bars indicate ± 1 standard deviation.

The κ_p/κ_o values obtained for the series of capillaries at Tris concentrations of 5, 10, and 20 mM are plotted in figure 5.1. An important observation regarding the

shape of the plots is that, within experimental error, the κ_p/κ_o ratio is essentially independent of Tris concentration, as evidenced by the shapes of the curves. This observation is critical in that it supports the assertion that electroosmotic conductivity is negligible under these conditions. Were it not, variation in the conductivity ratio with Tris concentration would be expected. Increasing the buffer concentration will compress the double layer resulting in a decreased zeta potential (as well as an increased electrokinetic radius), which equations 5.4 and 5.5 predict will affect the extent of electroosmotic current, specifically a decrease in λ with increasing Tris concentration due to the squared dependence on ζ. The shapes of the curves permit the κ_p/κ_o values for each column to be averaged; these values are shown in the table 5.3.

It can be seen that as the nominal pore size of the packing increases from 100 to 1000 Å, κ_p/κ_o values increase. Between the 1000 and 4000 Å packings, however, no noticeable difference exists. It is interesting to note that the κ_p/κ_o values for the widest pore media (1000 and 4000 Å) exceed those of the smallest (100 Å) by a factor of approximately 2. The fact that the nominal particle diameters of these packings are identical (d_p = 7 μm), and that the columns were packed using the same procedure, allows the assumption to be made that the interstitial porosities of the five columns are essentially identical. On this basis it can be concluded that the differences in the κ_p/κ_o values are due to the extent of intraparticle current flow. Comparison of these experimentally determined values with those predicted from various theoretical and

semi-empirical expressions derived for porous media consisting of hard spheres provides a method for testing this hypothesis.

Table 5.3. Experimental and theoretical κ_p/κ_o values. Theoretical values calculated using the equations above in which $\varepsilon_i = 0.4$ and $\theta = 1 - \varepsilon_i$.

Column	$(\kappa_p/\kappa_o)_{exp}$	$(\kappa_p/\kappa_o)_S$	$(\kappa_p/\kappa_o)_{BG}$	$(\kappa_p/\kappa_o)_{MT}$
100 Å	0.26 ± 0.02			
300 Å	0.35 ± 0.02			
500 Å	0.47 ± 0.02	0.28*	0.26*	0.29*
1000 Å	0.55 ± 0.03			
4000 Å	0.55 ± 0.03			

*Pore size independent values

S = Slawinski equation [118]:

$$\frac{\kappa_p}{\kappa_o} = \frac{\varepsilon_i}{(1.3219 + 0.3219\varepsilon_i)^2}$$

BG = Boyack-Giddings equation [117, 121]:

$$\frac{\kappa_p}{\kappa_o} = \varepsilon_i C T^{-2}$$

$$T = 1 + 0.173(1 - \varepsilon_i)$$

$$C = (1-\theta)^{-1}\left[\frac{1+\theta}{(1-\theta^{0.67})}\right]^{-1}$$

MT = Meredith-Tobias equation [120]:

$$\frac{\kappa_p}{\kappa_o} = 8\frac{(2-\theta)(1-\theta)}{(4+\theta)(4-\theta)}$$

Table 5.3 shows experimental κ_p/κ_o values in addition to those determined using three equations found in the literature. The calculated values were determined

by neglecting particle porosity and assuming $\varepsilon_i = 0.4$. Immediately apparent is that the κ_p/κ_o values for the 100 Å packing agree quite well with each of the three calculated values (from theory). Additionally, the 100 Å data closely approach experimental values obtained by Van Der Put and Bijsterbosch [122] for spherical polystyrene particles ($\kappa_p/\kappa_o = 0.28 \pm 0.02$). The agreement between these values implies that intraparticle ion transport is indeed negligible for the 100 Å packing. The larger pore sizes, however, differ significantly from the predicted conductivity values. It is evidently intraparticle current that results in the increased conductivities of the columns packed with larger pore particles.

In wide pore media, the free cross sectional area contributed by current-carrying pores will have the effect of increasing κ_p/κ_o. In this case an effective total porosity ε_t' is needed to replace ε_i in equation 5.3. The effective porosity is greater than ε_i and simply represents the combined contributions of the interstices and the current carrying intraparticle through-pores to the overall free cross sectional area. In principle, differences in intraparticle pore geometry and connectivity for the various packing materials could result in larger obstruction factors for some media, further increasing κ_p/κ_o.

It could be argued that the free cross sectional area available for current transport should be calculated based on the total column porosity ε_t. This, however, assumes that ion transport can occur in any pore, regardless of size or connectivity. Furthermore, the data obtained for the 100 Å column show that although the particles

have a considerable porosity (ε_p = 0.5 determined by mercury intrusion porosimetry), intraparticle current is negligible. Therefore, inclusion of pores of this size for the 100 Å column would not yield an accurate method of normalization.

Although a precise assessment of pore connectivity in these packings would be at best a formidable task, pore size distribution data and κ_p/κ_o values can be used to estimate the diameter above which the intraparticle pores are likely to transport current. Intuitively, it would be expected that larger diameter pores have a greater probability of extending through the particles. Following this reasoning, packings with a greater fraction of large pores would be expected to exhibit higher values of κ_p/κ_o.

Pore size distributions, median pore diameters and particle porosities (ε_p) for the packings determined by mercury intrusion porosimetry are shown in figure 5.2. With the exception of the 100 Å media, the distributions are bimodal, having one maximum at approximately 120 Å and another at some larger diameter, the value of which varies with the material. The wide pore HPLC packings employed in this study have been shown to comprise a mixture of particle types [113]; the shapes of the distributions reflect the heterogeneity of the materials. From the pore size distribution data and table 5.3, it is evident that κ_p/κ_o increases with the median pore size of the packings up to 1000 Å. No significant difference exists between the 1000 Å and 4000 Å columns. Interestingly, a median pore diameter of approximately 1600 Å, significantly different from the nominal value, was determined for the 4000 Å packing. This likely accounts for the high degree of similarity in κ_p/κ_o values between the 1000 and 4000 Å columns.

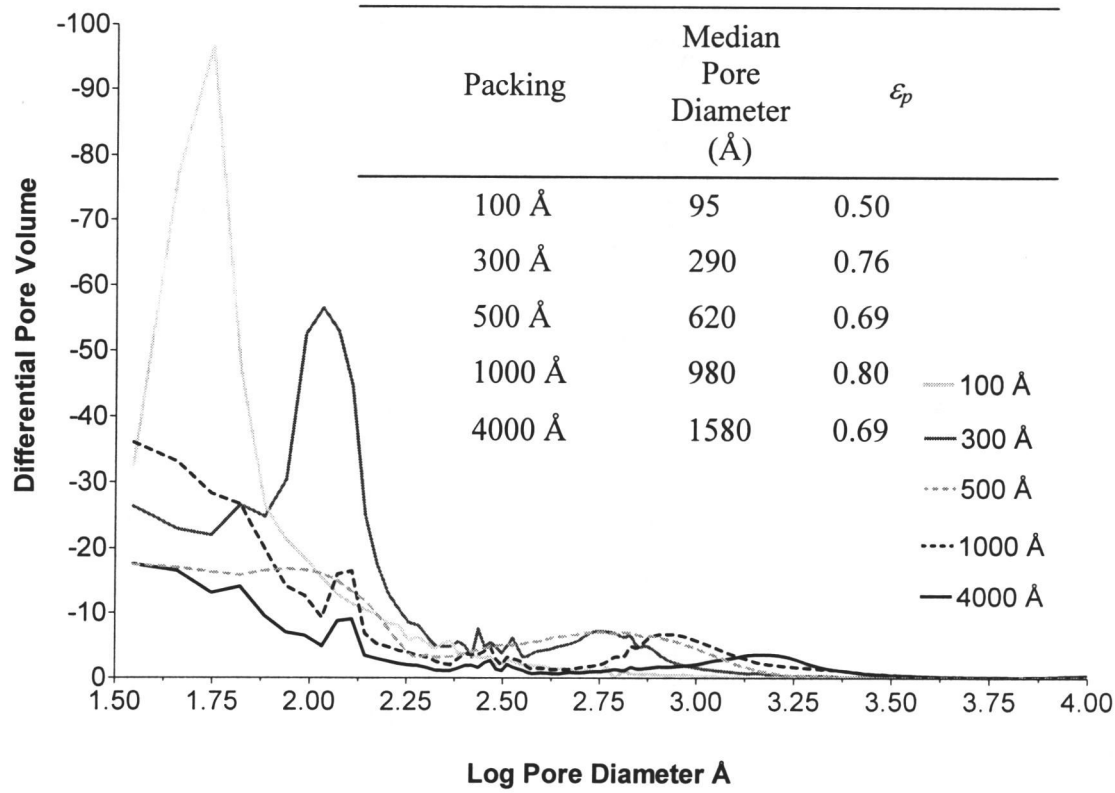

Figure 5.2. Pore size distributions for the packings determined by mercury intrusion porosimetry.

These data allow the estimation of an "effective" total porosity, which, in addition to the interstitial volume, includes only the fraction of intraparticle void volume contributed by putative intraparticle through-pores in each column. Values of effective total porosity ε_t' were determined by first selecting a cutoff pore diameter below which current transport was assumed to be negligible. It has been shown previously (table 5.3) that current flow in the 100 Å capillary occurs nearly exclusively in the interstitial region. Therefore, the pore size distribution of this

packing was used as the basis from which to assign a cutoff point. Specifically, the range of pore sizes contributing most to the cumulative pore volume of the 100 Å pore size packing were assumed not to participate in current transport. To this end, and to evaluate results at different cutoff points, three cutoffs, at 300, 500, and 700 Å, were chosen. From the pore size distribution data, effective particle porosity ε_p' values were determined by neglecting the volume contribution of pores below each cutoff. Setting $\varepsilon_i = 0.4$ and using the following relation, values of ε_t' were subsequently obtained.

$$\varepsilon_t' = \varepsilon_i + \varepsilon_p'(1 - \varepsilon_i) \tag{5.8}$$

In table 5.4 the fractions of intraparticle pore volume contributed by pores below each cutoff diameter are shown for each packing material. Additionally, values of ε_t', calculated for each column by truncating at the appropriate pore diameter (300, 500, or 700 Å) are provided.

Table 5.4. Intraparticle pore volume fraction contributed by pores below the cutoff diameter and effective total porosity ε_t' values for the columns employed in the study.

Column	Intraparticle Volume Fraction Below Cutoff			ε_t'		
	300 Å	500 Å	700 Å	300 Å	500 Å	700 Å
100 Å	0.78	0.84	0.88	0.47	0.45	0.44
300 Å	0.52	0.61	0.74	0.63	0.58	0.52
500 Å	0.28	0.40	0.56	0.70	0.65	0.58
1000 Å	0.26	0.30	0.35	0.77	0.75	0.72
4000 Å	0.18	0.22	0.24	0.75	0.74	0.72

As expected, the pore volume fraction below each cutoff is greatest for the 100 Å packing. For example, 84% of the cumulative pore volume falls below the cutoff diameter of 500 Å for the 100 Å packing, versus 22% for the 4000 Å material.

The effective total porosity values were next used to calculate obstruction factors for the columns. Rearranging equation 3 and substituting ε_t' for ε_i yields the following expression for the obstruction factor.

$$\xi = \frac{\kappa_p}{\kappa_o \varepsilon_t'} \tag{5.9}$$

Table 5.5. Obstruction factors for the capillary columns.

Column	$\xi \pm$ s.d		
	300 Å cutoff	500 Å cutoff	700 Å cutoff
100 Å	0.55 ±0.05	0.58 ±0.05	0.59 ±0.05
300 Å	0.56 ±0.03	0.60 ±0.04	0.67 ±0.03
500 Å	0.67 ±0.04	0.72 ±0.04	0.81 ±0.05
1000 Å	0.71 ±0.04	0.73 ±0.04	0.76 ±0.04
4000 Å	0.73 ±0.05	0.74 ±0.05	0.76 ±0.05

If the trends in experimental κ_p/κ_o values were due solely to differences in free cross sectional area available for current flow, then any variation in obstruction factors for the five columns should be insignificant. Although the values presented in table 5.5 do show a degree of convergence, they are seen to fall into two groups. At each cutoff, no difference exists, within experimental error, between obstruction factors for the 100 and 300 Å columns or the 500, 1000, and 4000 Å columns. Again invoking

the assumption that intraparticle current in the 100 Å column is negligible, it is evident that the discrepancies in conductivity ratios cannot be accounted for solely by differences in free cross sectional area.

Scanning electron micrographs of the packings are shown in figure 5.3, in which the particle subtypes present in each material are visible. With these images, several important observations regarding the morphology of the packing particles can be made. First, the particles comprising the packings can be divided into three general subtypes: narrow pore particles having a smooth appearance; intermediate pore size with a spongy appearance; and a wide pore subtype having a rough surface.

Expectedly, the 1000 and 4000 Å media contain a significant fraction of the wide pore subtype. These particles appear to have a more open structure relative to the other subtypes and are absent in the narrow pore packings. These images, as well as the results of transmission electron microscopic analysis of these packings [113], provide evidence that the wide pore subtype consists largely of through-pores. (TEM images of 1000 and 4000 Å Nucleosil packings from [113] are shown in figure 4.5.) The 100 Å packing, in contrast, appears more homogenous, consisting only of the smooth particles. These narrow pore smooth particles predominate in the 300 Å packing as well, although the intermediate subtype is also visible. Lastly, a mixture of smooth and intermediate pore size particles is found in the 500 Å packing. It is important to note that the fraction of smooth particles is less in the 500 Å packing than in the 300 Å. The conductivity data imply that current transport occurs through the intermediate particle subtype (i.e. to an appreciable extent, these pores behave as through-pores).

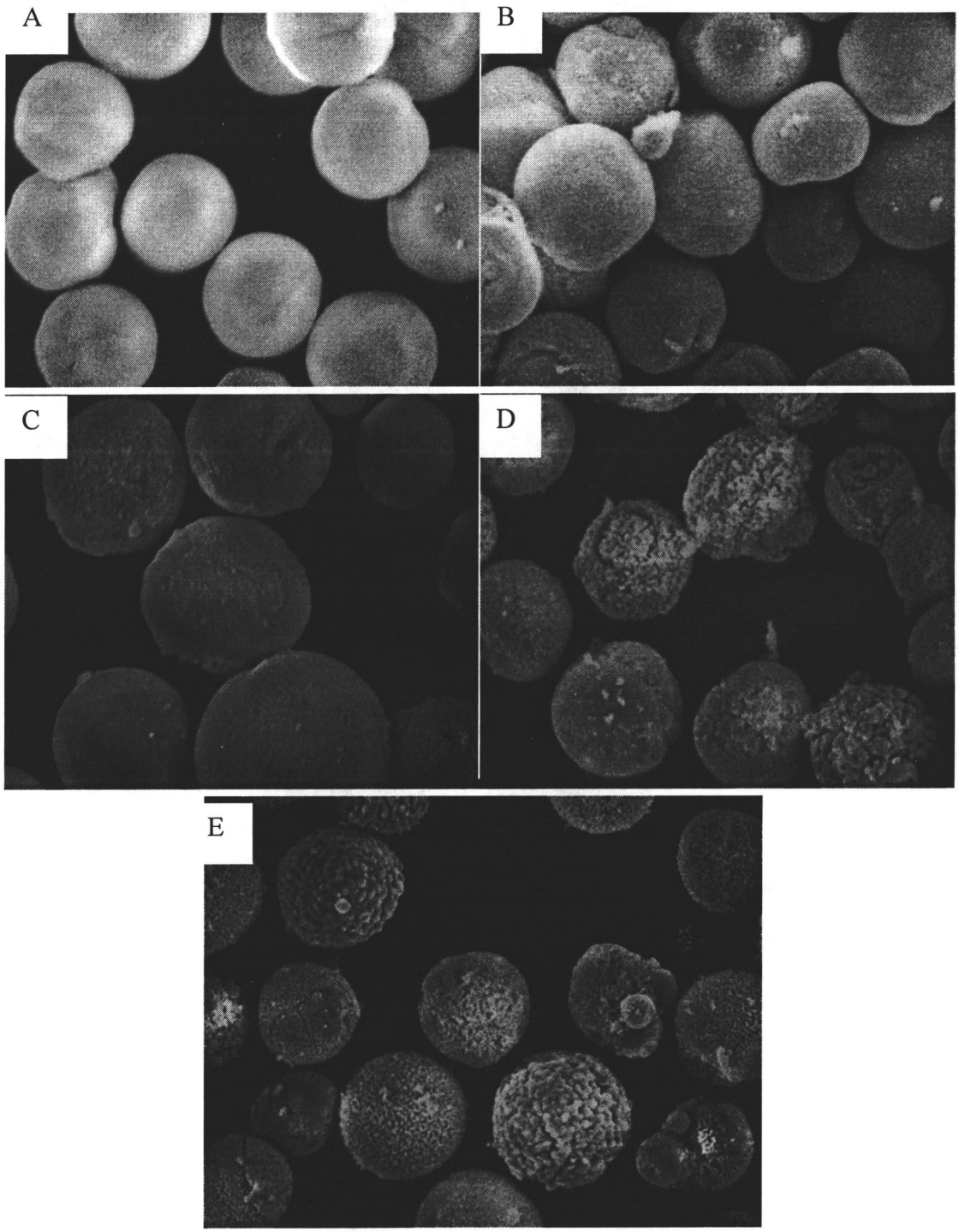

Figure 5.3. Scanning electron micrographs of the packings employed in this study. (A) 100 Å, (B) 300 Å, (C) 500 Å, (D) 1000 Å, (E) 4000 Å.

The differences in obstruction factors for the packings may be attributable to geometrical effects within the particle subtypes that comprise each packing material. The pores comprising the large-pore particle subtype found in the 1000 Å and 4000 Å packings may exhibit a decreased overall tortuosity and/or an increased constriction factor relative to the smaller pores in the intermediate subtype. This effect may be less pronounced for the intermediate pore size subtype of particle, resulting in the slightly smaller obstruction factor for the 500 Å column. The agreement in obstruction factors between the 100 and 300 Å columns is likely due to the fact that the extent of intraparticle current transport in the 300 Å column is relatively small. In this column, an insufficient fraction of particles having pores sufficient to allow current transport exists to have a discernable effect on the obstruction factor.

5.5 Conclusion

The results of this study indicate that macroporous packing materials support intraparticle current flow in chromatographic columns under typical CEC conditions. Columns packed with the widest nominal pore media, namely 1000 Å and 4000 Å, exhibited conductivities over two fold greater than that obtained for a column packed with conventional 100 Å pore diameter media, providing evidence of the existence of "through-pores" in these packings. The packed bed conductivity values and pore size distribution data obtained for the packing materials suggest that current transport is minimal through pores below approximately 300 – 700 Å in diameter. This value may represent the approximate diameter range above which pores have an increased

likelihood of being through-pores. Obstruction factors determined separately by neglecting the volume contribution of pores below 300, 500, and 700 Å in diameter were highest for the columns packed with 1000 Å and 4000 Å media, possibly due to geometrical effects.

It can be concluded from these results that the 1000 Å and 4000 Å media yield packed beds with greater intraparticle flow permeability relative to the smaller pore media. These findings, in concert with results obtained from a thorough study of chromatographic efficiency of macroporous packed columns in the perfusive regime [115], indicate that the use of these wide pore packings in CEC under conditions in which double layer thickness is small compared to the median pore diameter can serve to maximize gains in efficiency arising from electroosmotic perfusion.

6. CONCLUSION

The intent of this dissertation was to explore novel approaches by which selectivity and efficiency could be enhanced in microscale liquid chromatography. As outlined in the introduction, the research was focused in two areas: i) the development of high selectivity affinity sorbents based on molecular imprinted polymers for microscale HPLC and ii) the study of intraparticle, or perfusive electroosmotic flow in macroporous silica-based packings and its effect on efficiency in CEC. In this section, the major conclusions drawn from the research in these areas are summarized.

Molecular imprinted polymers (MIPs) were synthesized in bulk using nortriptyline (NOR), a representative tricyclic antidepressant drug, as the template molecule. After grinding and sieving to achieve the desired particle size, the MIPs were packed into fused silica capillary columns for chromatographic evaluation. To assess the selectivity of the MIP-based affinity sorbent, a group of tricyclic antidepressants structurally similar to the template and other related compounds were screened against the MIP.

Of particular interest in the chromatographic screening experiments was the extent of *selective* interaction of each test probe with the MIP sorbent (i.e. the "goodness of fit" of each compound into the NOR binding pocket). Thus, it was necessary to compensate for any nonspecific interaction between the compounds and the imprinted polymer. Retention behavior on a control or "blank" polymer, which was prepared identically to the MIP but in the absence of template, was used to assess nonspecific retention of the test probes.

Retention factors on the MIP and control polymers were employed in the calculation of a selection index for each test compound. Because retention on the control polymer is factored out, the selection index provides a measure of the extent of selective interaction (i.e. an affinity type interaction) of a given compound with the MIP.

Unsurprisingly, the template molecule was the most strongly retained on the MIP and had the highest selection index of all the compounds tested. Selection index values for the group of test probes revealed that the antidepressants sharing the major structural features of the template molecule, specifically the three rings and pendant secondary amine moiety, exhibited the most favorable interaction with the MIP. A secondary amine-containing antidepressant with a single ring (BUP) showed a much lower selection index than the secondary amine tricyclic compounds. Similar behavior was observed for the structural precursor IDB, which possesses the rings but not the pendant group. Caffeine was screened to evaluate the MIP's ability to discriminate against a structurally unrelated compound. Expectedly, caffeine exhibited virtually no interaction with the MIP.

A series of experiments designed to study the mechanism of interaction between the test probes and the MIP provided evidence of hydrogen bonding between the amine functionality on the analytes and a methacrylic acid moiety on the MIP. As mentioned above, the data show that selective interaction with the MIP is enhanced when a compound contains the three rings *and* pendant secondary amine.

These observations are consistent with what would be expected given the nature of noncovalent imprint formation. Specifically, affinity for the MIP is

maximized when size, shape and functional group complementarity exists between an analyte and the binding site.

These results demonstrate that retention based on molecular recognition (i.e. affinity interactions dependent upon size, shape and chemical functionality of analytes), is possible with MIP sorbents. As discussed in chapter 3, the high selectivity achievable with MIPs may render them useful in a preliminary screening step for potentially bioactive molecules. In addition, the wide range of applicability of noncovalent molecular imprint polymers and their relative ease of preparation allow for custom tailored affinity sorbents that could be useful in a variety of applications.

Macroporous particles in CEC are an alternative to very small diameter packings in maximizing chromatographic efficiency. In this dissertation, the chromatographic performance of columns packed with a series of commercially available reversed phase particles of various nominal pore diameters was investigated. Specifically, the buffer concentration of the mobile phase was varied, which affected the extent of intraparticle EOF, and the plate height of a weakly retained test probe was monitored.

The data showed that at low buffer concentrations efficiency, correlated with the nominal pore size of the packing (4000 Å > 1000 Å > 500 Å). As buffer concentration was gradually increased over two orders of magnitude, rate curves for the three columns converged (i.e. efficiencies were comparable). The observations are consistent with columns operated in a perfusive regime and were rationalized as follows. The critical parameter controlling the extent of perfusion in these packings is the mean intraparticle electrokinetic radius (κa). At low buffer concentrations, the

intraparticle κa is insufficient to yield appreciable perfusion in the comparatively narrow 500 Å packing. As a result, the 500 Å column functions as a "conventional" interstitial flow system with no perfusive efficiency gains. In contrast, the 4000 Å packing has a larger mean κa at the same buffer concentration because the mean intraparticle channel radius a is greater. Hence, the 4000 Å column operates in a perfusive mode under these conditions, evidenced by enhanced efficiency.

Likewise, the convergence of the rate curves for the different columns is attributable to more favorable mean intraparticle κa values as buffer concentration is increased. These observations are again consistent with expected results for perfusive flow in CEC columns.

It is clear upon examination of the chromatographic data presented in chapter 4 that rapid, high efficiency separations are best achieved with the widest pore packing, in this case 4000 Å, at buffer concentrations below 25 mM. This is because the low buffer concentrations that yield favorable κa values with wide pore packings also result in a more robust mean EOF velocity (recall that mean EOF velocity is proportional to double layer thickness).

A model by which the extent of intraparticle EOF in a given column could be estimated was presented in chapter 4 of this dissertation. Expressed in terms of an effective particle diameter, $d_{p.eff}$, values were calculated using a weighted average method, which accounted for i) the fraction of column void volume contributed by the interstital space and each of 995 intervals of intraparticle pore space encompassing diameters from 50 – 10000 Å as determined by mercury intrusion porosimetry and ii) the extent of double layer overlap in the interstitial and intraparticle regions.

Values of $d_{p.eff}$, obtained with the model show agreement with the general trends in the chromatographic data, specifically the pronounced differences in the packings at the lowest buffer concentration and the convergence as buffer concentration is increased. Substitution of $d_{p.eff}$, for d_p did not result in overlap of the rate curves for the various data sets. A significant degree of overlap in the curves would be expected if reductions in effective particle diameter were the sole factor leading to increased efficiency with these columns. Although differences in slope between the rate curves would be expected at higher velocities due to decreased stagnant mobile phase mass transfer (included in the C term of the Knox equation) independent of correction by $d_{p.eff}$,, the curves based on $d_{p.eff}$, differ at low to moderate reduced velocities, at which the coupled eddy diffusion/mobile phase mass transfer (the A term of the Knox equation) dominates. Differences in the A term between the packings could perhaps arise from geometrical effects, for example decreased tortuosity factors for the wide pore media, in the intraparticle flow channels.

Expanding on the research presented in chapter 4, the intraparticle flow permeability of CEC columns packed with various pore sizes of particles was investigated by comparing the electrical conductivity of the columns. In addition to the those studied in chapter 4, two packings of the same base silica and particle diameter were included, having nominal pore sizes of 100 and 300 Å. After determining the current due to electroosmosis to be negligible in the columns under the experimental conditions, observed differences in the conductivity ratio κ_p/κ_o were attributed to the extent intraparticle ion transport.

κ_p/κ_o values for the 100 Å column were in agreement with theory for nonporous spheres, indicating that intraparticle current was negligible. Conductivity ratios for the larger pore sizes, however, showed significant deviation from theory. For example, conductivity ratios for columns packed with the widest pore media (1000 and 4000 Å), were over twofold greater than that predicted for nonporous spheres. These results provide evidence for the existence of through-pores in these wide pore packings.

The conductivity data and pore size distributions of the packings determined by mercury intrusion porosimetry were used to estimate effective total porosity (ε_p') values for the columns. The effective total porosity is defined as the fraction of free space in the column through current flow due to ion transport can occur. Values of ε_p' were determined by selecting a pore diameter (300, 500, or 700 Å) below which pores were assumed not to allow ion transport and subsequently neglecting the pore volume contributed by pores below this diameter when calculating the particle porosity.

The ε_p' values were used to estimate obstruction factors for the columns, which are a measure of the effect of geometrical constraints on current flow in the packed bed. At each of the three cutoff pore diameters, obstruction factors for the 100 and 300 Å columns exhibited a marked difference from the three widest pore columns.

Transmission and scanning electron micrographs of these packings show that a packing of a given nominal pore diameter actually consists of a blend of various subtypes of particles differing in pore size and morphology. The 1000 and 4000 Å packings contain a substantial fraction of the particle subtype having wide pores with an open structure as determined by SEM and TEM. Differences in obstruction factors

between the columns could perhaps be due to an enhanced tortuosity factor in this large pore subtype.

The results of this study indicate that the intraparticle flow permeability is greatest in columns packed with the widest pore media, 1000 and 4000 Å. Collectively, the results presented in chapters 4 and 5 show that efficiency gains due to perfusive electroosmosis can be maximized when these wide pore media are employed.

With regard to intraparticle or perfusive electroosmosis in CEC, it has been demonstrated in this dissertation that i) substantial gains in efficiency are possible with macroporous, reverse-phase HPLC packings at relatively low buffer concentrations, ii) the extent of intraparticle EOF can be estimated and expressed in terms of an effective particle diameter, iii) pores that allow through-pore ion transport (and hence, EOF) exist in these packings, and iv) intraparticle flow permeability is maximized with wide pore packings.

BIBLIOGRAPHY

1) Turková, J. *Bioaffinity Chromatography*, Elsevier: Amsterdam, 1993.

2) Afeyan, N.B.; Gordon, N.F.; Mazsaroff, I.; Varady, L.; Fulton, S.P.; Yang, Y.B.; Regnier, F.E. *J. Chromatogr.*, **1990**, *519*, 1.

3) Giddings, J.C. *Dynamics of Chromatography;* Marcel Dekker: New York, 1965.

4) Bristow, P.A.; Knox J.H. *Chromatographia,* **1977**, *10*, 279.

5) Knox, J.H. *J. Chromatogr. Sci.*, **1980**, *18*, 453.

6) Ishii, D. ed. *Introduction to Microscale High-Performance Liquid Chromatography*; VCH: New York, 1988.

7) Snyder, L. Kirkland, J. *Introduction to Modern Liquid Chromatography*;, Wiley Interscience: New York, 1979.

8) Martin, M. Eon, C. Guiochon, G. *J. Chromatogr.*, **1975**, *108*, 229.

9) Mysels, K. *Introduction to Colloid Chemistry*; Interscience: New York, 1959.

10) Shaw, D.J. *Introduction to Colloid and Surface Chemistry*; Butterworth-Heinemann: Oxford, 1992.

11) Lükde, S.; Adam, T.; Unger, K.K. *J. Chromatogr. A*, **1997**, *786*, 229.

12) Reynolds, K.J.; Colón, L.A. *J. Liq. Chromatogr. Rel. Technol.*, **2000**, *23*, 161.

13) Knox, J.H.; Grant, I.H. *Chromatographia*, **1991**, *32*, 317.

14) Yan, C. Dadoo, R., Zhao, H., Zare, R. *Anal. Chem.*, **1995**, *67*, 2026.

15) Martin, A.J.P.; Synge, R.L.M. *Biochem J.*, **1941**, *35*, 1358.

16) Hamilton, P.B.; Bogue, D.C.; Anderson, R.A. *Anal. Chem.*, **1960**, *32*, 1782.

17) Huber,, J.F.K.; Hulsman, J.A.R.L. *Anal. Chim. Acta*, **1967**, *38*, 305.

18) Vallano, P.T.; Chirica, G.; Remcho, V.T. in the *Encyclopedia of Analytical Chemistry*; R.A. Meyers, ed., John Wiley and Sons: Chichester, 2000.

19) Done, J.N.; Knox, J.H.; Loheac, J. *Applications of High-Speed Liquid Chromatography*; John Wiley & Sons Ltd.: New York, 1974.

20) Horvath, Cs.; Preiss, B.A.; Lipsky, S.R. *Anal. Chem.*, **1967**, *39*, 1422.

21) Kirkland, J.J. *J. Chromatogr. Sci.*, **1969**, *7*, 7.

22) Scott, R.P.W.; Kucera, P. *J. Chromatogr.*, **1979**, *169*, 51.

23) Menet, H.G., Gareil, P.C., Rosset, R.H., *Anal. Chem.*, **1984**, *58*, 1770.

24) Nota, G.; Marino, G.; Buoncuore, V.; Ballio, A. *J. Chromatogr.* **1970**, *46*, 103.

25) Tsuda, T.; Novotny, M. *Anal. Chem.*, **1978**, *50*, 632.

26) Hibi, K.; Ishii, D.; Fujishima, I.; Takeuchi, T.; Nakanishi, T. *J High Res. Chromat. & Chromat. Commun.*, **1978**, (July), 21.

27) Tsuda, T.; Hibi, K.; Nakanishi, T.; Takeuchi, T.; Ishii, D. *J. Chromatogr.*, **1978**, *158*, 227.

28) Tijseen, R.; Bleumer, J.P.A.; Smit, A. *J. Chromatogr.*, **1981**, *218*, 137.

29) Poppe, H. *J Chromatogr., A*, **1997**, *778*, 3.

30) Swart, R.; Kraak, J.C.; Poppe, H. *Trends in Anal. Chem.*, **1997**, *16*, 332.

31) Dandeneau, R.D.; Zerenner, E.H. *J. High Res. Chromatogr. & Chromatogr. Commun.* **1979**, (June) 351.

32) Yang, F.J. *J. High Res. Chromatogr.& Chromatogr. Commun.*, **1980**, *3*, 589.

33) Kennedy, R.T.; Jorgenson, J.W. *Anal. Chem.*, **1989**, *61*, 436.

34) Tsuda, T.; Novotny, M. *Anal. Chem.*, **1978**, *50*, 271.

35) Hirata, Y.; Novotny, M.; Tsuda, T.; Ishii, D. *Anal. Chem.* **1979**, *51*, 1807.

36) Knox, J.H.; Parcher, J.F. *Anal. Chem.*, **1969**, *41*, 1599.

37) Knox, J.H.; Laird, G.R.; Raven, P.A. *J. Chromatogr.* **1976**, *122*, 128.

38) Wilson, W.H.; McNair, H.M.; Maa, Y.F.; Hyver, K.J. *J. High Resolut. Chromatogr.*, **1990**, *13*, 18.

39) Kennedy, R.T.; Jorgenson, J.W. *Anal. Chem*, **1989**, *161*, 1128.

40) Wilson, W. H., Ph.D. Dissertation, Virginia Polytechnic Institute & State University, 1990.

41) Gluckman, J.C.; Hirose, A.; McGuffin, V.L.; Novotny, M. *Chromatographia*, **1983**, *17*, 303.

42) Helmholtz, H. V. *Wiedemanns Ann. (Ann. Phys. Leipzig)*, **1877**, *7*, 337.

43) Tiselius, A. *Trans. Faraday Society*, **1937**, *33*, 524.

44) Hjerten, S. *Methods Biochem. Anal.*, **1970**, *18*, 55.

45) Jorgenson, J.W.; Lukacs, K.D. *J. Chromatogr.*, **1981**, *218*, 209.

46) Terabe, S.; Otsuka, K.; Ichikawa, K.; Tsuchiya, A.; Ando, T. *Anal. Chem.*, **1984**, *56*, 111.

47) Pretorius, V.; Hopkins, B.; Schieke, J. *J. Chromatogr.*, **1974**, *99*, 23.

48) Knox, J.H.; Grant, I.H. *Chromatographia*, **1987**, *24*, 135.

49) Euerby,M.R.; Gilligan, D.; Johnson, C.M.; Roulin, S.C.P.; Myers, P.; Bartle, K.D. *J. Microcol. Sep.*, **1997**, *9*, 373.

50) Taylor, M.R.; Teale, P.; Westwood, S.A.; Perrett, D. *Anal. Chem.*, **1991**, *69*, 2554.

51) Sandra, P.; Dermaux, A.; Ferraz, V.; Dittmann, M.M.; Rozing, G. *J. Microcol. Sep.*, **1997**, *9*, 409.

52) Li, D.; Knobel, H.H.; Remcho, V.T. *J. Chromatogr. B*, **1997**, *695*, 169.

53) Tan, Z.J.; Remcho, V.T. *Anal. Chem.*, **1997**, *69*, 581.

54) Fujimoto, C.; Fujise, Y.; Matsuzawa, E. *Anal. Chem.*, **1996**, *68*, 2753.

55) Palm A.; Novotny, M. *Anal. Chem.*, **1997**, *69*, 4499.

56) Liao, J-L; Chen, N.; Ericson, C.; Hjertén, S. *Anal. Chem.*, **1996**, *68*, 3468.

57) Ericson, C.; Liao, J-L; Nakazato, K.; Hjertén, S. *J. Chromatogr. A*, **1997**, *767*, 33.

58) Schweitz, L.; Andersson, L.I.; Nilsson, S. *Anal. Chem.*, **1997**, *69*, 1179.

59) Schweitz, L.; Andersson, L.I.; Nilsson, S. *J. Chromatogr. A*, **1997**, *792*, 401.

60) Peters, E.C.; Petro, M.; Svec, F.; Frechet, J.M.J. *Anal. Chem.*, **1997**, *69*, 3646.

61) Peters, E.C.; Petro, M.; Svec, F.; Frechet, J.M.J. *Anal. Chem.*, **1998**, *70*, 2288.

62) Peters, E.C.; Petro, M.; Svec, F.; Frechet, J.M.J. *Anal. Chem.*, **1998**, *70*, 2296.

63) Minakuchi, H.; Nakanishi, K.; Soga, N.; Ishizuka, N.; Tanaka, N. *Anal. Chem.*, **1996**, *68*, 3498.

64) Ishizuka, N.; Minakuchi, H.; Nakanishi, K.; Soga, N.; Tanaka, N. *J. Chromatogr. A*, **1998**, *797*, 133.

65) Hayes, J.D.; Malik, A. *Anal. Chem.*, **2000**, *72*, 4090.

66) Hayes, J.D.; Scott, T.J.; Malik, A. *Anal. Chem.*, **1997**, *69*, 3889.

67) Chirica, G.; Remcho, V.T. *Electrophoresis*, **1999**, *20*, 50.

68) Chirica, G.; Remcho, V.T. *Electrophoresis*, **2000**, *21*, 3093.

69) Dickey, F.H. *Proc. Natl. Acad. Sci. USA*, **1949**, *35*, 227.

70) Mosbach, K.; Mosbach, R. *Acta Chem. Scand.*, **1966**, *20*, 2807.

71) Hedborg, E.; Winquist, F.; Lundström, I.; Andersson, L.; Mosbach, K. *Sensors and Actuators A*, 1993, 37, 796.

72) Vlatakis, G.; Andersson, L.I.; Müller, R.; Mosbach, K. *Nature*, 1993, 361, 645.

73) Ohkubo, K.; Urata, Y.; Hirota, S.; Funakoshi, Y.; Sagawa, T.; Usui, S.; Yoshinaga,K. *J. Mol. Catal.*, **1995**, *101*, L111.

74) Mosbach, K.; Ramström, O. *Bio/Technology*, **1996**, *14*, 163.

75) Wulff, G. *Angew. Chem. Intl. Ed. Engl.*, **1995**, *34*, 1812.

76) Steinke, J.; Sterrington, D.C.; Dunkin, I.R. *Adv. Polymer Sci.*, **1995**, *123*, 81.

77) Remcho, V.T.; Tan, Z.J. *Anal. Chem.*, **1999**, *71*, 248A.

78) Ramström, O.; Nicholls, I.A.; Mosbach, K. *Tetrahedron: Asymmetry*, **1994**, *5*, 649.

79) Sellergren, B.; Shea, K. *J. Chromatogr. A*, **1993**, *654*, 17.

80) Fischer, L.; Müller, R.; Ekberg, B.; Mosbach, K. *J. Am. Chem. Soc.*, **1991**, *113*, 9358.

81) Kempe, M.; Mosbach, K. *J. Chromatogr. A*, **1994**, *664*, 276.

82) Nicholls, I.A.; Mosbach, K. *J. Chromatogr. A*, **1995**, *691*, 349.

83) Wulff, G.; Haarer, J. *Makromol. Chem.*, **1991**, *192*, 1329.

84) Kriz, D.; Ramström, O.; Mosbach, K. *Anal. Chem.*, **1997**, *69*, 345A.

85) Czarnik, A. *Anal. Chem.*, **1998**, *70*, 379A.

86) Boutin, J.A.; Lambert, P.H.; Bertin, S.; Volland, J.P.; Fauchère, J.L. *J. Chromatogr. B*, **1999**, *725*, 17.

87) Woodbury, C.P.; Venton, D.L. *J. Chromatogr. B*, **1999**, *725*, 113.

88) Evans, D.M.; Williams, K.P.; McGuinness, B.; Tarr, G.; Regnier, F.; Afeyan, N.; Jindal, S. *Nature Biotechnol.*, **1996**, *14*, 504.

89) Tan, Z.J.; Cipolletti, M.; Remcho, V.T. *Proceedings of the 21st International Symposium on Capillary Chromatography and Electrophoresis*, Wintergreen, VA, USA, May 18-22 1997, p. 466.

90) Ramström, O.; Ye, L.; Krook, M.; Mosbach, K. *Anal. Commun.*, **1998**, *35*, 9.

91) Olson, D.L.; Lacey, M.E.; Sweedler, J.V. *Anal. Chem.*, **1998**, *70*, 257A.

92) Budavari, S. ed., *The Merck Index 12th Edition*, Merck & Co., Inc.: Whitehouse Station, NJ, 1996.

93) Sellergren, B.; K. Shea, K. *J. Chromatogr. A*, **1995**, *690*, 29.

94) O'Brien, T.P.; Snow, N.H.; Grinberg, N.; Crocker, L. *J. Liq. Chrom. Rel. Technol.*, **1999**, *22*, 183.

95) Sellergren, B. *J. Chromatogr. A*, **1994**, *673*, 133.

96) Hosoya, K.; Yoshizako, K.; Shirasu, Y.; Kimata, K.; Araki, T.; Tanaka, N.; Haginaka, J. *J. Chromatogr. A*, **1996**, *728*, 139.

97) Mayes, A.G.; Mosbach, K. *Trends Anal. Chem.*, **1997**, *16*, 321.

98) Thoma, K.; Albert, K. *Pharm. Acta Helv.*, **1980**, *55*, 8.

99) Armstrong, D.W.; Chen, S.; Chang, S. *J. Liq. Chrom.*, **1992**, *15*, 545.

100) Colón, L.A.; Guo, Y.; Fermier, A. *Anal. Chem.*, **1997**, *69*, 461A.

101) Dittmann, M.M.; Wienand, K.; Bek, F.; Rozing, G.P. *LC-GC* **1995**, *13*, 802.

102) Crego, A.L.; González, A.; Marina, M.L. *Crit. Rev. Anal. Chem.* **1996**, *26*, 261.

103) Vallano, P.T.; Remcho, V.T. *J. AOAC International* **1999**, *82*, 1604.

104) Li, D.; Remcho, V.T. *J. Microcolumn Sep.* **1997**, *9*, 389.

105) Unger, K.K. *Porous Silica*, Elsevier: Amsterdam, 1979; Chapter 2.

106) Stol, R.; Kok, W.T.; Poppe, H. *J. Chromatogr. A* **1999**, *853*, 45.

107) Knox, J.H.; Kennedy, G. *J. Chromatgr. Sci.* **1972**, *10*, 549.

108) Rice, C.L.; Whitehead, R. *J. Phys. Chem.* **1965**, *69*, 4017.

109) Von Smolouchowski, M. in I. Graetz, ed., *Handbuch der Elektrizität und des Magnetismus*, Barth, Leipzig, 1921.

110) Wan, Q-H. *Anal. Chem.* **1997**, *69*, 361.

111) Wan, Q-H. *J. Phys. Chem. B* **1997**, *101*, 4860.

112) Wilke, C.R.; Chang, P.; *Am. Inst. Chem. Eng.*, **1955**, *1*, 264.

113) Tanaka, N.; Hashidzume, K.; Araki, M.; Tsuchiya, H.; Okuno, A.; Iwaguchi, K.; Ohnishi, S.; Takai, N. *J. Chromatogr.* **1988**, *448*, 95.

114) Schwer, C.; Kenndler, E. *Anal. Chem.* **1991**, *63*, 1801.

115) Vallano, P.T.; Remcho, V.T. *Anal. Chem.*, **2000**, *72*, 4255.

116) Wan, Q-H. *J. Phys. Chem. B*, **1997**, *101*, 8449.

117) Boyak, J.R., Giddings, J.C. *Arch. Biochem. Biophys.*, **1963**, *100*, 16-25.

118) Slawinski, A. *J. Chim. Phys.*, **1926**, *23*, 710-727.

119) Bruggeman, D.A.G. *Ann. Phys.*, **1935**, *24*, 636-664.

120) Meredith, R.E., Tobias, C.W. *J. Electrochem. Soc.*, **1961**, *108*, 286-290.

121) Edward, J.T. *Adv. Chromatogr.*, **1966**, *2*, 63-98.

122) Van Der Put, A.G., Bijsterbosch, B.H. *J. Colloid Interface Sci.*, **1980**, *75*, 512-524.